SYSTEM DESIGN AND ASSESSMENT NOTES

NOTE 41

8 July 2014

STUDY AND CLASSIFICATION OF POTENTIAL IEMI SOURCES

Nicolas MORA, Felix VEGA, Gaspard LUGRIN, Farhad RACHIDI

EMC Laboratory

Swiss Federal Institute of Technology in Lausanne (EPFL)

Lausanne, Switzerland

Marcos RUBINSTEIN

University of Applied Sciences of Western Switzerland (HEIG-VD)

Yverdon, Switzerland

Corresponding author: nicolas.mora@epfl.ch

Abstract: In this note, we assess the capabilities of publicly reported high-voltage (HV) pulsers and high-power electromagnetic (HPEM) radiators that could be regarded as potential IEMI sources. We are interested in using the methods proposed in the literature to characterize the signals generated by "real" sources for which authors have provided relevant information or even the waveforms in the papers. We also apply the definitions proposed to classify the available sources in terms of their transportability, technological development, and cost level in order to see the trends that are followed by both the conducted and radiated sources. As a product of this note, two Appendices including the waveform and spectral parameters of 39 sources, and the classification of 21 conducted sources and 55 radiated sources are attached.

TABLE OF CONTENTS

1 INTRODUCTION

The assessment of the vulnerability of critical systems against intentional electromagnetic interferences (IEMI) has attracted considerable interest in the EMC community in the past decade or so [1-6]. Prior to any analysis of the consequences of a successful IEMI attack, a good knowledge of the expected high power electromagnetic environments (HPEM-E) is required in order to decide the scope of the considered methodology. To do this, several questions need to be addressed, including:

- What is the expected voltage waveform that could be injected in the cables of the facility under study?
- What is the maximum field level expected in the vicinity of the facility under study?
- What are the frequencies of the fields that will be illuminating the facility walls?
- Can the possible IEMI sources be transported to the vicinity of the facility?
- How much money does a malefactor require to acquire such a source?

One would expect that, given the size of hand-made electronic equipment and general purpose facilities, the majority of the sources should be built around some hundreds of MHz to some GHz (about 1 GHz according to the Baum's law[7]). There are several good surveys in the literature addressing some of these questions by making reference to the development of so-called non-lethal weapons in the US [8, 9]. In addition, useful analytical predictions of the expected field levels of sources can be found in [10, 11]. However, many advances have been made in the past few years and the survey on available sources can be revisited by including recently reported sources of different types and, in particular, mesoband sources of the past decade [12-16].

Revisiting the survey is also warranted since, although general classification methods of sources according to their transportability and availability properties have been proposed [10, 17, 18], these methods have not been used in a systematic way to address available sources.

In this note, we assess the capabilities of publicly reported HV pulsers and HPEM radiators that could be regarded as potential IEMI sources. We are interested in using the methods proposed in the literature to characterize the signals generated by "real" sources for which authors have somehow provided relevant information or even the waveforms in the papers. We also apply the definitions proposed to classify the sources in terms of their transportability, technological development, and cost level in order to see the trends that are followed by both, conducted and radiated sources. As a product of this note, two Appendices including the waveforms and spectral parameters of about 39 sources, and the classification of 21 conducted sources and 55 radiated sources are attached.

We start by reviewing the definitions of the waveform and spectral attributes that have been given in the literature in Section 2. The proposed classification of the sources according to their field strength, and their availability is described in Section 3.

In Section 4, we describe the adopted procedure to digitize the source waveforms extracted from papers, and the processing steps to produce the "wavecards" containing all the relevant parameters associated with each source. We also introduce a technique for an efficient evaluation of the Fourier transform of the signals and the extraction of their spectral characteristics. The technique is based on the use of the matrix pencil method (MPM) to expand the time domain waveforms into a series of damped complex exponentials, whose poles and residues can be used to calculate waveform's Fourier transform analytically. We also present the use of the so-called Blumer index for improving the time required for estimating the band-ratio of a given spectrum.

In Section 5, we analyze the general trends and characteristics of the sources by using comprehensive pie charts and bar plots.

An overview of the possible source limitations due to physical constraints of the implemented technologies is presented in Section 6. The purpose of this section is to provide some figures representing the maximum expected limits of a potential IEMI source.

Finally, conclusions are given in Section 7.

2 WAVEFORM PARAMETERS

In this section, the waveform attributes used in this work for the characterization of the radiated and conducted emissions of different types of IEMI sources will be defined. An effort is made to include the classification parameters of typical emissions that regularly appear in the measurements reported in the literature, out of the many different waveforms that could be encountered in the field.

Radiated and conducted signals can be classified by using their time-domain characteristics or their frequency spectrum. The time and frequency characterization of the sources is essential for the evaluation of the threat level.

The waveform characteristics definitions will be presented in two subsections. The first part will cover the time-domain waveform attributes of typical measured outputs of IEMI generators and the so-called susceptibility norms that are generally used to evaluate the equipment susceptibility levels. In the second part, the frequency spectrum attributes will be presented.

2.1 Time-domain parameters

2.1.1 Waveform attributes

2.1.1.1 Single pulse attributes

One of the typically measured waveforms from Hyperband/Sub-hyperband generators, also called UWB generators (e.g. [19-24]), is a single pulse that can be represented by the waveform presented in Fig. 2.1 [25]:

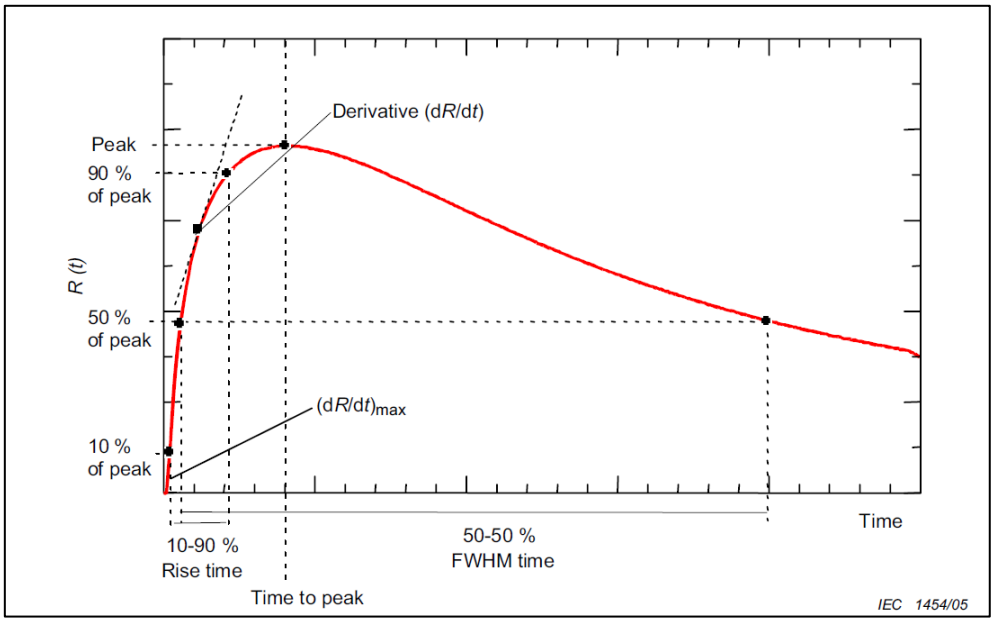

Fig. 2.1 Illustrative plot of a monopolar pulse and its waveform attributes. Adapted from [25]

The time domain waveform attributes characterizing this type of signals, namely the peak amplitude, the time-to-peak, the 10-90 % rise-time, the full-width-at-half-maximum (FWHM), and the peak derivative are also shown in Fig. 2.1. Notice that the time domain signal $R(t)$ has been truncated to illustrate its significant characteristics. In the late times, $R(t)$ should vanish to zero to ensure causality.

a Peak Amplitude

The peak amplitude of the waveform $R_{\max}$ is defined as the maximum value of the signal during its rise. For a pulse-like function, it corresponds to its absolute maximum value:

$$R_{\max} = \max(|R(t)|) \tag{2.1}$$

b Time to peak

The time to peak $\Delta t_{\max}$ is defined as the time it takes the waveform to achieve its maximum amplitude, starting from a zero amplitude level:

$$\Delta t_{\max} = t\big|_{R(t)=R_{\max}} - \max(t\big|_{R(t)\approx 0}) \tag{2.2}$$

c Peak derivative

The peak derivative $\left(\frac{dR}{dt}\right)_{\max}$ is calculated as the maximum derivative of the waveform before achieving its peak amplitude:

$$\left(\frac{dR}{dt}\right)_{\max} = \max(\frac{dR}{dt}), t < t\big|_{R(t)=R_{\max}} \tag{2.3}$$

d 10-90% rise time

The 10-90% rise time Δt_{10-90} is defined as the time it takes the waveform to increase from 10% to 90% of $R_{\max}$, during its rising period:

$$\Delta t_{10-90} = t\big|_{R(t)=0.9R_{\max}} - t\big|_{R(t)=0.1R_{\max}}, t < t\big|_{R(t)=R_{\max}} \tag{2.4}$$

e Maximum rate of rise

An alternative definition for the rise-time that has been proposed for the analysis of Nuclear Electromagnetic Pulses (NEMP) is the so-called maximum rate of rise[1] t_{mr} [26]. The maximum rate of rise of an impulsive-like signal can be defined as the ratio of its peak amplitude and its peak derivative:

$$t_{mr} = \frac{R_{\max}}{\left(\frac{dR}{dt}\right)_{\max}} \tag{2.5}$$

[1] The denomination maximum rate of rise has been used in the EMP community for designating this quantity and it shall not be confused with the peak derivative.

f Full-width-at-half -maximum (FWHM)

The FWHM Δt_{50-50}, also commonly addressed as the "duration" of the pulse, is the time elapsed between the instant when the waveform reaches 50% of $R_{\max}$, during its rising period, and the instant when it decays to 50% of $R_{\max}$ during its falling period:

$$\Delta t_{50-50} = t\big|_{R(t)=0.5R_{\max} \wedge \frac{dR}{dt}<0} - t\big|_{R(t)=0.5R_{\max} \wedge \frac{dR}{dt}>0} \tag{2.6}$$

2.1.1.2 Damped sinusoid attributes

Another common type of waveform used for the analysis of HPEM generators is the damped sinusoid waveform. This is the typical oscillatory profile of the so-called mesoband generators (e.g. [8, 15, 27-30]). For this kind of waveforms, there are three additional parameters that may be of interest. These will be defined in the next three subsections. A plot of a damped sinusoid function is presented in Fig. 2.2:

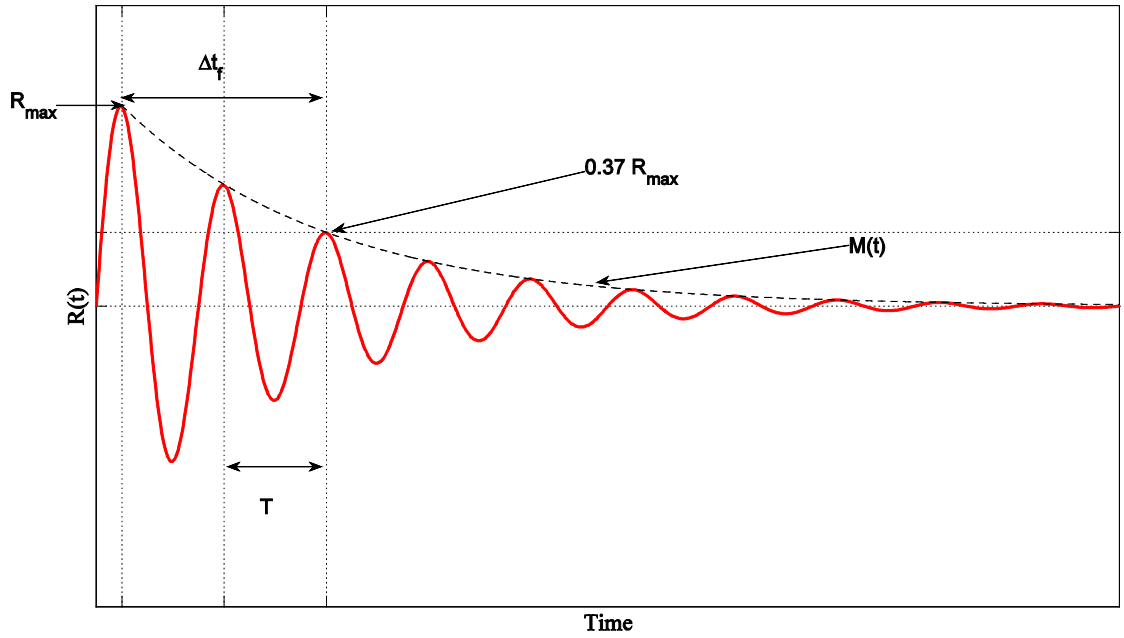

Fig. 2.2 Plot of a damped sinusoidal function and its waveform attributes.

g Fall-time

The fall-time Δt_f is the time taken by the exponential envelope $M(t)$ to decay from the peak amplitude $R_{\max}$ to a value of $\frac{1}{e} \approx 37\%$ of $R_{\max}$ (see Fig. 2.2):

$$\Delta t_f = t\big|_{M(t)\approx 0.37R_{\max}} - t\big|_{R(t)=R_{\max}} \tag{2.7}$$

This value, which is also addressed as the e-folding time, gives an idea of the damping factor associated with the damped exponential envelope that attenuates the sinusoid, as illustrated with a dashed black line in Fig. 2.2.

h Average period

The average period T is the period of the sinusoidal function that is being modulated by the damped exponential. It can be estimated by measuring the time between two successive local maxima, minima, or zero crossings as illustrated in Fig. 2.2. The average period T can be used to estimate the average frequency of the damped sinusoid ${f_0}^{\text{avg}}$ as:

$$ {f_0}^{\text{avg}} = \frac{1}{T} \tag{2.8} $$

i Average quality factor

The quality factor of a damped sinusoid gives a measure of the energy concentration in its fundamental frequency. Qualitatively, it is a figure that measures the ability of delivering energy at a tuned frequency before the waveform extinguishes. The average quality factor Q^{avg} can be estimated from the average period and the fall time as [31]:

$$ Q^{\text{avg}} = \pi \frac{\Delta t_f}{T} = \pi {f_0}^{\text{avg}} \Delta t_f \tag{2.9} $$

In practical cases, the typically measured waveforms may not reproduce a perfect damped sinusoid, but rather an oscillatory waveform. However, the aforementioned parameters can be used to estimate the properties in an average sense. As an illustration, an example of a measured oscillatory signal for which the attributes of damped-sinusoid-like waveforms are analyzed is shown in Fig. 2.3.

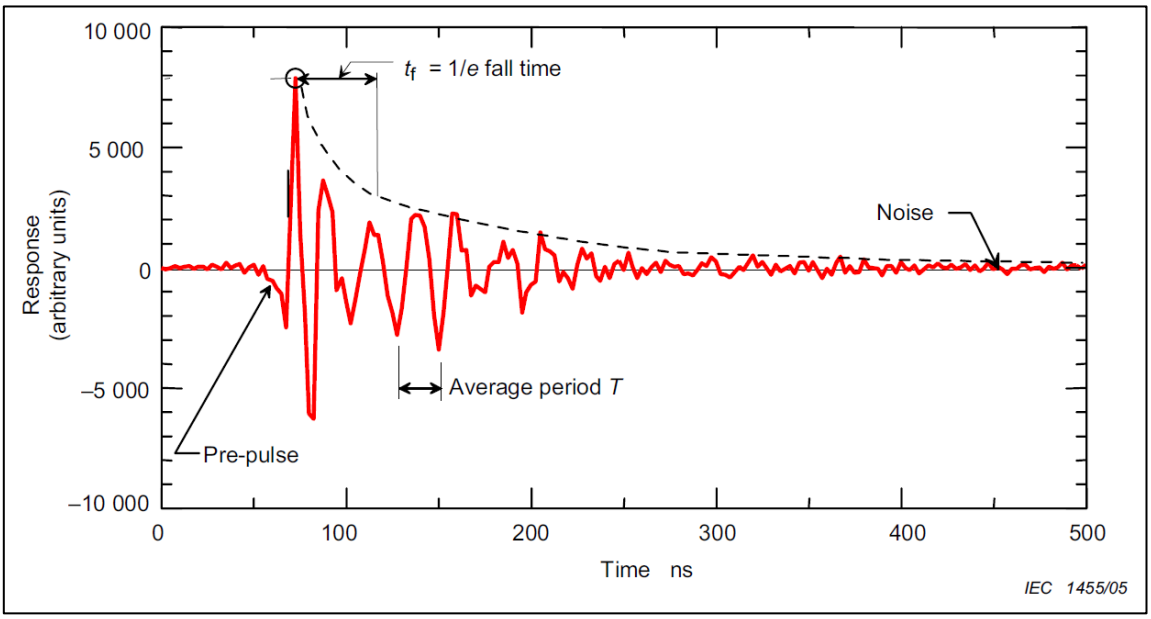

Fig. 2.3 Illustration of an oscillatory measured signal. Image reproduced from [25]

2.1.1.3 Continuous Wave (CW) attributes

Continuous wave (CW) sources are also commonly analyzed in the field of IEMI (e.g.[32-34]). CW outputs are generally bursts of sinusoidal pulses as schematically illustrated in Fig.

2.4. The CW bursts can be viewed as a sinusoidal waveform with a central frequency f_0 whose amplitude is modulated by a periodic binary pulse train with a given duty cycle and a repetition rate, similar to what is know as On-Off keying or OOK in digital communications [35].

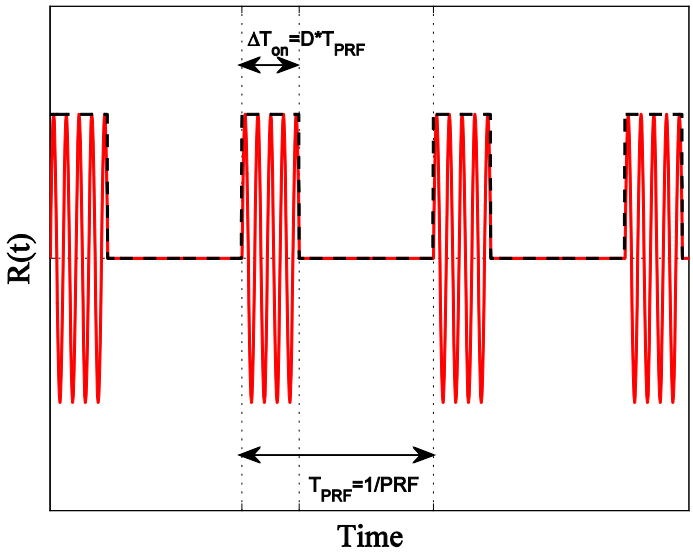

Fig. 2.4 Illustration of a CW burst

j Pulse repetition frequency (PRF)

The pulse repetition frequency (PRF) of the burst is the frequency of the transition between an ON-OFF-ON state of the CW generator; i.e. the inverse of the period of the modulating pulse train T_{PRF}:

$$PRF = \frac{1}{T_{PRF}} \tag{2.10}$$

Notice that the PRF can be also defined for repetitive monopolar pulse and damped sinusoid generators. In these cases, the PRF corresponds to the time elapsed between the onset instants of two successive waveforms.

k Duty cycle

The duty cycle of the burst is the time frame during which the CW source output is active (see Fig. 2.4), expressed as a fraction of the burst period. The duty cycle can be calculated as a function of the *PRF* and the active time frame ΔT_{on} as:

$$D = \frac{\Delta T_{on}}{T_{PRF}} = PRF \cdot \Delta T_{on} \tag{2.11}$$

2.2 N-norms

The so-called N-norms are parameters that are used to characterize time domain waveforms, and have been historically proposed to define the susceptibility limits of equipment. The

particular interest on using norms stems from the fact that they can be used to specify the effect of a given field on systems [25, 36]. The calculation of the N-norms is based on the application of mathematical operators over the entire waveform. A summary of the definition of the norms $N_1 - N_5$, together with an indication as to why the norm is of particular interest is presented in Table 2.1 reproduced from [9, 25].

Table 2.1 N–norms used for high power transient waveforms [9, 25]

Norm	Name	Use
$N_1 = \left\|R(t)\right\|_{\max}$	Peak (absolute) value	Circuit upset/electric breakdown/arc-over effects
$N_2 = \left\|\frac{\partial R(t)}{\partial t}\right\|_{\max}$	Peak (absolute) derivative	Component arcing / circuit upset
$N_3 = \left\|\int_0^t R(t)dt\right\|_{\max}$	Peak (absolute) impulse	Dielectric puncture (if R denotes E field)
$N_4 = \int_0^\infty \left\|R(t)\right\|dt$	Rectified total impulse	Equipment Damage
$N_5 = \left\{\int_0^\infty \left\|R(t)\right\|^2 dt\right\}^{\frac{1}{2}}$	Square root of action integral	Component burnout

Notice that the first two norms correspond to the already described *peak Amplitude* and the *peak derivative* of the waveforms. If the ratio N_1/N_2 is calculated, the *maximum rate of rise* is also obtained. Thus, one could think of a new definition of the rise time "based on norms" as [37]:

$$t_N = \frac{N_1}{N_2} = \frac{\text{peak amplitude}}{\text{peak derivative}} = t_{mr} \tag{2.12}$$

where the subscript *N* denotes the calculation of the rise time on a "norm" basis.

2.3 Frequency domain parameters

The frequency domain properties of the waveforms are obtained from the frequency spectrum of the signals. The frequency spectrum can be evaluated by calculating the Laplace transform along the imaginary *j* axis, or by directly calculating the Fourier transform of the time domain waveform. Consider the illustration of the frequency spectrum of a damped sinusoid waveform in Fig. 2.5.

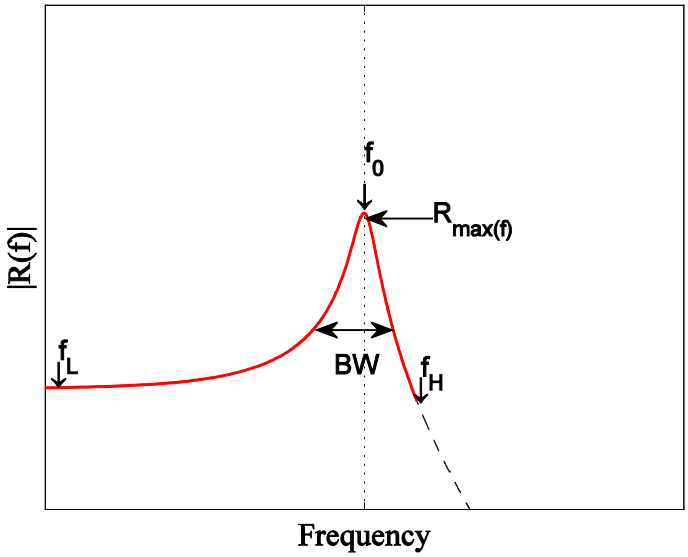

Fig. 2.5 Illustration of the frequency spectrum of a damped sinusoid waveform

a Peak spectral amplitude

The peak spectral amplitude $R_{\max(f)}$ corresponds to the maximum amplitude of the frequency spectrum of the waveform:

$$R_{\max(f)} = \max(|R(f)|) \tag{2.13}$$

b Center frequency

The center frequency f_0 corresponds to the frequency at which $R_{\max(f)}$ is evaluated:

$$f_0 = f\big|_{|R(f)|=R_{\max(f)}} \tag{2.14}$$

For a signal exhibiting several local maxima, a single central frequency cannot be uniquely defined. In this case, the term "resonant frequencies" is used to refer to the points where the local maxima are evaluated.

c Band-ratio

The band-ratio is a fraction that is commonly used to classify the nature of the output of an HPEM generator. The band-ratio of a spectrum is defined as [9, 10, 34]:

$$br = \frac{f_H}{f_L} \tag{2.15}$$

where the low- and high- frequency limits, f_L and f_H are defined as the smallest interval in which 90% of the energy is contained [10, 34]:

$$\inf\left\{(f_H - f_L) : \{f_H, f_L\} \text{ in } A_{0.9}\right\}$$

$$A_{0,9} = \frac{\left\{\int_{f_L}^{f_H} \left|\tilde{R}(f)\right|^2 df\right\}^{\frac{1}{2}}}{\left\{\int_{0}^{\infty} \left|\tilde{R}(f)\right|^2 df\right\}^{\frac{1}{2}}} = 0.9 \tag{2.16}$$

Notice that the frequency domain version of the N_5 norm is used in (2.16) to calculate the frequency interval. For spectra with large DC content, the lowest frequency limit is nominally defined as 1 Hz. This is illustrated in Fig. 2.5, although the 1 Hz value is not explicitly shown in the figure.

The interval between f_L and f_H is sometimes addressed as the 90% energy bandwidth BW_{90}:

$$BW_{90} = f_H - f_L \tag{2.17}$$

d Quality factor

The quality factor of resonant signals has already been defined from the time domain characteristics of the waveform. Conversely the quality factor of a signal can be estimated from its spectral characteristics as [31]:

$$Q = \frac{f_0}{BW_{-3dB}} \tag{2.18}$$

where BW_{-3dB} is the frequency interval bounded by the -3dB frequency limits measured from the center frequency.

3 PROPOSED CLASSIFICATIONS OF IEMI SOURCES

During the past decade or so, the study of IEMI has led to different classification attempts for the fields generated by HPEM sources, also addressed as intentional electromagnetic environments (IEME). Among the first, if not the first, Giri has proposed the classification of IEME according to spectral attributes and to the E-field strength of the generated waveforms [10, 38].

Other classifications have been proposed in the literature based on an evaluation of the likelihood of an IEMI attack in terms of the possibility of physically approaching a source to a target, or the required expertise to operate the source. In general, forecasting the occurrence of an IEMI attack is a very complex task since many subjective criteria are involved. However, some authors (e.g. [18]) have tried to address the possibility of having a given HPEM weapon nearby a target by evaluating the following two factors:

(i) The *availability* of the source: how difficult is to build or acquire a given source?

(ii) The *transportability* of the source: how difficult is it to transport a given source?

The evaluation of each of these factors is subject to the criteria of the EMC expert and the security expert of the facility. However, some guidelines in the classification can be obtained from the available publications.

In this section, we will review the classifications appearing in the literature according to the spectral and amplitude attributes of the IEME, and more subjective concepts like the availability and transportability of the sources.

3.1 Spectral classification

The first attempt to classify HPEM generators was developed by Giri in [38]. The proposed classification was made according to the spectrum of the generated IEME by using both, the percent bandwidth and the band-ratio of the generated signals. As it has been discussed in [9, 10], the use of the percent bandwidth to classify IEME may be inadequate in the context of UWB signals because it comes from a "communications point of view". On the other hand, the band-ratio concept was derived from a physical insight into the generated fields by the already existing HPEM sources at that time. The proposed classification was later standardized by IEC in 2005 [11]. The classification of the IEME according to the band-ratio (see Section 2.3) is presented in Tab. 3.1[9, 10].

Tab. 3.1 Classification of IEME according to the band-ratio

Band type	**Band-ratio (*br*)**
Hypoband	≤ 1.01
Mesoband	$1.010 < br \leq 3$
Sub-hyperband	$3 < br \leq 10$
Hyperband	$br \geq 10$

3.2 E-field strength classification

Another approach for the classification of IEME generated by HPEM sources is to examine the generated E-field at a given distance from the source [10]. The main interest is to predict the possible threat imposed to electronic equipment in proximity of the IEME due to a given HPEM source. There are several publications dealing with the susceptibility of electronic IT equipment (see e.g. [24, 32, 39-43]). A general reference summarizing the different susceptibility studies up to 2004 can be found in [44].

Regarding the possible effects induced by strong radiators on electronic equipment, Giri has proposed a 4-level consequence classification according to the order of magnitude of the generated E-field and the coupling mechanism [41]. The proposed classification is presented in Tab. 3.2. Notice that the front-door/back-door coupling mechanism (see [32] for the definition of the coupling mechanisms) has also an impact on the required amplitudes to produce a certain consequence.

Tab. 3.2 Classification of electromagnetic effects according to E-field strength [41]

Effect	Consequence	Front-door / back-door coupling	Order of magnitude (V/m)
Noise	Harmless	Front door	10^0
False information	Can be critical	Front door	10^1
Transient upset	System may recover	Backdoor	10^2
Permanent damage	Can be critical	Backdoor	10^3

Sabbath has also proposed a classification of the E-fields according to the so-called threat level as reported in Tab. 3.3 [45]. However, there is little information available in the literature about the rationale behind the choice of the amplitudes.

Tab. 3.3 Classification of the E-field strength according to the threat level [45]

Threat level	Description	Amplitude
XL	Extreme low	< 0.1 kV/m
L	Low	0.1-1kV/m
M	Intermediate	1-10kV/m
H	High	10-100kV/m
XH	Extreme high	>100kV/m

3.3 E-field - range classification

Unlike HEMP environments, the IEME produced by HPEM radiators is range-dependent and the amplitude of the expected fields at a given distance will depend on the technology of the source and the antenna. The radiated fields generated by any antenna in the far field region are

inversely proportional to the distance and, therefore, a constant range-normalized E field is expected. The range-normalized radiated E-field of a source is defined as its "far voltage" V_{far} [10]:

$$V_{far} = rE_f \tag{3.1}$$

where r is the range and E_f is the far-field generated by the source.

Although this parameter is commonly addressed in the literature, to the best of the authors' knowledge, no source classification has been proposed according to their far voltages. Three of the highest reported far voltages in the literature are:

(i) JOLT [19, 46]: 5.3 MV

(ii) GIMLI [47]: 1.4 MV

(iii) Prototype IRA [48]: 1.281MV

The generation of HPEM fields typically requires the excitation of a given antenna with a high-voltage pulser. Another parameter of HPEM sources that has been used in the literature to compare their performance is the ratio of the far-voltage to the pulser peak-voltage V_{far}/V_0. It describes the efficiency of the source in transforming an initial pulse into a desired far field.

Notice that this ratio depends on both, the antenna, and the characteristics of the pulser (including the switching speed). For impulse radiating antennas, the far voltage amplitude is related to the derivative of the input pulse and, therefore, the rise-time plays a significant role in obtaining high V_{far}/V_0 ratios.

Three of the highest reported V_{far}/V_0 ratios in the literature are:

(i) Prototype IRA [48]: 10.68 (V_{far}=1281 kV obtained with a ±60kV/100ps pulser)

(ii) JOLT [19, 46]: 5.3 (V_{far}=5.3 MV obtained with a 1MV/180ps pulser)

(iii) IRA II [9]: 4.60 (V_{far}=690kV obtained with a ±75 kV/85ps pulser)

3.4 Source availability

The source *availability* describes its attainability according to the level of sophistication of the underlying technologies. Different categorizations have been proposed in the literature to evaluate this property of the sources.

3.4.1 Giri and Tesche -2004

Giri and Tesche have proposed in [10] the classification of the source technology as:

(i) Low-tech systems: characterized by a marginal performance, minimal technical capabilities, and easily assembled and deployed while hiding behind dielectric walls in trucks and similar vehicles.

(ii) Medium-tech systems: require the skills of a qualified electrical engineer and relatively more sophisticated components such as a commercially available radar system that can be modified to become a weapon system.

(iii) High-tech systems: require specialized and sophisticated technologies and perhaps even specifically tuned to cause severe damage to a specific target.

3.4.2 Sabath and Garbe - 2009

In a more recent publication, Sabath and Garbe used the term technological challenge to describe the knowledge and effort needed to design, assemble and operate a source [17]. They suggest considering the level of sophistication of the underlying technologies, the level of knowledge to design and operate the source, the availability of the components in the market, and the costs to classify the sources as:

(i) Low tech systems

(ii) Medium tech systems

(iii) High tech systems

(iv) Highly sophisticated systems

Unfortunately, there is very little explanation about how to classify a given source into one of the above categories.

3.4.3 ITU -2009

In the same year, the term *availability* was proposed in [18] to measure both the cost and the technological sophistication of a source. The categories proposed by ITU in this document are:

(i) Consumer

(ii) Hobbyist

(iii) Professional

(iv) Bespoke

Again, no clear criteria were provided as to how to classify a source into a given category; but some examples are given.

Among all the criteria that have been proposed in the literature to classify the availability of a source, perhaps the easiest to measure is the cost of a source. Sabath and Garbe have proposed the following reasonable ranges in [17]:

(i) Low cost : less than 1k€

(ii) Moderate cost: between 1k€ and 100 k€

(iii) Medium cost: between 100k€ and 1M€

(iv) High cost: more than 1M€

3.5 Source transportability

Source *transportability* evaluates the requirements in terms of size, weight, and energy supply that determine the level of difficulty with which a source could be physically moved close to a target. As for the *availability*, the categories for evaluating the transportability of a source are subject to the criteria of the experts. However, there are some guidelines in recent publications that could serve as a tool for the classification.

3.5.1 Sabath and Garbe - 2009

The term used to characterize the transportability of a source in [17] is mobility. They have proposed the following categories for its evaluation:

(i) Stationary: the source is part of a fixed installation

(ii) Transportable: a source that can be transported between various locations, but during operation the system has to be stationary at one location.

(iii) Mobile: a source that can be integrated into a mobile platform and can operate during motion of the platform

(iv) Very mobile: a mobile source that has the ability to operate undiscovered in urban environments

(v) Highly mobile: a mobile source that has the ability to operate undiscovered within a building or transportation systems

3.5.2 ITU – 2009

The ITU [18] proposed the term *portability* to describe the *transportability* of the sources. Four portability levels are distinguished:

(i) Pocket size or body worn: applies to threat devices that can be hidden in the human body and/or in the clothing

(ii) Briefcase or backpack-sized: applies to threat devices that are too large to be hidden in the human body and/or in the clothing, but are still small enough to be carried by a person (such as in a briefcase or a backpack)

(iii) Motor-vehicle size: applies to threat devices that are too large to be easily carried by a person, but large enough to be hidden in a typical consumer motor vehicle

(iv) Trailer-sized: applies to threat devices that are too large to be either easily carried by a person or hidden in a typical consumer motor vehicle. Such threat devices require transportation using a commercial/industrial transportation vehicle

4 SELECTED WAVEFORMS CLASSIFICATION

In order to assess potential IEMI sources and the waveforms that they are able to generate, we have collected papers published in peer-reviewed journals, conference papers, standards, conference presentations, online catalogs and brochures, and some books in which possible conducted and radiated sources were reported. The characteristics of all the sources were extracted into a database of waveforms and sources that we can use to identify some trends. The choice of the considered publications was made so that at least some basic characteristics of the sources were mentioned and measured. Of course, the information that can be collected about each source varies according to the kind of publication and, therefore, not all the parameters of the sources could be retrieved.

As potential IEMI sources, we have chosen the published HV sources and HPEM radiators that, due to their transportability and ease of operation, would most easily be deployed against urban or rural facilities. Note that the transportability of the source alone is not an objective criterion since, for example, many of the hyperband radiators are difficult to transport due to the size of the antenna. Similarly, many of the most powerful radiators require a heavy primary source and a pulsed power stage that imply the use of big trucks and are difficult to operate undiscovered. Efforts were made to include as many sources as possible, provided that they can operate without any fixed installation, using primary energy sources that can be operated using batteries or transportable power plants. In many cases, the transportability of the sources could not be evaluated in a straightforward way due to lack of information.

In general, conducted sources offering pulsed outputs in the range of some hundreds of kV with moderate durations (hundreds of ns) are available on the market, and their transportability is only marginally constrained by their size and weight. High-energy sources require the use of bigger capacitors and inductors for storage, which will result in an increase of the weight of the source. The sources that are included in the database are mainly test-sources that are common in EMC laboratories for ESD/lightning/NEMP testing. Note that low voltage sources could also be considered as potential conducted sources, and some examples have been included in the database.

On the other hand, the choice of HPEM radiated sources is more complex since both, the HV pulser and the antenna, have to be considered. As already mentioned, the output antennas of typical hyperband radiators are likely to have big sizes due to the lower-frequency-range radiation requirement (below about 200 MHz). Also, highly sophisticated radiators with increased gains due to the use of reflectors require some stability to ensure the correct focusing of the beams and, therefore, they are less likely to be operated while in movement. The radiated sources that were included in the database were mainly obtained from peer-reviewed journal papers, conference papers, and standards. This reveals that many of the available sources are still in development phase and their commercial fabrication is not very common. We did not consider in our database the HPM radiators [49] (typically present in radars and testing facilities) that require heavy primary power for cooling and feeding the CW outputs.

The collected information has been put into two separate databases containing:

(i) The reported waveform of the source output, its frequency spectrum, and a list of various time-domain and spectral attributes presented in Section 2.

(ii) A collection of the source characteristics including its classification according to the criteria presented in Section 3.

The first database is available in Appendix A in the form of a collection of "wavecards" containing all the above-mentioned information. The steps and operations performed to calculate all the waveform and spectral attributes are briefly presented in Section 4.2.

The second database is available in Appendix B in the form of a spreadsheet. Some of the criteria for classifying the sources are briefly described in Section 4.3.

4.2 The wavecards database

In this subsection, we briefly explain the required steps for the creation of the wavecards included in Appendix A.

4.2.1 Digitizing the source waveform

The first step in the creation of the wavecard is to digitize the reported waveform that is found in the document. To this aim, we used a scanner to digitize the paper based documents and a PDF reader for the documents available in electronic format to obtain an image of the waveform. We used the Engauge digitizer© (free distribution tool) to convert the images into numerical vectors to be processed by the main software. It is important to highlight that digitizing a signal from paper does not ensure that the whole spectral attributes of the signal will be correctly reproduced. Nevertheless, we expect a fair approximation of the real measured signal and its properties.

To illustrate the process, we will use Fig. 4.1 that shows an example of a waveform image and its digitized version after using the Engauge digitizer©. The waveform corresponds to the far voltage of the HPEM source reported in [50].

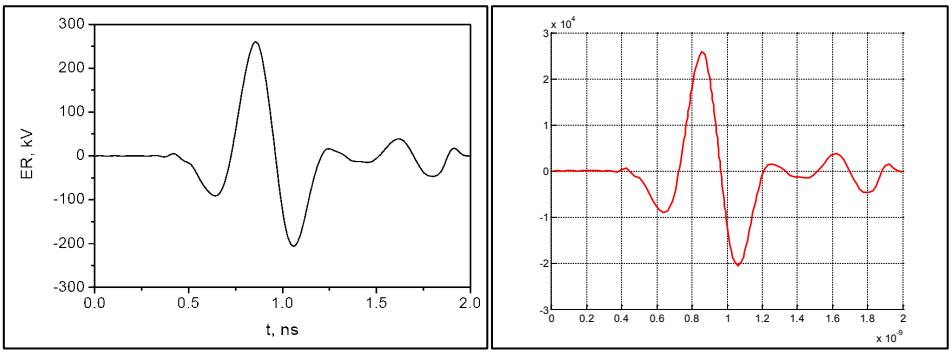

Fig. 4.1 Digitized image (right panel) of the far voltage waveform of the source reported in [50] (left panel)

Since the waveform points provided by the Engauge digitizer© are not sampled with a uniform time step, the whole waveform is interpolated using 1024 points with a uniform time

step. Notice that the selected interpolation sampling rate is independent of the sampling rate of the scope that was used to record the waveform.

It is quite normal that the digitized signals do not vanish to zero in the late times because of the truncation of the original waveform in the document or because of digitizing errors of the program. Therefore, we have decided to window the signals with a quasi-rectangular unitary pulse created using the complementary error function [51]:

$$u_{erfc}(t) = \frac{1}{2}\left(\mathrm{erfc}\left(\frac{t - t_b}{0.55 t_d} \right) - \mathrm{erfc}\left(\frac{t - t_a}{0.55 t_f} \right) \right) \tag{4.1}$$

where t_a-t_b is the FWHM of the pulse, t_d is the 10-90% rise-time of the pulse, and t_f is the 90-10% fall-time of the pulse.

A plot of the erfc window for the case t_d=t_f=*5*, t_a=*90* and t_b=*10* is shown in Fig. 4.2

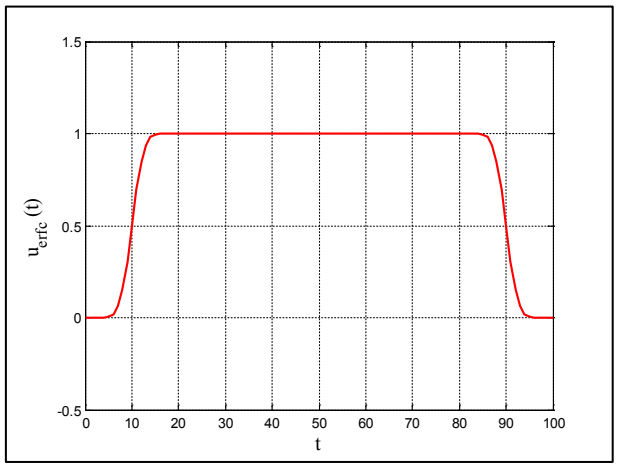

Fig. 4.2 Example of the u_{erfc} function for t_d=t_f=5, t_a=90 and t_b=10.

To carry out the windowing of the selected waveforms, the time constants in (4.1) are chosen so that the early rise of the window does not modify the early time behavior of the digitized signal. On the other hand, the fall time is also chosen so that the windowed signal smoothly converges to zero in the late times. Notice that the use of the erfc function ensures a smooth transition in the rising and falling edges of the window and, therefore, numerical spectral noise due to discontinuities is reduced.

After windowing the digitized signal, zero padding up to 2048 samples is performed in order to increase the resolution of the FFT that is performed in the next step. An example of the windowed version of the waveform in Fig. 4.1 is presented in Fig. 4.3. Note that the effect of the window is unnoticeable and a smooth transition to zero is ensured in the early and late times.

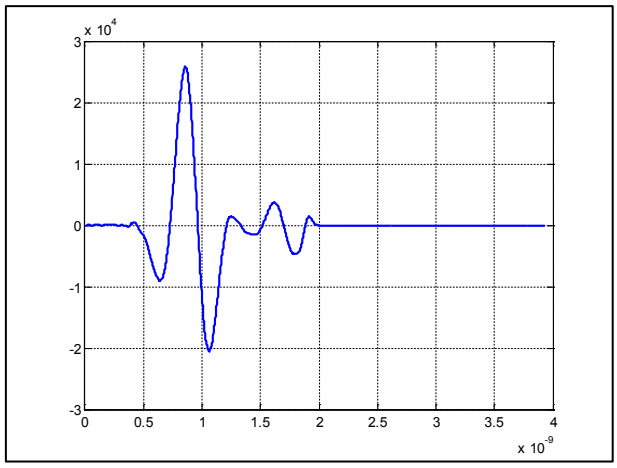

Fig. 4.3 Windowed version of the digitized signal in Fig. 4.1

4.2.2 Estimation of the FFT of the waveform

Once the time domain waveform digitized, the spectrum of the signal was calculated with an FFT. Unless a better frequency resolution was required, the FFT was performed with exactly 2048 samples. The FFT information was used to calculate the following spectral attributes (see Section 2): peak spectral amplitude, center frequency, quality factor, -3dB bandwidth, 90% energy bandwidth, and the band-ratio.

The accuracy of the -3dB bandwidth and, consequently, the quality factor, depend on the frequency resolution of the FFT and, therefore, zero padding can be used to reduce the frequency step. On the other hand, the estimation of the band-ratio of a given signal with by way of equations (2.15)-(2.17) becomes time-consuming if the FFT of the spectrum has to be calculated over a large number of frequency points.

The 90% energy bandwidth BW_{90} is iteratively calculated by testing in all the possible frequency points of the discrete spectrum of the HPEM signature and, for each pair of tested frequency points, an integration procedure has to be performed. Thus, it is desired to compute the BW_{90} from spectra containing a reduced number of points, but containing the necessary amount of information for correctly calculating the limits. Notice that traditional sampling schemes with reduced equidistant linear or logarithmic steps may fail to efficiently represent spectra since resonances may be lost.

4.2.3 Alternative method for the estimation of the Fourier transform of the signal

Due to the previously mentioned issues, an alternative method for estimating the frequency spectrum of the waveforms was used in this work. Consider the approximation of the digitized waveform $r(t)$, as the sum of *m* damped complex sinusoids:

$$r(t) \approx \sum_{i=1}^{m} A_i e^{s_i t} u(t) \qquad (4.2)$$

where the residues A_i and the poles s_i are complex numbers and *u(t)* is the Heaviside function. The damped exponential condition of the basis will ensure the existence of the

Fourier transform of $r(t)$ since the real part of the complex poles is negative and, therefore, the signal must vanish at infinite times, i.e.:

$$s_i = \sigma_i + j\omega_i, \sigma_i < 0 \tag{4.3}$$

The Fourier transform of $r(t)$ can be then approximated as:

$$R(\omega) = \Im(r(t)) \approx \Im(\sum_{i=1}^{m} A_i e^{s_i t} u(t)) = \sum_{i=1}^{m} A_i \Im(e^{s_i t} u(t)) = \sum_{i=1}^{m} \frac{-A_i}{s_i - j\omega} \tag{4.4}$$

Notice that in order to get a good approximation of the original waveform, a sufficient number of poles *m* has to be chosen.

The interest of this method relies in the fact that if the residues and poles of the original waveform can be retrieved, its Fourier transform can be analytically estimated with the use of (4.4) at any desired frequency point, and the algorithms for calculating the band-ratio can be improved since it is no longer required to sample the spectrum with a regular frequency step.

4.2.3.1 Estimation procedure

In order to retrieve the residues and the poles of the signals, we used the matrix-pencil-method (MPM) in [52]. This technique has proven to be very efficient in the extraction of the residues and poles of signals containing noise. To choose the number of *m* poles that correctly reproduce the waveform, the signal is first expanded into an increased number of complex conjugated pole pairs (typically 25 pairs). It is expected that the poles that contribute most to the expansion of the signal are those having the largest residues. Thus, the retrieved poles are sorted according to a decreasing absolute value of their residues. Then, the number of poles *m* is chosen to minimize the normalized mean square error (MSE) between the original signal and the approximated signal with the *m* poles [53]:

$$MSE = \frac{\sqrt{\sum_t |r(t) - r_{rec}(t)|^2}}{\sum_t |r(t)|} \tag{4.5}$$

where $r_{rec}(t)$ is the signal reconstructed using (4.2).

Finally, the Fourier transform is calculated analytically using (4.4) for the desired frequency points.

Fig. 4.4 presents an example of a measured signal and its reconstruction with the MPM. The red signal corresponds to the vertical electric field generated by the EPFL switching oscillator connected to a monopole antenna [13]. The time domain waveforms are presented in the top panel, and the frequency spectra are shown in the lower panel. The waveform in blue was reconstructed by using 26 poles resulting in $\mathrm{MSE} = 2.3 \times 10^{-3}$. The spectrum in red was calculated by using a fast Fourier transform (FFT) of the original waveform and the spectrum in blue from equation (4.4).

Even though the reconstruction of the time domain signal is in very good agreement with the measurement, some differences can be observed in the spectra at low and high frequencies.

The advantage of the analytical spectrum is that, since the reconstructed signal must vanish in the late times, it must give a causal Fourier transform. On the other hand, the spectrum calculated with the FFT may contain truncation errors.

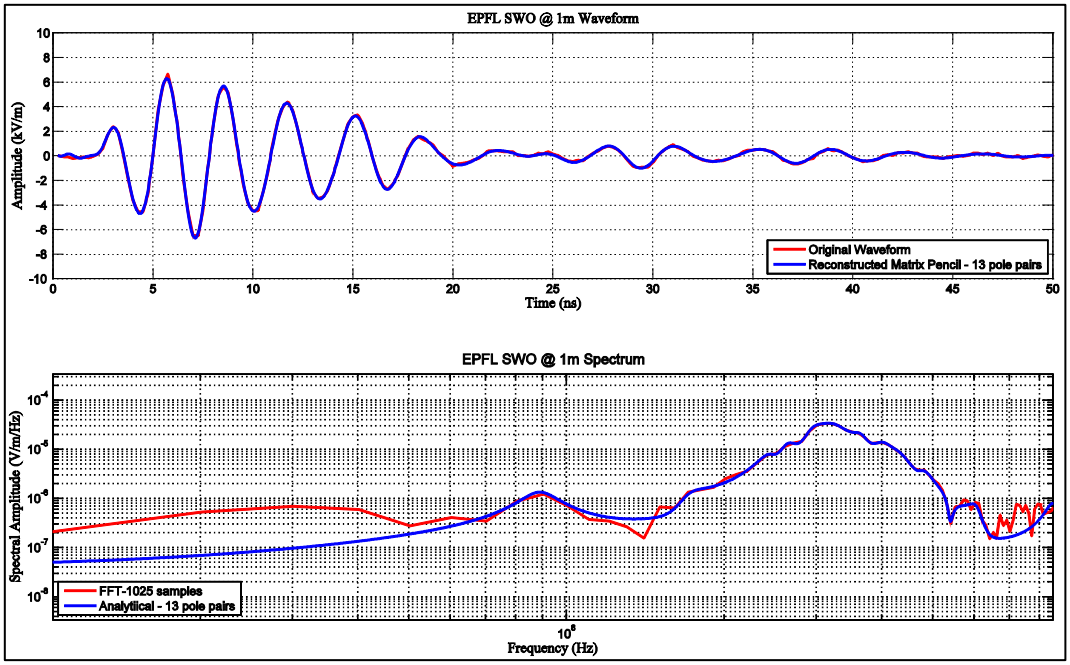

Fig. 4.4 Example of the reconstruction of a measured signal with the MPM and the analytical calculation of its spectrum.

4.2.4 Calculation of the waveform and its spectral attributes

The digitized waveform and its spectrum being available from the FFT or the analytical approach, the following parameters can be straightforwardly calculated with the equations presented in Section 2:

(i) Peak amplitude (N_1)

(ii) Peak derivative (N_2)

(iii) Peak impulse (N_3)

(iv) Rectified total impulse (N_4)

(v) Sq. Root. action integral (N_5)

(vi) Time to peak

(vii) 10-90 rise-time

(viii) Max. rate of rise

(ix) FWHM

(x) Fall time

(xi) Peak spectral amplitude

(xii) Average frequency (Time domain approach)

(xiii) Center frequency (Frequency domain approach)

(xiv) -3dB bandwidth

(xv) Average quality factor (Time domain approach)

(xvi) Quality factor (Frequency domain approach)

The calculation of the band-ratio *br* of the signal defined in Eq. 2.15, and the 90% *Bandwidth* BW_{90} defined in Eq. 2.17, are not straightforward. Both require that the spectrum of the signal be calculated in a limited number of frequency points to bound the algorithm's calculation time and to obtain enough accuracy in the spectrum calculation (no information missing) so that the frequency limits f_l and f_h can be correctly calculated. If the spectrum contains a reduced number of frequencies, but the resonances of the signal and the important concentrations of energy are missing, the band-ratio is not correctly calculated. Thus, a method to evaluate the accuracy of the spectra is needed.

4.2.4.1 Estimation of the band-ratio with the aid of the Blumer Index

The Blumer index can be used to estimate the accuracy of a measured or numerically calculated spectrum [54]. The index serves as a tool to determine if the information contained in a given number of points of a spectrum is good enough to reproduce a causal signal, or if more frequency samples are required. The Blumer index is derived from the Hilbert transform properties of causal signals and it can be calculated as:

$$B = \left\{ 1 - \frac{\sum_{\omega_{\min}}^{\omega_{\max}} \left| \mathrm{Re}\{R(\omega)\} \right|^2 \Delta\omega - \sum_{\omega_{\min}}^{\omega_{\max}} \left| \mathrm{Im}\{R(\omega)\} \right|^2 \Delta\omega}{\sum_{\omega_{\min}}^{\omega_{\max}} \left| \mathrm{Re}\{R(\omega)\} \right|^2 \Delta\omega + \sum_{\omega_{\min}}^{\omega_{\max}} \left| \mathrm{Im}\{R(\omega)\} \right|^2 \Delta\omega} \right\} \times 100\% \qquad (4.6)$$

where $\omega_{\min}$, and $\omega_{\max}$ are the minimum and maximum frequency points in the spectrum, respectively, and $\Delta\omega$ is the frequency step between consecutive frequency points. Notice that for an accurate causal spectrum, the Blumer index is B=100%; since the sum over the real part of the spectrum should be equal to the sum of the imaginary part to satisfy Hilbert transform properties.

To overcome the above-mentioned issues for the estimation of the band-ratio of the studied waveforms, we have used an adaptive non-uniform sampling scheme proposed in [54]. In this scheme, in the vicinity of spectral peaks, a large number of data points are sampled. On the other hand, at frequencies where the spectrum changes less rapidly, a lower sampling rate is used. To test the accuracy of the discrete spectral representation of the selected waveform, the Blumer index of the spectrum is evaluated. If the index is below a user-defined threshold (usually around 98-100%), the spectrum is sampled again with an iterative scheme until the threshold is reached. This procedure reduces the errors arising from the under-sampling of the spectrum, and/or from truncation the spectrum at the upper and lower frequency limits. As a consequence, the calculation time of the band-ratio is significantly reduced because fewer

frequency points need to be tested. Further details in the iterative selection of the frequency points can be found in [54].

To illustrate the use of the adaptive scheme, the Blumer index, and its influence in the estimation of the band-ratio of a signal, we have calculated the spectrum of the waveform presented in Fig. 4.4 by using the traditional FFT, and the analytical expression in (4.4) with three different (and reduced) numbers of frequency samples: 10, 33, and 106 (see Fig. 4.5). The samples were obtained iteratively with the adaptive scheme with the following Blumer index thresholds: 77%, 97% and 99%, respectively.

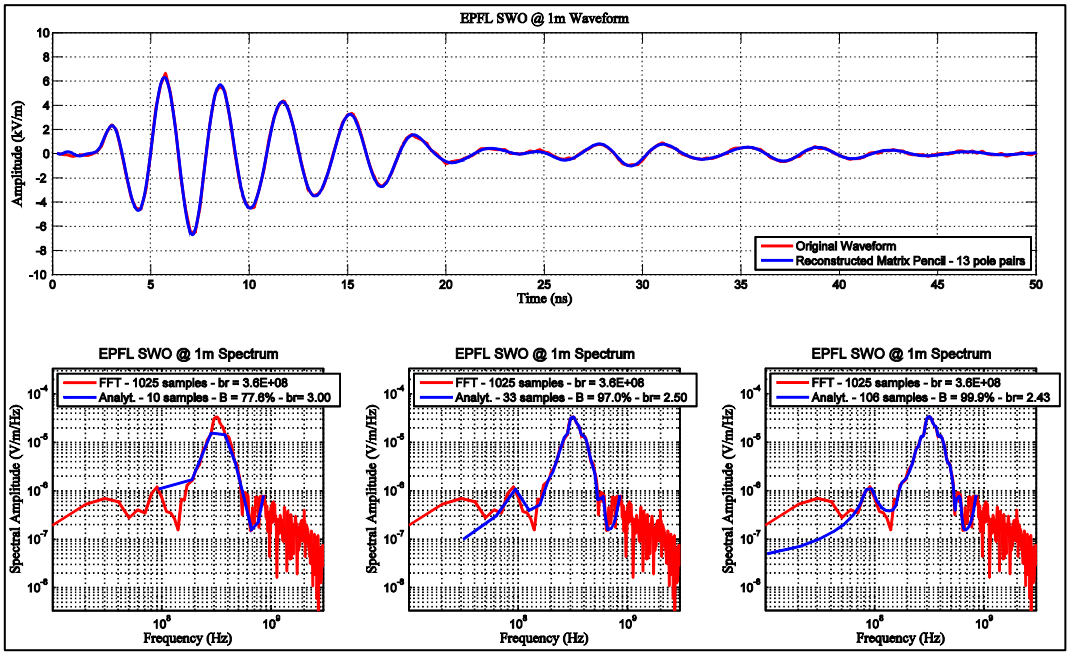

Fig. 4.5 Illustration of the use of the Blumer Index in the calculation of the band-ratio.

A summary of the band-ratio results obtained with the FFT and the proposed scheme using the Blumer index is reported in Tab. 4.1.

Tab. 4.1 Comparison of the band-ratio results obtained with the FFT and the analytical-Blumer index approach

Scheme	Number of samples	Blumer index	Band-ratio
FFT	1025	N/A	3.6×10^8
Analytical – Blumer	10	77.6%	3.00
Analytical – Blumer	33	97%	2.50
Analytical – Blumer	106	99%	2.43

Given the damped oscillatory behavior of the waveform, a reduced band-ratio is expected (mesoband or sub-hyperband signal). Notice that the band-ratio and the resulting BW_{90} estimated from the spectrum obtained with the FFT are not correctly calculated since the frequency-sampling scheme of the FFT is linear and, therefore, very large frequency steps are

obtained. Also, some important resonances could be missed. In order to reduce the frequency step size, zero padding could be used, but also the number of samples of the FFT would be increased, leading to an increase in the calculation time of the band-ratio.

On the other hand, with the adaptive scheme, the band-ratio is estimated by using non-equidistant frequencies that are chosen as the frequencies where the majority of the energy is concentrated. The obtained band-ratios with the adaptive scheme correspond to a mesoband signal, as expected. Notice that the adaptive scheme already provides a Blumer index of 97% with about 33 samples, and 99% with 106 samples and, therefore the algorithm for estimating the band-ratio requires much less time than with an FFT.

4.2.5 Example of a wavecard

Finally, once the parameters have been calculated, the wavecard is generated. An example showing the wavecard of the source in [50] is presented in Fig. 4.6. Notice that additional information such as the name, the year of publication, and the band type have been also added to the contents of the wavecard.

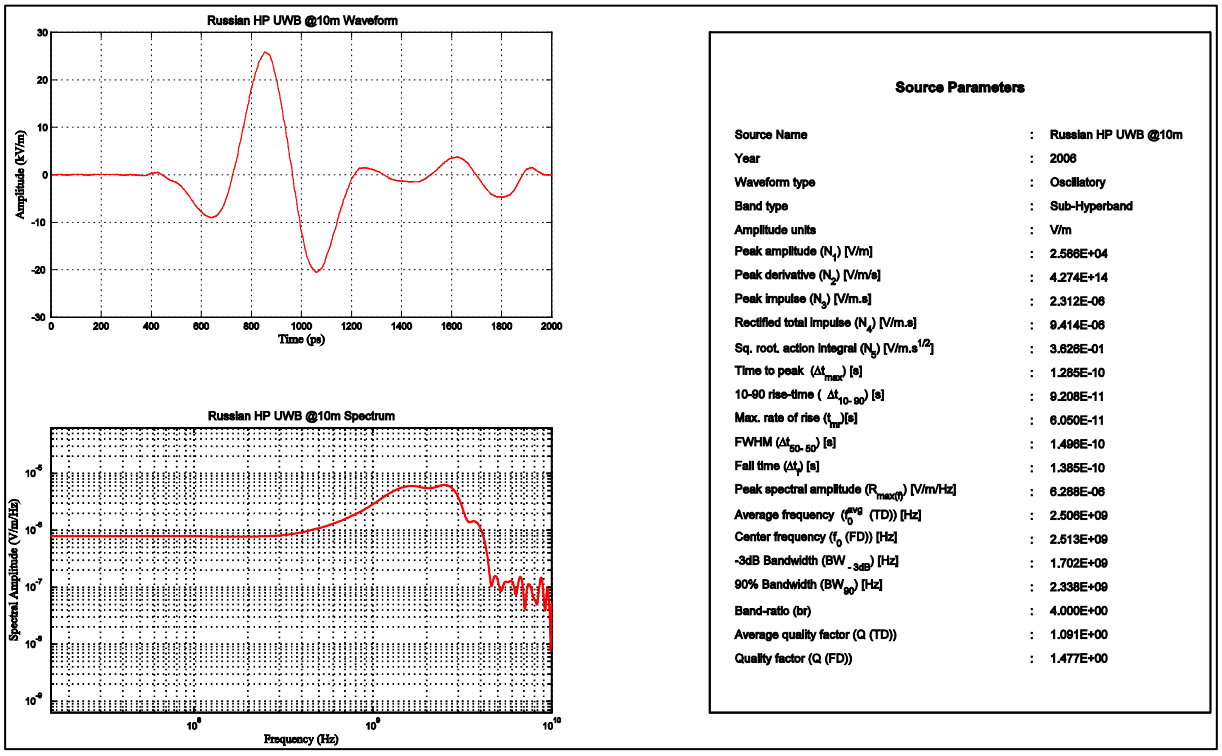

Fig. 4.6 Example of the wavecard of the source reported in [50]

4.3 The potential IEMI sources database

The second database generated with the survey is a spreadsheet containing a collection of all the identified potential conducted and radiated sources and their relevant characteristics/ attributes.

The following characteristics were included in the conducted source collection:

(i) *Year:* the year of the source construction (if available) or the publication year of the document that reports the source (for the first time).

(ii) *Source Name:* the name that was used to identify the source in the database

(iii) *Peak Voltage (kV):* the maximum voltage in kV that can be generated by the source

(iv) *PRF (Hz):* the pulse repetition frequency of the source in Hz, as explained in Eq. 2.10.

(v) Average/center frequency: the average frequency of the source (only for mesoband or CW sources, or sub-hyperband sources with a very low band ratio).

(vi) Band type: the band-type of the source according to its band-ratio, as it was explained in Tab 3.1 if the waveform is available. Else, the band-type is inferred according to the information available from the publication.

(vii) Technology Level: the classification of the source according to the technological sophistication criteria proposed by Giri and Tesche in [10] and reviewed in Section 3.4 of this note.

(viii) Cost Level: the classification of the source according to its cost as proposed by Sabath and Garbe in [17] and reviewed in Section 3.4 of this note.

(ix) Portability level: the classification of the source according to its portability level as proposed by the ITU in [18] and reviewed in Section 3.5 of this note.

(x) Reference: the reference from which the information about the source has been obtained.

(xi) Wavecard: the name of the wavecard associated to the source (if available in Appendix A).

And the following characteristics for the radiated source collection:

(i) *Year:* the year of the source construction (if available) or the publication year of the document that reports the source (for the first time).

(ii) *Source Name:* the name that was used to identify the source in the database

(iii) *Peak Field (kV/m):* the reported peak electric field in kV/m generated by the source at a given distance

(iv) *Test distance (m):* the distance in m at which the peak electric field has been measured

(v) Far Voltage (kV): the far-field generated by the source as explained in Section 3.3 of this note.

(vi) Vpeak (pulser) (kV): the peak voltage in kV generated by the source's main pulser

(vii) *rEp/Vp*: the far-voltage/pulser-peak-voltage ratio as explained in Section 3.3 of this note.

(viii) rise-time $_{10\text{-}90}$ (ps): the 10-90 rise time of the source in ps obtained from the wavecard (if available). Else, the rise-time is inferred from the information available in the publication.

(ix) *PRF (Hz):* the pulse repetition frequency of the source in Hz, as explained in Eq. 2.10.

(x) *Min frequency (MHz):* the minimum frequency of the source in MHz (only for mesoband or CW sources, or sub-hyperband sources with a very low band ratio).

(xi) Average/center frequency (MHz): the average/center frequency of the source in MHz (only for mesoband or CW sources, or sub-hyperband sources with a very low band ratio).

(xii) Max frequency (MHz): the maximum frequency of the source in MHz (only for mesoband or CW sources, or sub-hyperband sources with a very low band-ratio).

(xiii) Band type: the band-type of the source according to its band-ratio, as it was explained in Tab 3.1 if the waveform is available. Else, the band-type is inferred according to the information available from the publication.

(xiv) Technology Level: the classification of the source according to the technological sophistication criteria proposed by Giri and Tesche in [10] and reviewed in Section 3.4 of this note.

(xv) Cost Level: the classification of the source according to its cost as proposed by Sabath and Garbe in [17] and reviewed in Section 3.4 of this note.

(xvi) Portability level: the classification of the source according to its portability level as proposed by the ITU in [18] and reviewed in Section 3.5 of this note.

(xvii) Primary source DC voltage: the DC charging voltage of the Marx generator of the primary source of the pulser.

(xviii) Pulser: brief description of the source pulser

(xix) Output antenna: brief description of the source antenna

(xx) Reference: the reference from which the information about the source has been obtained.

(xxi) Wavecard: the name of the wavecard associated to the source (if available in Appendix A).

5 ANALYSIS OF THE POTENTIAL IEMI SOURCES CHARACTERISTICS

The information gathered in the databases has been analyzed to identify possible trends or common factors that could lead to a better understanding of the expected characteristics of IEMI sources. In this section, we present our findings in the form of pie charts and bar plots from which general trends can be identified, providing insight into the potential risk of IEMI sources.

In the first part, we deal with the information collected from conducted sources, and in the second part the information collected from radiated sources.

5.1 Conducted Sources

In general, the technologies required to produce portable HV sources have seen significant progress in the last 50 years or so, and it is quite difficult to identify trends since there are little constraints for their customized fabrication. However, the cost of test sources remains moderate, perhaps because they are still used only for research and development purposes.

5.1.1 Portability level

A percentage pie chart illustrating the portability level of the 21 conducted sources in the database is presented in Fig. 5.1. As it can be appreciated, almost all the sources can be transported in a briefcase, which implies that they can be operated undiscovered.

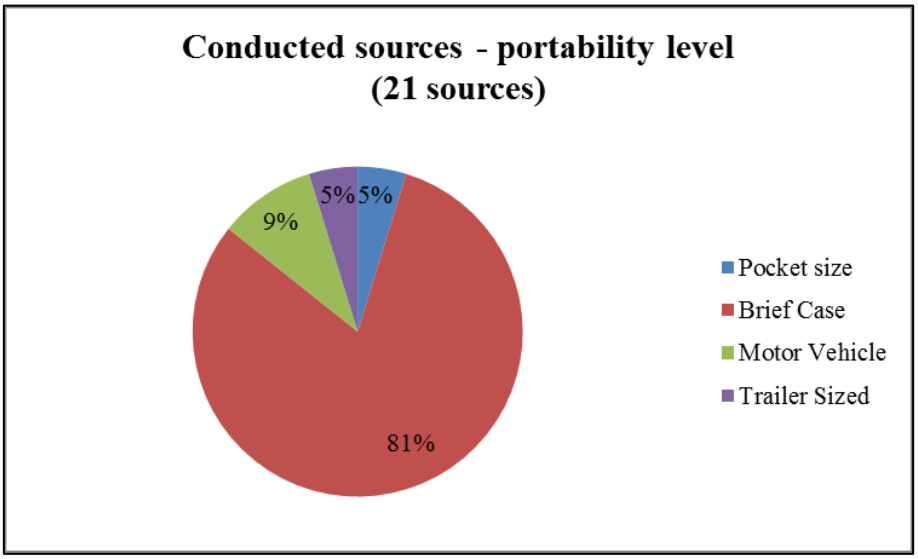

Fig. 5.1 Portability level of the conducted sources

5.1.2 Techonology level

A percentage pie chart illustrating the technology level of the 21 conducted sources in the database is presented in Fig. 5.2. About half of the reported sources require high technology development for their fabrication, suggesting that half of the devices are used for very specific research and development purposes and, therefore, their availability is limited. The other sources belonging to the medium-tech and low-tech category are more likely to be purchased from a commercial producer.

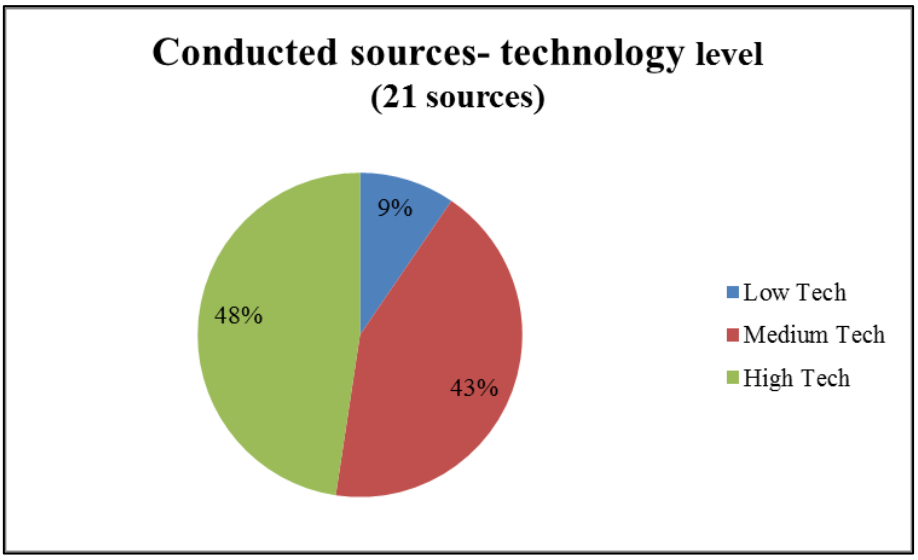

Fig. 5.2 Technology level of the conducted sources

5.1.3 Cost level

A percentage pie chart illustrating the cost level of the 21 conducted sources in the database is presented in Fig. 5.3. As expected from the previous analyses, the majority (81%) of the sources can be purchased or fabricated at a moderate cost. This could be understood as a consequence of the maturity of the required technologies and availability of the primary components.

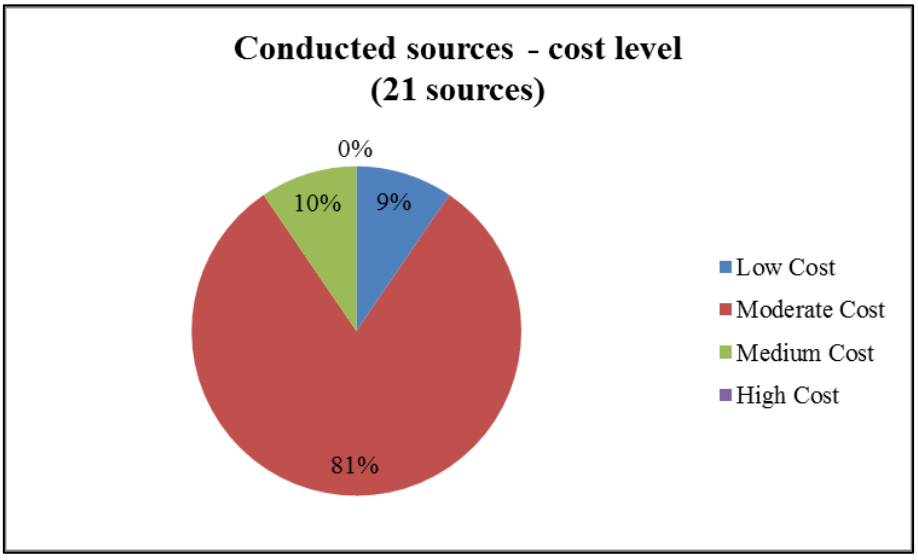

Fig. 5.3 Cost level of the conducted sources

5.1.4 Portability level vs. technology level

The portability level of the 21 sources is plotted against their technology level in the bar plot of Fig. 5.4. It can be seen that the technological level does not restrict the portability of the sources. About half of the sources that fit inside a briefcase are high-tech sources, and the

other half are mainly moderate-tech and only one is low tech. Only one of the studied sources fits inside a pocket and uses low-tech technology.

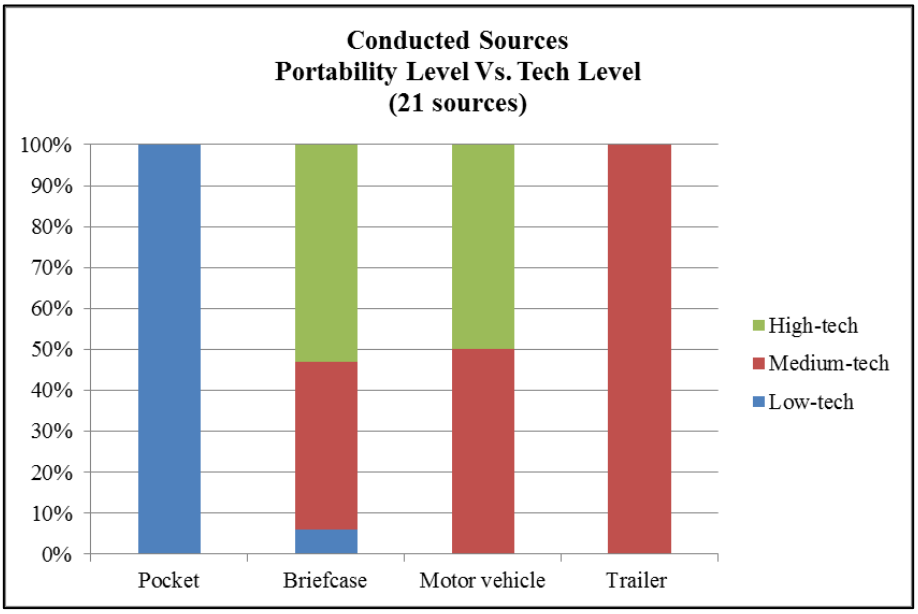

Fig. 5.4 Portability level vs. technology level of the conducted sources

5.1.5 Portability level vs. cost level

The portability level of the 21 sources is plotted against their cost level in the bar plot of Fig. 5.5. Surprisingly, the most portable sources are those exhibiting a low or moderate cost. This can be explained, at least in part, by the fact that the cost is related to the required energy storage capacity of the source, which in turn is related to its transportability level. This implies that conducted sources could be very available for a malefactor.

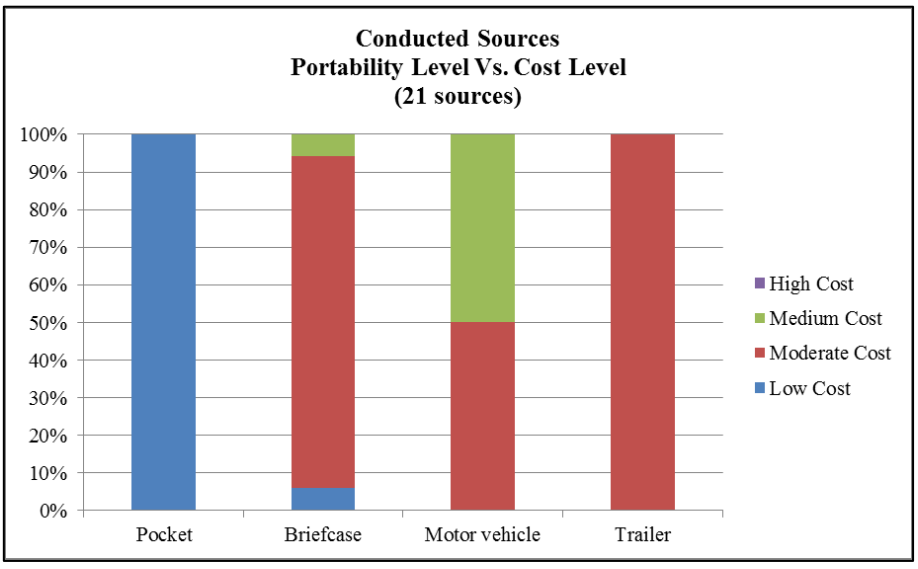

Fig. 5.5 Portability level vs. cost level of the conducted sources

5.1.6 Portability level vs. peak voltage

The portability level of the 21 sources is plotted against their peak voltage in the bar plot of Fig. 5.6. For an IEMI scenario, conducted voltage levels exceeding some kV are not likely to propagate efficiently due to insulation breakdown inside the cables. This is why we have chosen to classify in a single voltage level the sources above 10 kV. According to the bar plot, it is concluded that sources producing peak voltages below 10 kV (the sources labeled "more than 10 kV" are of course included since they can be operated at voltages lower than their maximum rating) are available at any portability level. The main factor leading to less portability is perhaps the increase of the energy storage requirement of the source. Interestingly, the percentage of pocket-sized sources with peak voltage level lower than 1 kV is negligible in the studied dataset.

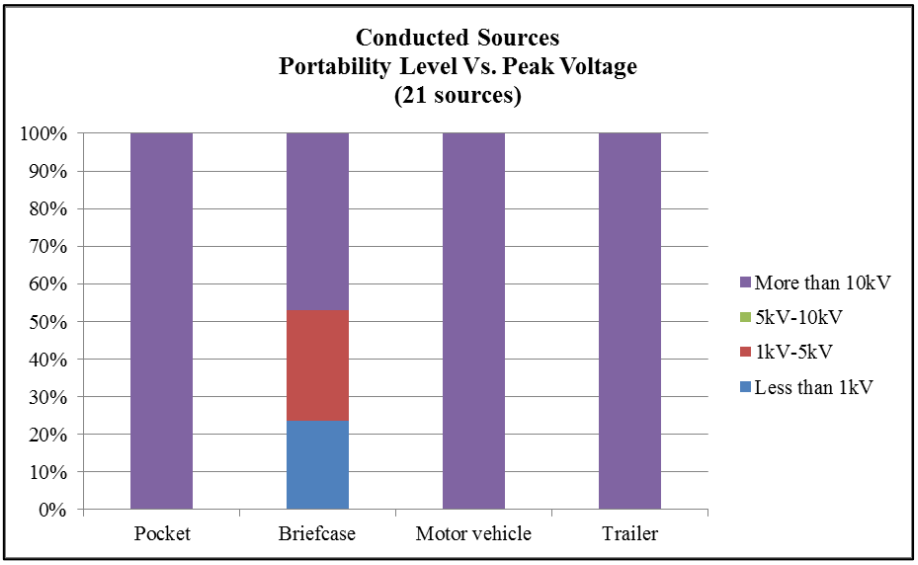

Fig. 5.6 Portability level vs. peak voltage of the conducted sources

5.2 Radiated Sources

The radiated sources that were studied were mainly published in scientific journals, and there are a few sources that can be purchased from a commercial provider. This implies that these sources still have a limited availability, perhaps due to the technological effort and test equipment required to produce them. However, due to the possibility of producing elevated fields with such sources, they constitute a major threat, particularly since many of them can be easily transported. More insight about the source characteristics can be found in what follows.

5.2.1 Portability level

A percentage pie chart illustrating the portability level of 54 of the 55 radiated sources in the database is presented in Fig. 5.7. Notice that there is one source for which the portability level could not be inferred from the available information. According to the chart, the majority of the reported sources require a vehicle or a trailer to be transported. This is due certainly to the size of the antenna and to the weight of the primary pulser. Notice that the classification of the transportability does not consider the possibility of operating the source inside the vehicle.

Thus, the question of operating it undiscovered remains open. Only a few (18%) can be transported in a briefcase, and there are no pocket sized sources reported in the literature.

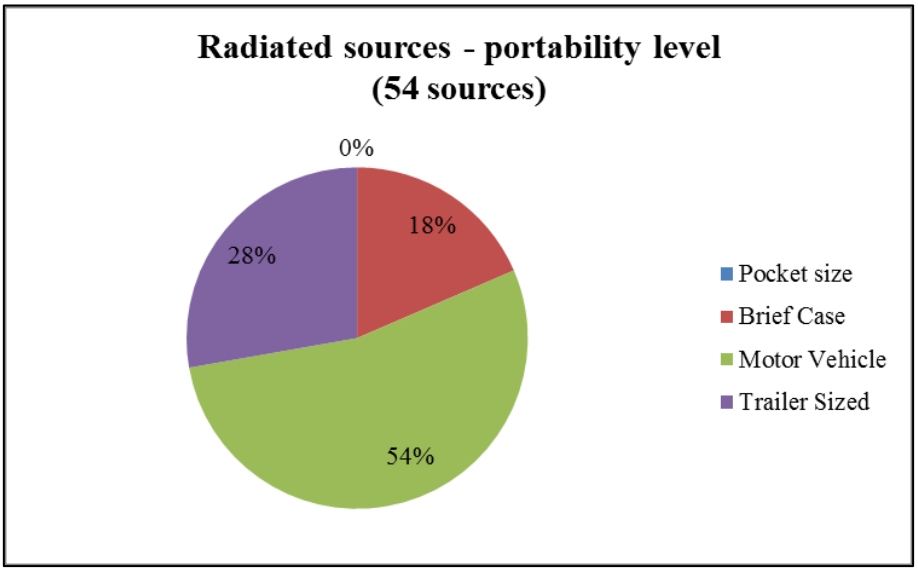

Fig. 5.7 Portability level of the radiated sources

5.2.2 Technology level

A percentage pie chart illustrating the technology level of the 55 radiated sources in the database is presented in Fig. 5.8. This figure illustrates the fact that the radiated sources are still under development and, therefore, the required technical effort is high and the availability of the required components is limited.

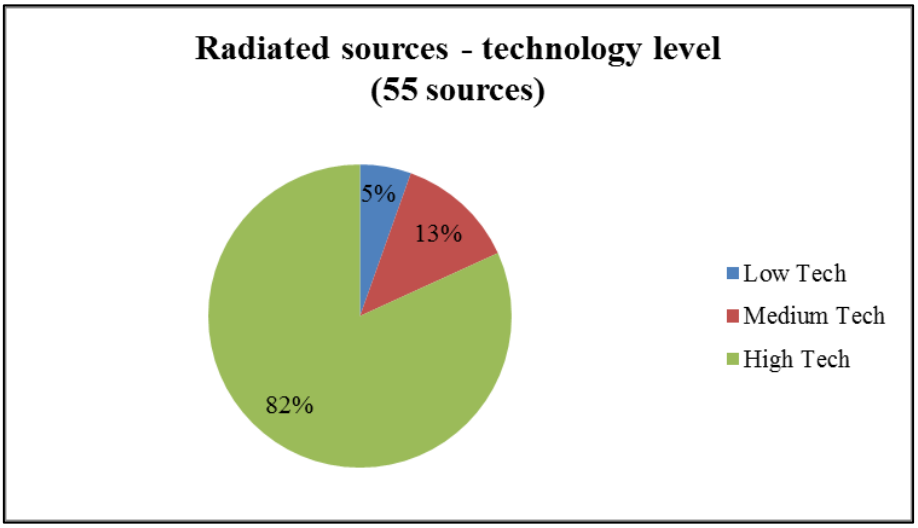

Fig. 5.8 Technology level of the radiated sources

5.2.3 Cost level

A percentage pie chart illustrating the cost level of the 55 radiated sources in the database is presented in Fig. 5.9. The majority of the sources are classified as having medium and high cost. As expected, the cost level reflects the high sophistication of some of the devices and the

limited availability of the components. However, 24% of the sources can be obtained at a moderate cost, which implies that there are some already mature tools that are available on the market.

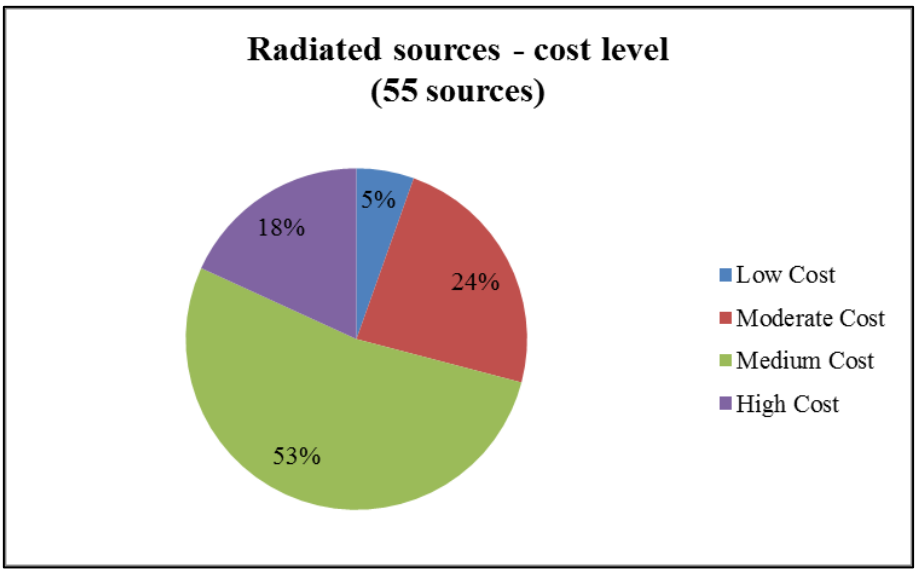

Fig. 5.9 Cost level of the radiated sources

5.2.4 Far voltage

A percentage pie chart illustrating the far voltage of 35 of the 55 radiated sources in the database is presented in Fig. 5.10. Notice that there are 20 sources for which the far voltage could not be obtained from the available information. We have chosen the far voltage categories by following the considerations of the threat levels proposed in Tab. 3.2 and Tab. 3.3. According to the classification, the large majority (about 83%) of the sources produce far voltages between 10 and 1000 kV, which at a distance of 10 m would produce fields in the range of 1-100 kV/m. These levels are high enough to induce false information or transient upset in some systems and, in some cases, permanent damage. Sources producing lower levels may not imply a risk against electronics, but they remain useful for laboratory testing. A very reduced number of sources (3 sources) produce more than 1 MV of far voltage. These sources can be regarded as the most dangerous among the sources for which their far voltage is available in the literature.

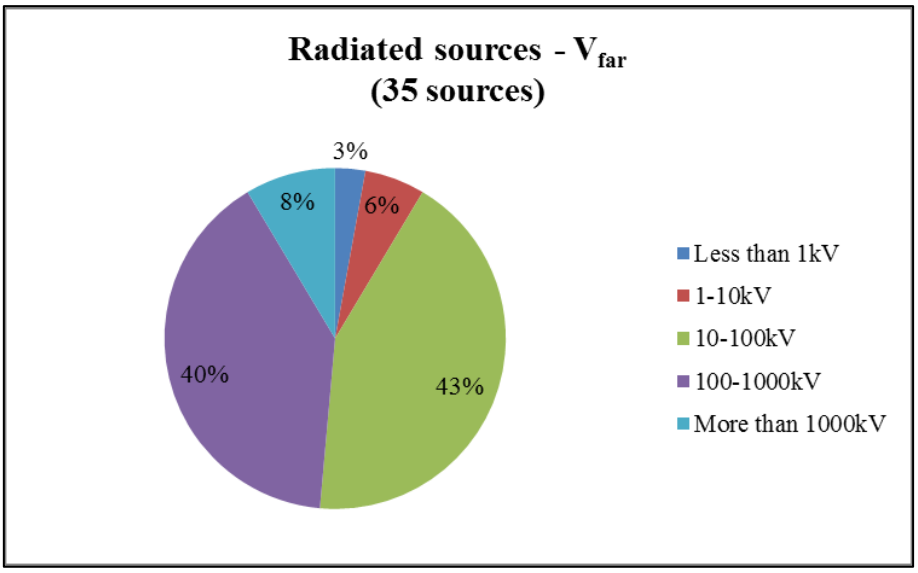

Fig. 5.10 Far voltage of the radiated sources

5.2.5 V_{far}/V_p ratio

A percentage pie chart illustrating the ratio of the far voltage to the peak pulser voltage V_{far}/V_p for 35 of the 55 radiated sources in the database is presented in Fig. 5.11. As mentioned in 5.2.4, there are 20 sources for which the far voltage could not be obtained from the available information. The majority of the sources exhibit a ratio between 0 and 2, which gives an idea of the average conversion efficiencies available. Very few have a ratio above 5 which appears to be the conversion limit with the present technologies.

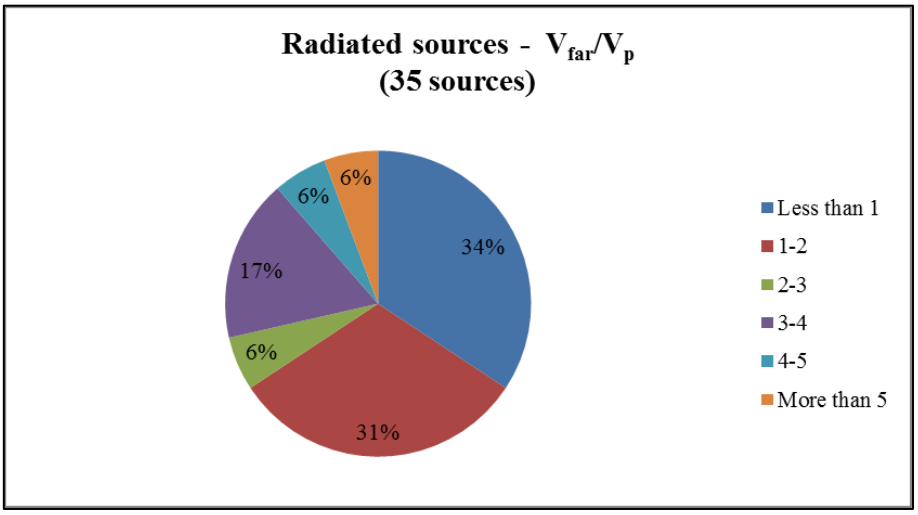

Fig. 5.11 Far voltage/ peak pulser voltage ratio of the radiated sources

5.2.6 Portability level vs. technology level

The portability level of 54 of the 55 sources is plotted against their technology level in the bar plot of Fig. 5.12. As mentioned in 5.2.1, there is one source for which the portability level could not be inferred from the available information. The main conclusions that can be drawn from the plot can be summarized as follows: 1) Regardless of their technology level, none of

the sources in the database can be classified into the pocket transportability level. 2) There exist low and high-tech sources that can be transported in a briefcase, motor vehicle or a trailer. 3) Only sources considered Medium-tech require at least a motor vehicle to be transported. Interestingly, high-tech sources are present at all portability levels (except in the pocket availability level).

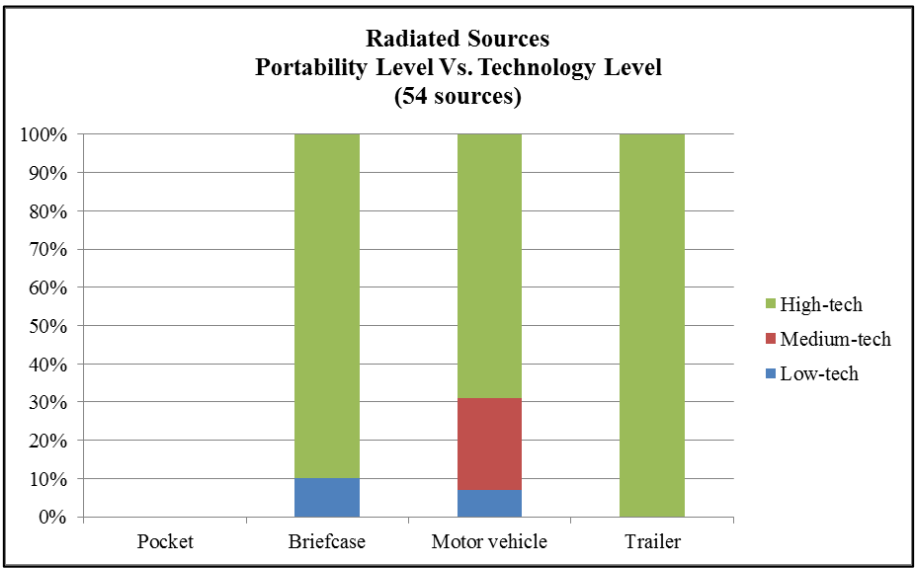

Fig. 5.12 Portability level vs. technology level of the radiated sources

5.2.7 Portability level vs. cost level

The portability level of 54 of the 55 sources is plotted against their cost level in the bar plot of Fig. 5.13. As mentioned in 5.2.1, the portability level of one of the sources could not be inferred from the available information. A similar picture to that of the comparison between portability and technology level is shown in Fig. 5.13. It can be seen from this figure that the cost of the source is likely to be in the medium cost category at any transportability level. However, notice that while only about 10% of the moderate cost sources fall in the briefcase transportability bin, this percentage climbs to almost 50% for the motor vehicle sized sources. This implies that, from an availability point of view, sources are more likely to be transported in vehicles since they may exhibit a lower cost.

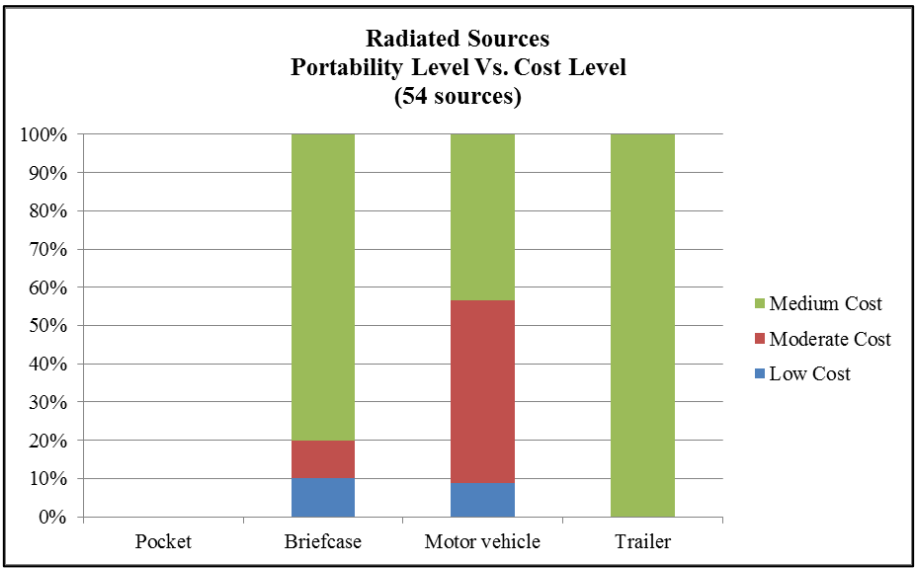

Fig. 5.13 Portability level vs. cost level of the radiated sources

5.2.8 Portability level vs. far voltage

The portability level of 35 of the 55 sources is plotted against their far voltage in the bar plot of Fig. 5.14. Notice again that, as in 5.2.4, there are 20 sources for which the far voltage could not be obtained from the available information. From the bar plot, it can be observed that considerable far voltage levels (up to 1000 kV) can already be generated with sources fitting into suitcases. This implies a high threat level for malefactors with the available resources to acquire such a source. In general, all the far voltage levels are also available at motor vehicle sized and trailer sized sources.

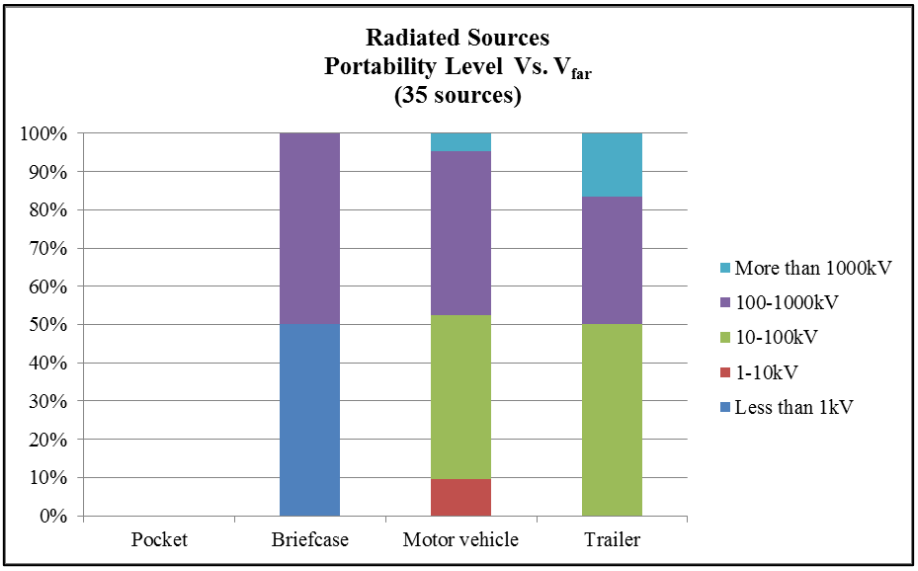

Fig. 5.14 Portability level vs. far voltage of the radiated sources

5.2.9 Band-type

We have tried to address the band-type of the sources in order to identify possible trends in their fabrication. A percentage pie chart illustrating the band-type of 52 of the 55 radiated sources in the database is presented in Fig. 5.15. Notice here that there are 3 sources for which the band-type could not be inferred from the available information. According to the chart, similar numbers were found for mesoband, sub-hyperband and hyperband sources. Thus, it appears that from a band-type point of view, there is not a preferential kind of source.

As expected, there are a few CW sources since many of the HPM sources were not included due to the transportability and operability issues explained in Section 4. Many of the consulted references that included the use of LPM or HPM tubes were presented fixed installations and, therefore, they were not considered in the database.

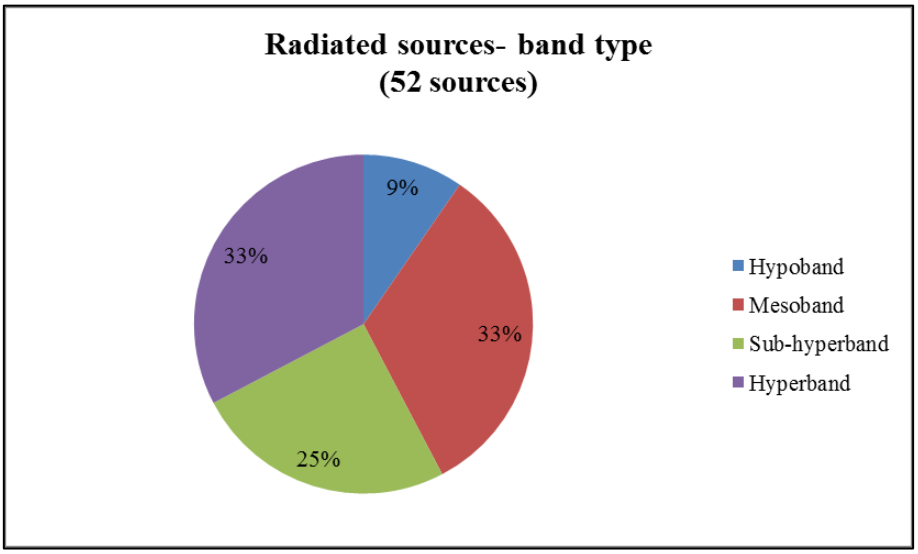

Fig. 5.15 Band-type of the radiated sources

5.2.10 Year

In order to get an insight into the research and development activities performed in this area, we have assessed the number of sources vs. the publication year. A bar plot illustrating the publication year of the 55 radiated sources in the database is presented in Fig. 5.16. It can be observed that there were only a handful of publications about this subject before 1995, and a few in the period ranging from 1995 to 2000. An increased activity occurred in 2000-2010, with about the same number of publications in the first 5 years of this period as in the second 5-year period. In the three-year period from 2010-2013, there is about the same number of publications than that corresponding to 2005-2010, suggesting an increase of the research and development interest.

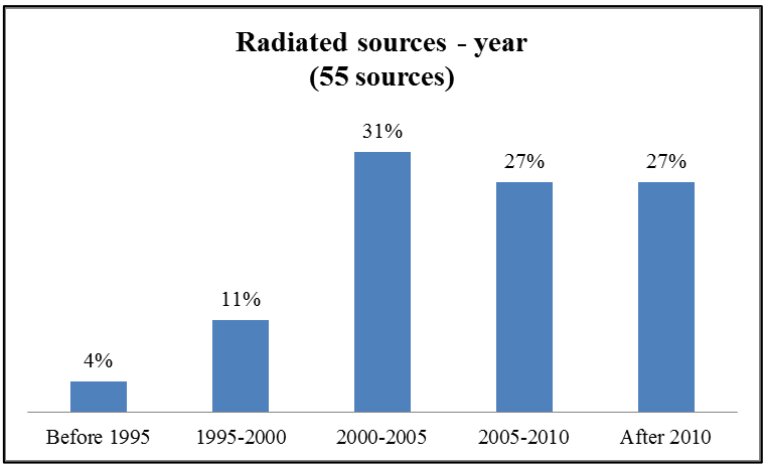

Fig. 5.16 Publication year of the radiated sources

5.2.11 Year vs. band-type

Finally, we have assessed the band-type vs. the publication year to see if there is an increased interest through time for a specific kind of source. The publication year of 52 of the 55 sources is plotted against their band-type in the bar plot of Fig. 5.17. Notice that there are 3 sources for which the band-type could not be inferred from the available information. The bar plot shows a trend to produce hyperband radiators before 2000. Mesoband sources appear in 2000 and, since 2010, there the majority of the reported sources belong to this category. Notice that from the waveform analysis, it was found that some of the oscillating sources exhibited a very low band-ratio between 3 and 4. Thus, part of the sub-hyperband sources between 2005 -2010 could be added to the mesoband sources due to their approximated behaviors. Finally, as it was mentioned before, there has been considerable development on hypoband sources during the last decades or so; however, due to their increased power and low transportability, very few were considered in the database and they have not appeared in the literature since 2010.

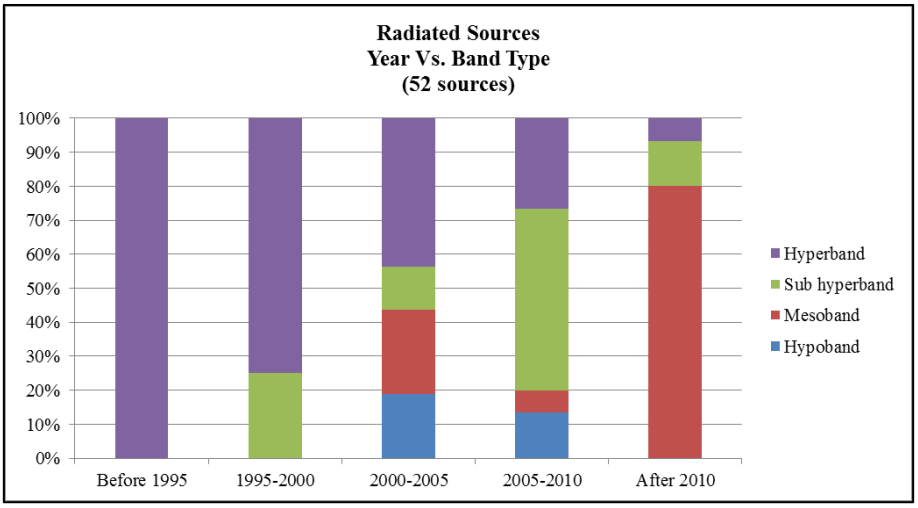

Fig. 5.17 Publication year vs. bandtype of the radiated sources

6 OVERVIEW OF THE EXPECTED LIMITS OF POTENTIAL IEMI SOURCES AND THEIR CURRENT TECHNOLOGIES

Having studied the trends based on the collected information on sources, we have tried to understand the types of threats that can be achievable with today's technologies and markets. These trends would certainly be modified as soon as the transportability of the sources increases or the costs are reduced due to technological improvement or market growth. We have explained the interest in generating intense fields in the range between some hundreds of MHz and some GHz due to the expected sizes of handmade electronic equipment and the so-called Baum's law [7]. However, radiated IEMI could also be generated at higher frequencies (perhaps with less impact on electronics) or at higher field levels.

The generation of HPEM fields is fundamentally limited by physical constraints (proper to the current technologies) that we will briefly overview in this section. When thinking about the feasibility of potential IEMI sources, the most important constraint is perhaps the physical limitation rather than the current technological limitation. However, it is quite difficult to think about the first one without the other one.

There are many schemes for generating HPEM fields. A block diagram describing a simple HPEM generation scheme is presented in Fig. 6.1.

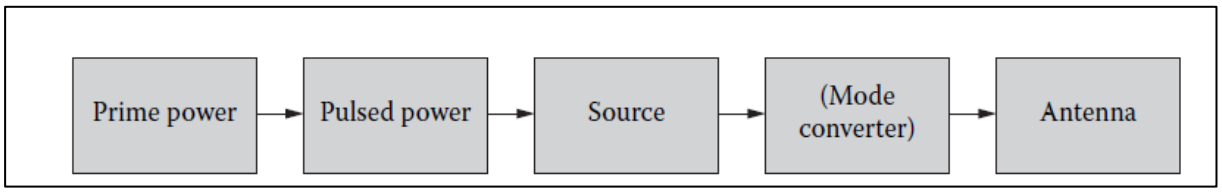

Fig. 6.1 HPEM fields generation scheme. Image adapted from [49].

One of the most common setups starts from a primary DC source that charges a capacitor bank, which in turn feeds a Marx or an inductive generator constituting the so-called primary source. The output of the primary source is injected into subsequent pulse-forming stages in which the rise time is reduced and the desired pulsed power waveform is obtained. At this point, depending on the application, the pulsed power stage can feed a microwave cavity, an HPM tube, or some form of peaking switch whose output is mode-converted and connected to an output antenna. For a conducted source, the output is directly connected to the target, or to a suitable inductive or capacitive probe that will couple to the target.

6.1 Technological limits

The electric field flowing in each of the stages of the HPEM generation chain is limited by the so-called gas breakdown limit for short pulses (roughly less than 1μs). For longer pulses, the key issue is the wall heating (see e.g. page 124 of [49]). The amplitude of the electric field inside the generation chain will depend on the waveguide geometry and the primary excitation signal. When the total field propagating along a gas-filled medium is raised beyond the breakdown limit, a plasma channel is created that is able to sustain a high current value and a conduction current in the gas will short down the original field. In general, a spark develops when the accelerated electrons (due to the high intensity electric field) are capable of

producing large electron avalanches. If this wave is intensive enough, the current in the intensified channel increases, becoming unstable until the total breakdown occurs [55].

The breakdown field of air and other types of gases have been extensively studied for switching applications [56-59] and for HPM generation [60]. For air at standard temperature and pressure (STP) conditions immersed in a uniform field configuration (e.g. DC field in a parallel plate arrangement), the breakdown field is roughly 3MV/m. The study of breakdown under slowly changing non-uniform field conditions is much more complex and its analysis has to be worked out separately for each gas pressure and field configuration. There are some analytical formulas in the literature that provide the breakdown field between canonical sets of electrodes (e.g. spheres, cylinders, cylinder-plates, etc.) for different gases with a fair agreement with experiments [57, 61].

Breakdown data for various gases show higher breakdown fields for shorter duration pulses. For instance, the breakdown of air at one atmosphere pressure is a factor of 2.3 higher for a 10-ns pulse than for DC [57]. In general, the 3MV/m breakdown threshold for uniform field configurations is typically used in HPEM antenna design with a safety margin of 3 (i.e. 1MV/m at the antenna output) to account for possible enhancement points that may lead to gas breakdown [37]. If higher field values are needed, antennas are usually insulated in SF6 [16, 46] which breaks down at about 9MV/m and exhibits a similar propagation constant as air.

6.1.1 Hyperband radiators

The far electric field of hyperband HPEM radiators having aperture antennas as an output (e.g. a HIRA [9]) is governed by the slew rate of the driving voltage and the size of the aperture. The difficulty in building high voltage transient pulsers generating hundreds of kV with rise times in the order of hundreds of picoseconds constitutes a technological limitation for the generation of such signals. High performance peaking gaps tolerate pressures up to about 100 atm and withstand E fields in the range of MV/cm. It is believed that the maximum derivative that could be expected from a gas switch is in the order of the 10^{15} V/s [9, 62]. Assuming a maximum derivative of $10x10^{15}$ V/s, we can obtain a rough estimation of the strongest/fastest achievable pulser for hyperband radiators. For instance, the fastest 100kV pulser would switch at no less than 10 ps and the fastest 1MV pulser should close at no less than 100ps.

As already mentioned in Section 3.2, among the most powerful transient generators available for purchase is the JOLT [46]. This system is capable of delivering a radiated far field with a rise-time of about 80ps, a FWHM of the order of 100ps, and a far voltage of 5.3MV. To achieve these results, the JOLT is driven by a 1MV pulser switching in about 200ps (dV/dt of about 5×10^{15} V/s). In the near field, this system could generate up to 800kV/m [37].

6.1.2 Mesoband radiators

Mesoband generators can be built from quarter wave switched oscillators charged with a DC voltage [14]. These systems will also be limited by the above-mentioned switching

constraints. Furthermore, given the expected size of these devices, high voltage management becomes an issue. Also, if the desired oscillating frequencies of the quarter wave oscillators exceed the GHz range, the design of the devices becomes complicated since the mechanical precision requirements for constructing metal profiles at such small dimensions are expensive and not always feasible.

One of the most powerful reported mesoband systems based on a switching oscillator is the so-called MATRIX system [8]. This system could be charged up to 150kV and it oscillated between 180 MHz and 600MHz. The estimated far-voltage (rE_{peak} product) of the original MATRIX system was about 90kV. Newer versions of the MATRIX systems include oscillators working at higher frequencies (1 and 2GHz) but charged at lower DC voltages (50-65kV) [30, 63] due to the above-mentioned breakdown constraints.

Another way to obtain mesoband HPEM radiated waveforms is by connecting a wire antenna to a HV impulse generator. Among the most powerful reported systems, the DIEHL suitcase generators [64] are capable of producing about 225kV/m at 1m, oscillating at a center frequency of 350MHz. These systems use a tunable coil antenna that is pulsed with a 600kV Marx generator. The main technological challenge of such systems is the compaction of the Marx generator into such a small volume (100x55x82cm^3 according to [64]).

A bigger, but still transportable mesoband radiation system based on the excitation of wire antennas with a powerful Marx generator was presented in [16]. The system was capable of generating a 2MV/300ps pulse to drive a set of helical antennas with 9 different central frequencies ranging from 200 MHz to 6GHz. Due to breakdown issues at the generator/antenna interface, the helical antennas had to be insulated in an SF6 radome.

6.1.3 Hypoband radiators

Among the IEMI radiators, the so-called Low Power Microwave (LPM) sources and High Power Microwave (HPM) radiators are the most dangerous since they are very energetic and may induce permanent effects due to heating of semiconductors. HPM devices are defined as those that exceed 100MW in peak power and span the range of frequencies between 1 and 300GHz [9, 49]. Conventional tubes may work in a continuous wave regime up to some MW of output power. If higher output power is required, HPM radiators can be tailored to emit continuous wave bursts of short duration in the hundreds of nanoseconds to some microseconds range (10^{-6} duty factors), and reach output power of some GW. Given the size and the weight of the required supply source and the cooling mechanisms of such generators, LPM and HPM sources are very difficult to transport and they are typically installed in military vehicles or big infrastructures such as airports or military bases.

In order to understand the positioning of LPM and HPM tubes, a comparison of the peak vs. average power for conventional and HPM tubes is presented in Fig. 6.3. The peak power of a device is plotted against its average power. It can be appreciated that conventional tubes (shaded in light gray) span a big range in the plot while HPM tubes (shaded in dark gray) have not been developed to produce substantial average power levels. The black straight lines are traced to identify the limits between 1, 10^{-2}, 10^{-4}, and 10^{-6} duty factors.

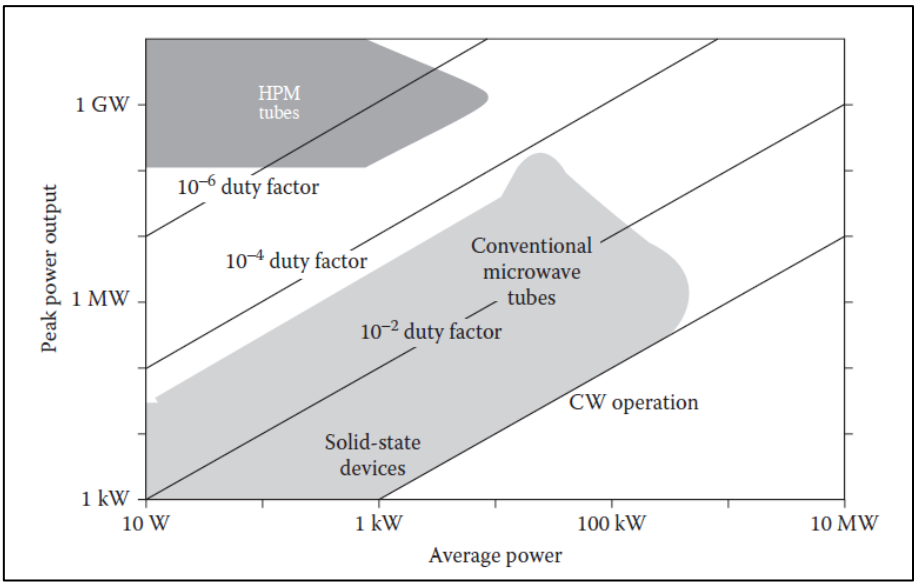

Fig. 6.2 Peak vs. average power for LPM and HPM sources. Figure taken from [49].

Naturally, the expected peak E field of an HPM radiator is lower than that of a hyperband or mesoband radiator. It was believed in the late 90s that HPM devices were fundamentally limited above a peak power of approximately 10GW and pulse energy of 1kJ [49, 65]. However, it is believed that with the aid of phase locking, multiple sources can conceivably increase the single device levels. For example, the output levels of a feasible multiple pulse weapon considered by Taylor and Giri in [65] was 10GW of peak power, 100ns pulse width, and 1 kJ of energy per pulse at a repetition rate of 1kHz. The ultimate limits on HPM source peak power are not well known. They are set by a trade-offs between breakdown (multipactor), mode competition, and intense beam-field interactions.

Fig. 6.3 presents a plot of the peak power generated by a representative sample of high power sources adapted from [49]. It appears that the peak power of many sources falls off as Pf^2 at high frequency.

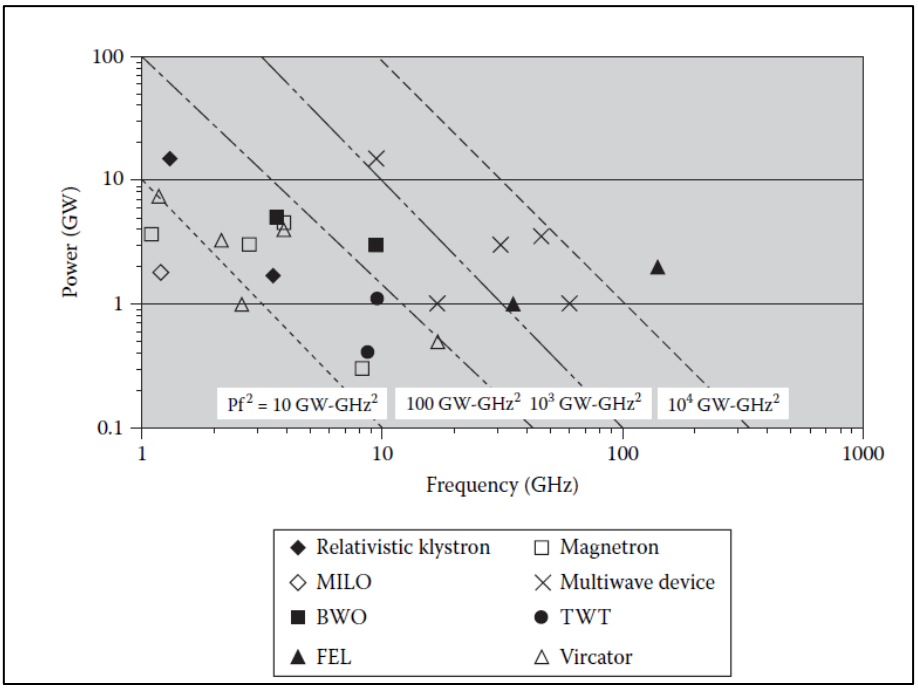

Fig. 6.3 Peak powers of HPM sources. Figure taken from [49].

Among the most powerful and simple to build HPM sources is the virtual cathode oscillator or Vircator. The Vircator is a very attractive source for IEMI given the fact that it is a tunable CW generator in the 1-10GHz range, it does not require an applied magnetic field and it is a low impedance device (permits high power operation at low voltage). However, it is a very inefficient source (about 1-15%) and it is traditionally operated with explosives like single shot electrical generators at the input in order to reduce space.

7 CONCLUSIONS

In this note, we have presented a study and classification of potential IEMI sources that were collected from available publications. The study comprises the calculation of the waveform and spectral parameters of the voltage measured at the output of conducted sources and the electric field at a given distance of radiated sources. The waveforms have been digitized from the original papers, and a signal processing program has been created to obtain the parameters.

We have proposed an alternative method to represent the digitized signals as an expansion of complex exponentials from which the Fourier Transform can be calculated analytically. This alternative method facilitates the calculation of the spectral parameters of the signals because the spectra can be calculated at arbitrary frequency points. We have also shown how to improve the calculation time of the band-ratio of the signals by using the Blumer index. From these results, we have created a set of wavecards each containing a summary of the characteristics of a waveform, including its spectral parameters. The complete wavecard set can be found in Appendix A.

We have also collected the main characteristics of the sources into a spreadsheet and tried to classify them according to the proposed criteria for assessing the strength, availability and transportability of sources that were presented in Section 3 of this note. The spreadsheet is also available in Appendix B of this note.

The information in the spreadsheets was used to generate pie charts and bar plots that illustrate some tendencies and characteristics of the analyzed conducted and radiated sources. It was found that potential IEMI conducted sources are more available than radiated sources. Due to the maturity of the market, and the lower frequency requirements, these sources are commercially available from various EMC test vendors. Voltage levels in the range of several kV can be achieved with sources exhibiting all of the defined portability levels (including pocket-size), and their acquisition prices remain moderate for the majority of the conducted sources. Thus, they can be regarded as likely to be deployed by an IEMI malefactor.

On the other hand, radiated sources appear to be still in a development phase and are only available for purchase as test-sources. They seem to require at least a vehicle to be transported and, according to the classification (made to the best of the authors' knowledge), the typical costs of such sources remain high due to the required high technology in the implementation and testing. However, there are already some prototypes that can be transported in a briefcase and whose field level outputs are capable of theoretically producing malfunctions and damages –if close enough- in electronics. A trend to produce hyperband radiators was identified in the early 2000s. In more recent years, the survey reveals a growing activity in the development of mesoband sources.

In the last chapter of this note, we have tried to underline the physical limitations that constrain the development of current technologies in the generation of faster and stronger HPEM sources.

8 ACKNOWLEDGEMENTS

This work was initially inspired on the idea of studying the “waveforms taxonomy” of purely analytical signals suggested by Dr. Giri a couple of years ago. The wavecards constitute the first implementation of such idea but applied to digitized waveforms from available publications.

The authors would like to convey their gratitude to Bertrand Daout, Marc Sallin, Werner Hirschi, Scott Tyo, and Dave Giri for the useful discussions on the expected limitations of HPEM sources.

This study was financially supported by Swisselectric Research in the framework of the project “Impact of Intentional Electromagnetic Interference (IEMI) on Electric Power Systems”.

9 REFERENCES

[1] "Special Issue on high-power electromagnetics (HPEM) and intentional electromagnetic interference (IEMI),," *Electromagnetic Compatibility, IEEE Transactions on,* August 2004.

[2] R. Thottappillil, D. Mansson, and M. Backstrom, "Response of electrified railway facilities to intentional electromagnetic interference: Review of research at Uppsala University," in *Electromagnetic Compatibility and 19th International Zurich Symposium on Electromagnetic Compatibility, 2008. APEMC 2008. Asia-Pacific Symposium on*, 2008, pp. 291-294.

[3] D. Mansson, M. Backstrom, and R. Thottappillil, "Classifying facilities with respect to Intentional EMI," in *Electromagnetic Compatibility, 2009. EMC 2009. IEEE International Symposium on*, 2009, pp. 249-254.

[4] D. Mansson, M. Backstrom, and R. Thottappillil, "Intentional EMI against critical infrastructures, a discussion on mitigation philosophy," in *Electromagnetic Compatibility (APEMC), 2010 Asia-Pacific Symposium on*, 2010, pp. 134-137.

[5] W. A. Radasky, "High power electromagnetic (HPEM) threads and the electric power system," ed. Chicago, USA, 2010.

[6] W. A. Radasky, "The potential impacts of three High Power Electromagnetic (HPEM) threats on Smart Grids," *Electromagnetic Compatibility Magazine, IEEE,* vol. 1, pp. 107-110, 2012.

[7] C. E. Baum, "A time-domain view of choice of transient excitation waveforms for enhanced response of electronic systems," presented at the International Conference Electromagnetics Advanced Applications (ICEAA 2001), 2001.

[8] W. D. Prather, C. E. Baum, R. J. Torres, F. Sabath, and D. Nitsch, "Survey of worldwide high-power wideband capabilities," *Electromagnetic Compatibility, IEEE Transactions on,* vol. 46, pp. 335-344, 2004.

[9] D. V. Giri, *High-power electromagnetic radiators : nonlethal weapons and other applications*. Cambridge, MA: Harvard University Press, 2004.

[10] D. V. Giri and F. M. Tesche, "Classification of intentional electromagnetic environments (IEME)," *Electromagnetic Compatibility, IEEE Transactions on,* vol. 46, pp. 322-328, 2004.

[11] IEC, "61000-2-13 : Electromagnetic compatibility (EMC) - Part 2-13:Environment –High-power electromagnetic (HPEM)environments –Radiated and conducted," ed: IEC, 2005.

[12] M. Armanious, "DESIGN AND ANALYSIS OF A HIGH POWER MODERATE BAND RADIATOR USING A SWITCHED OSCILLATOR," DOCTOR OF PHILOSOPHY, COLLEGE OF OPTICAL SCIENCES, THE UNIVERSITY OF ARIZONA, 2010.

[13] F. Vega, "Analytical Methods for the Study and Design of Integrated Switched Oscillators and Antennas for Mesoband Radiation," DOCTEUR ÈS SCIENCES, FACULTÉ DES SCIENCES ET TECHNIQUES DE L'INGÉNIEUR, ÉCOLE POLYTECHNIQUE FÉDÉRALE DE LAUSANNE, 2013.

[14] D. V. Giri, F. M. Tesche, M. D. Abdalla, M. C. Skipper, and M. Nyffeler, "Switched Oscillators and Their Integration into Helical Antennas," *Circuit and Electromagnetic System Design Notes,* vol. 58, 2009.

[15] D. V. Giri, F. M. Tesche, M. D. Abdalla, M. C. Skipper, and M. Nyffeler, "Switched Oscillators and Their Integration Into Helical Antennas," *Plasma Science, IEEE Transactions on,* vol. 38, pp. 1411-1426, 2010.

[16] D. V. Giri, "Helical antennas energized by transient marx generators," in *High Power Microwave Defense & Security Workshop*, Saint-Louis, France, 2011.

[17] F. Sabath and H. Garbe, "Risk potential of radiated HPEM environments," in *Electromagnetic Compatibility, 2009. EMC 2009. IEEE International Symposium on*, 2009, pp. 226-231.

[18] ITU, "High-power electromagnetic immunity guide for telecommunication systems," in *K. 81* ed, 2009.

[19] C. E. Baum, W. L. Baker, W. D. Prather, J. M. Lehr, J. P. O'Loughlin, D. V. Giri*, et al.*, "JOLT: A Highly Directive, Very Intensive, Impulse-Like Radiator," *Sensor and Simulation 0480,* November 2003.

[20] F. M. Tesche and D. V. Giri, "Swiss Impulse Radiating Antenna (SWIRA) Characterization in the Presence of a Local Ground Plane (Earth)," *Sensor and Simulation Notes,* vol. 557, 2011.

[21] Y. V. Parfenov, L. N. Zdoukhov, W. A. Radasky, and M. Ianoz, "Conducted IEMI threats for commercial buildings," *Electromagnetic Compatibility, IEEE Transactions on,* vol. 46, pp. 404-411, 2004.
[22] D. Mansson, R. Thottappillil, and M. Backstrom, "Propagation of UWB Transients in Low-Voltage Power Installation Networks," *Electromagnetic Compatibility, IEEE Transactions on,* vol. 50, pp. 619-629, 2008.
[23] J. H. Hagmann, S. Dickmann, and S. Potthast, "Application and propagation of transient pulses on power supply networks," in *EMC Europe 2011 York*, 2011, pp. 7-12.
[24] D. Nitsch, M. Camp, F. Sabath, J. L. ter Haseborg, and H. Garbe, "Susceptibility of some electronic equipment to HPEM threats," *Electromagnetic Compatibility, IEEE Transactions on,* vol. 46, pp. 380-389, 2004.
[25] IEC, "61000-4-33 : Electromagnetic compatibility (EMC) - Part 4-33: Testing and measurement techniques - Measurement methods for high-power transient parameters," ed: IEC, 2005.
[26] C. Romero, M. Paolone, F. Rachidi, M. Rubinstein, D. Pavanello, and D. V. Giri, "A Statistical Analysis on the Risetime of Lightning Current Pulses in Negative Upward Flashes Measured at Säntis Tower," in *2012 International Conference on Lightning Protection (ICLP)*, Vienna, Austria, 2012.
[27] F. M. Tesche, "Transformer Responses to Fast Transient Excitations," The Defense Procurement Agency of the Federal Department of Defense, Civil Protection and Sports, NEMP Laboratory2002.
[28] J. S. Tyo, M. C. Skipper, M. D. Abdalla, S. P. Romero, and D. V. Giri, "Performance limitations of transmission line oscillators for high powermesoband sources," in *Pulsed Power Conference, 2007 16th IEEE International*, 2007, pp. 298-301.
[29] D. Belt, J. Mankowski, J. Walter, J. Dickens, and M. Kristiansen, "Analysis of Mesoband Single Element Pulsed Ring-Down Antennas for Implementation in Phased Array Systems," in *IEEE International Power Modulators and High Voltage Conference, Proceedings of the 2008*, 2008, pp. 152-155.
[30] M. Armanious, J. S. Tyo, M. C. Skipper, M. D. Abdalla, W. D. Prather, and J. E. Lawrance, "Interaction Between Geometric Parameters and Output Waveforms in High-Power Quarter-Wave Oscillators," *Plasma Science, IEEE Transactions on,* vol. 38, pp. 1124-1131, 2010.
[31] D. V. Giri, "HPE 201-2009: Damped Sinusoid Basics," ed. Chateau d'Oex, Switzerland, 2009.
[32] M. G. Backstrom and K. G. Lovstrand, "Susceptibility of electronic systems to high-power microwaves: summary of test experience," *Electromagnetic Compatibility, IEEE Transactions on,* vol. 46, pp. 396-403, 2004.
[33] D. Mansson, R. Thottappillil, M. Backstrom, and O. Lunden, "Vulnerability of European Rail Traffic Management System to Radiated Intentional EMI," *Electromagnetic Compatibility, IEEE Transactions on,* vol. 50, pp. 101-109, 2008.
[34] IEC, "61000-4-35 :Electromagnetic compatibility (EMC) –Part 4-35: Testing and measurement techniques – HPEM simulator compendium," ed: IEC, 2009.
[35] A. Das, *Digital Communication Principles and System Modelling*. Berlin: Springer Berlin, 2013.
[36] C. E. Baum, "Norms and Eigenvector norms," *Mathematics Notes* vol. 63, 1979.
[37] D. V. Giri, "Personal Communication," N. Mora, Ed., ed, 2012.
[38] D. V. Giri, "Classification of Intentional EMI based on bandwidth," presented at the AMEREM 2002, Annapolis, 2002.
[39] R. Hoad, N. J. Carter, D. Herke, and S. P. Watkins, "Trends in EM susceptibility of IT equipment," *Electromagnetic Compatibility, IEEE Transactions on,* vol. 46, pp. 390-395, 2004.
[40] O. H. Arnesen, E. Krogager, M. Backstrom, S. Bo-Sande, J. Godo, S. Harkonen*, et al.*, "HIGH POWER MICROWAVE EFFECTS ON CIVILIAN EQUIPMENT," presented at the URSI General Assembly, New Delhi, 2005.
[41] D. V. Giri, "Documented Electromagnetic Effects (EME)," in *EUROEM 2008*, Lausanne, Switzerland, 2008.

[42] F. Brauer, F. Sabath, and J. L. ter Haseborg, "Susceptibility of IT network systems to interferences by HPEM," in *Electromagnetic Compatibility, 2009. EMC 2009. IEEE International Symposium on*, 2009, pp. 237-242.
[43] F. Brauer, S. Fahlbusch, J. L. ter Haseborg, and S. Potthast, "Investigation of Hardening Measures for IT Equipment against Radiated and Conducted IEMI," *Electromagnetic Compatibility, IEEE Transactions on,* vol. 54, pp. 1055-1065, 2012.
[44] IEC, "61000-1-5 :Electromagnetic compatibility (EMC) –Part 1-5: General –High power electromagnetic (HPEM) effects on civil systems Reference," ed: IEC, 2004.
[45] F. Sabath, "Effects of documented HPEM attacks on systems. Course HPE 201-2011: High-Power Electromagnetics Course - Effects," ed. Schloss Noer, Germany, 2011.
[46] C. E. Baum, W. L. Baker, W. D. Prather, J. M. Lehr, J. P. O'Loughlin, D. V. Giri*, et al.*, "JOLT: a highly directive, very intensive, impulse-like radiator," *Proceedings of the IEEE,* vol. 92, pp. 1096-1109, 2004.
[47] P. Delmote, J. P. Duperoux, F. Bieth, and S. Pinguet, "UWB HPM at ISL: The GIMLI project and other applications," in *High Power Microwave Defense & Security Workshop*, Saint-Louis, France, 2011.
[48] D. V. Giri, H. Lackner, I. D. Smith, D. W. Morton, C. E. Baum, J. R. Marek*, et al.*, "Design, fabrication, and testing of a paraboloidal reflector antenna and pulser system for impulse-like waveforms," *Plasma Science, IEEE Transactions on,* vol. 25, pp. 318-326, 1997.
[49] J. Benford, E. Schamiloglu, and J. A. Swegle, *High power microwaves*. New York [u.a.]: Taylor & Francis, 2007.
[50] A. M. Efremov, V. I. Koshelev, B. M. Kovalchuk, V. V. Plisko, and K. N. Sukchushin, "High-Power Sources of Ultrawideband Radiation with Subnanosecond Pulse Length," presented at the 14th International Symposium on High Current Electronics, Tomsk, Russia, 2006.
[51] F. Vega, "DESIGN OF A HIGH POWER ULTRA WIDEBAND SYSTEM USING A FAST IMPULSE CURRENT GENERATOR," Doctor of Philosophy, Electrical and Electronics Engineering Department, National University of Colombia, 2011.
[52] Y. Hua and T. K. Sarkar, "Matrix pencil method for estimating parameters of exponentially damped/undamped sinusoids in noise," *Acoustics, Speech and Signal Processing, IEEE Transactions on,* vol. 38, pp. 814-824, 1990.
[53] J. Chauveau, N. de Beaucoudrey, and J. Saillard, "Selection of Contributing Natural Poles for the Characterization of Perfectly Conducting Targets in Resonance Region," *Antennas and Propagation, IEEE Transactions on,* vol. 55, pp. 2610-2617, 2007.
[54] A. Rubinstein, "Simulation of electrically large structures in EMC studies - application to automotive EMC," Swiss Federal Institute of Technology -EPFL, 2004.
[55] E. Nasser, *Fundamental of Gaseous Ionization and Plasma Electronics*: Wiley Interscience, 1971.
[56] G. Schaefer, M. Kristiansen, and A. H. Guenther, *Gas discharge closing switches*. New York, N.Y: Plenum Press, 1991.
[57] J. C. Martin, "Nanosecond pulse techniques," *Proceedings of the IEEE,* vol. 80, pp. 934-945, 1992.
[58] J. C. Martin, T. H. Martin, A. H. Guenther, and M. Kristiansen, *J.C. Martin on pulsed power*. New York: Plenum Press, 1996.
[59] V. Carboni, H. Lackner, D. V. Giri, and J. M. Lehr, "The Breakdown Fields and Risetimes of Select Gases Under Conditions of Fast Charging (~20 ns and less) and High Pressures (20-100 atmospheres)," *Switching Notes,* vol. 32, 2002.
[60] R. J. Barker and E. Schamiloglu, *High-power microwave sources and technologies*. New York, NY: IEEE Press, 2001.
[61] S. T. Pai and Q. Zhang, *Introduction to high power pulse technology*. Singapore [u.a.]: World Scientific, 1995.
[62] J. M. Lehr, C. E. Baum, W. D. Prather, and F. J. Agee, "Fundamental Physical considerations for ultrafast spark gap switching," *Switching Notes,* vol. 28, 1997.
[63] M. Armanious, J. S. Tyo, M. C. Skipper, M. D. Abdalla, W. D. Prather, and G. Gruen, "Electrostatic field management and electrodynamic modeling of switched quarter-wave

oscillators," *Dielectrics and Electrical Insulation, IEEE Transactions on,* vol. 18, pp. 1054-1065, 2011.
[64] DIEHL, "HPEM Case Brochure," DIEHL, Ed., ed, 2011.
[65] C. D. Taylor and D. V. Giri, *High-power microwave systems and effects*. [Washington]: Taylor and Francis, 1994.

SYSTEM DESIGN AND ASSESSMENT NOTES

NOTE 41

8 July 2014

APPENDIX A

EXTRACTION OF THE WAVEFORM AND SPECTRAL ATTRIBUTES OF POTENTIAL IEMI SOURCES REPORTED IN THE LITERATURE

Wavecard database

Corresponding author: nicolas.mora@epfl.ch

TABLE OF CONTENTS

A-1 INTRODUCTION

In this Appendix, the parameters of some potential conducted and radiated IEMI sources that were published in the literature (peer reviewed journal articles, standards, books, conference articles, reports, conference presentations, manuals, and brochures) are calculated by using the definition of the waveform attributes presented in Section 2 of this note. The parameters are obtained from the digitized waveforms of the voltage output of conducted sources, and the electric field at a given distance produced by radiated sources. Almost all the time domain waveforms were digitized from the waveform image available in the printed paper, the spectrum was numerically calculated, and the parameters list was also numerically calculated.

For each of the sources, a "wavecard" containing: (i) the digitized time domain waveform, (ii) the spectrum of the time domain waveform, and (iii) a list with several waveform parameters, was generated

To better understand the list of parameters, a brief explanation of the fields is given as follows:

(i) *Source Name:* the name that was used to identify the source in the wavecard database

(ii) *Year:* the year of the source construction (if available) or the publication year of the document that reports the source (for the first time).

(iii) *Waveform type*: classification of the source waveform depending on its nature. The waveform can be classified in three categories: Single Pulse, Oscillatory or CW.

(iv) *Band type:* the band-type of the source according to its band-ratio, as it was explained in Tab 3.1.

(v) *Amplitude units:* the units of the waveform. Typically V for conducted sources and V/m for radiated sources.

(vi) *Peak amplitude (N_1) [Units]:* the value of the N_1 norm according to the definition of Tab 2.1. The units of the N_1 are the same amplitude units.

(vii) *Peak derivative (N_2) [Units/s]:* the value of the N_2 norm according to the definition of Tab 2.1. The units of the N_1 are the amplitude units divided by time in seconds.

(viii) *Peak impulse (N_3) [Units . s]:* the value of the N_3 norm according to the definition of Tab 2.1. The units of the N_3 are the amplitude units multiplied by time in seconds.

(ix) *Rectified total impulse (N_4) [Units . s]:* the value of the N_4 norm according to the definition of Tab 2.1. The units of the N_4 are the amplitude units multiplied by time in seconds.

(x) *Sq. Root. action integral (N_5) [Units. $s^{1/2}$]:* the value of the N_5 norm according to the definition of Tab 2.1. The units of the N_5 are the amplitude units multiplied by the square root of time in seconds.

(xi) *Time to peak[s]:* the time to peak $\Delta t_{\max}$ as defined in Eq. 2.2. For signals in which a single impulsive behavior cannot be defined, the time to peak is measured on the rising edge of the signal before reaching the maximum peak. This parameter is measured in seconds.

(xii) *10-90 rise-time [s]:* the 10-90% rise time Δt_{10-90} as defined in Eq. 2.4. For signals in which a single impulsive behavior cannot be defined, the rise-time is measured in the rising edge of the signal before reaching the maximum peak. This parameter is measured in seconds.

(xiii) *Max. rate of rise [s]:* the maximum rate of rise t_{mr} as defined in Eq. 2.5.

(xiv) *FWHM [s]:* This field contains the FWHM Δt_{50-50} as defined in Eq. 2.6. For signals in which a single impulsive behavior cannot be defined, the FWHM is measured in the rising and falling edges of the signal before and after reaching the maximum peak. This parameter is measured in seconds.

(xv) *Fall time [s]:* For impulsive like signals, this parameter corresponds to the e-folding time of the signal. For oscillatory signals, this field contains the e-folding time Δt_f of the envelope of the signal as it was introduced in Eq. 2.7. For CW signals, the fall time has no significant meaning and therefore is omitted; thus appearing as a "NaN" value. This parameter is measured in seconds.

(xvi) *Peak spectral Amplitude [Units/Hz]:* contains the maximum amplitude of the FFT spectrum of the signal. This parameter is measured in the amplitude units divided by frequency in Hz.

(xvii) *Average frequency (TD) [Hz]:* the average frequency of the signal estimated from the average period in time domain as it was introduced in Eq. 2.8. For signals of the waveform type "Single Pulse", this parameter is not calculated and therefore displayed with "NaN" value. This frequency is measured in Hz.

(xviii) *Center frequency (FD) [Hz]:* the center frequency of the signal estimated as in Eq. 2.14. For signals of the waveform type "Single Pulse", this parameter is not calculated and therefore displayed with "NaN" value. This frequency is measured in Hz.

(xix) *-3dB bandwidth [Hz]:* the bandwidth BW_{-3dB} calculated as the difference of the -3dB limits starting from the peak spectral amplitude of the signal spectrum. This parameter is measured in Hz.

(xx) *90% Bandwidth [Hz]:* the 90% energy bandwidth BW_{90} defined in Eq. 2.17. This parameter is measured in Hz.

(xxi) *Band Ratio:* the band ratio of the signal as defined in Eq 2.15.

(xxii) *Average quality factor (TD):* the quality factor of the source calculated from a time domain approach as presented in Eq. 2.9. This parameter is not calculated for signal of the waveform type "Single Pulse" and "CW".

(xxiii) *Quality factor (FD):* the quality factor of the source calculated from a frequency domain approach as presented in Eq. 2.18. This parameter is not calculated for signal of the waveform type "Single Pulse" and "CW".

A-2 CONDUCTED SOURCES

A-2.1 GaAs Voltage Source in [A-1]

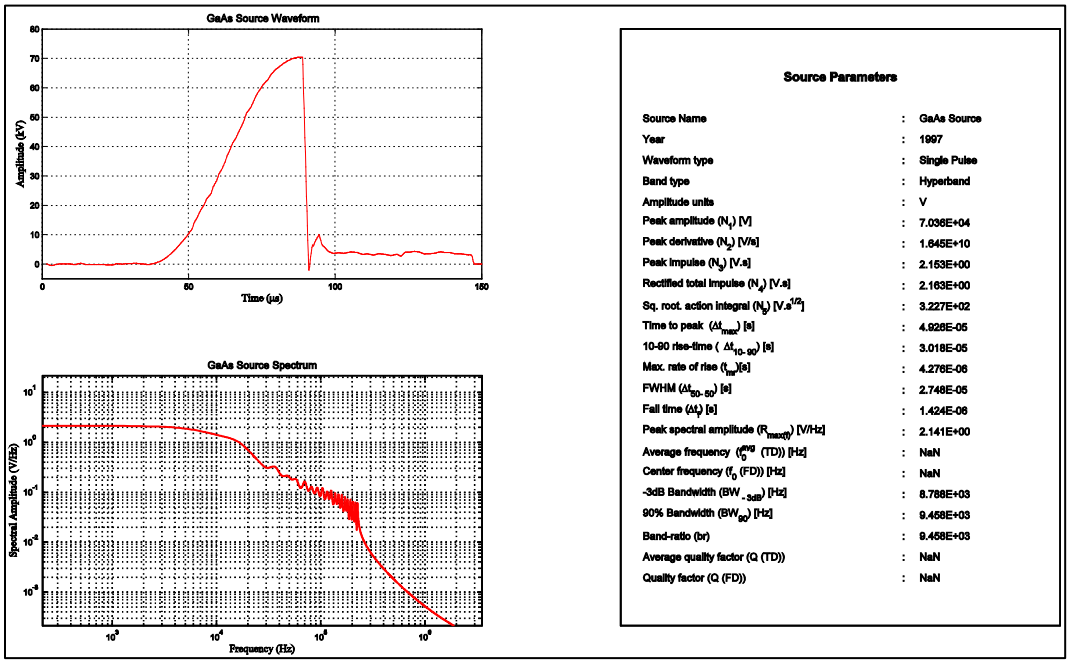

Source Parameters

Source Name	:	GaAs Source
Year	:	1997
Waveform type	:	Single Pulse
Band type	:	Hyperband
Amplitude units	:	V
Peak amplitude (N_1) [V]	:	7.036E+04
Peak derivative (N_2) [V/s]	:	1.645E+10
Peak impulse (N_3) [V.s]	:	2.153E+00
Rectified total impulse (N_4) [V.s]	:	2.163E+00
Sq. root. action integral (N_5) [V.s$^{1/2}$]	:	3.227E+02
Time to peak (Δt_{max}) [s]	:	4.926E-05
10-90 rise-time (Δt_{10-90}) [s]	:	3.018E-05
Max. rate of rise (t_{rm})[s]	:	4.276E-06
FWHM (Δt_{50-50}) [s]	:	2.748E-05
Fall time (Δt_f) [s]	:	1.424E-06
Peak spectral amplitude ($R_{max(f)}$) [V/Hz]	:	2.141E+00
Average frequency (f_0^{avg} (TD)) [Hz]	:	NaN
Center frequency (f_0 (FD)) [Hz]	:	NaN
-3dB Bandwidth (BW_{-3dB}) [Hz]	:	8.788E+03
90% Bandwidth (BW_{90}) [Hz]	:	9.468E+03
Band-ratio (br)	:	9.468E+03
Average quality factor (Q (TD))	:	NaN
Quality factor (Q (FD))	:	NaN

A-2.2 Voltage source in [A-2]

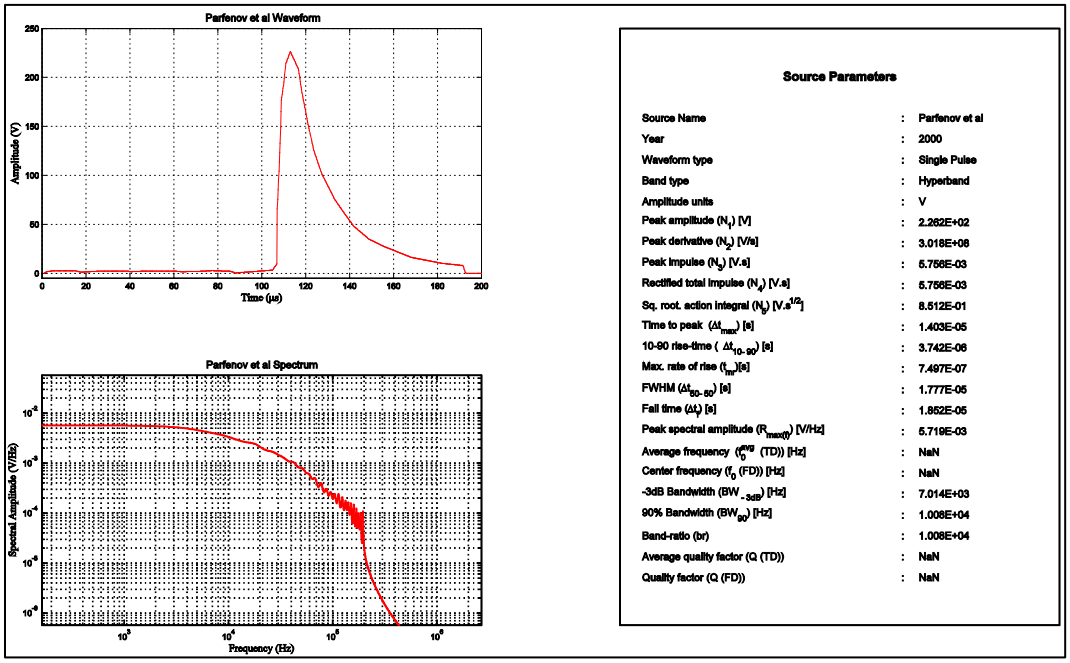

Source Parameters

Source Name	:	Parfenov et al
Year	:	2000
Waveform type	:	Single Pulse
Band type	:	Hyperband
Amplitude units	:	V
Peak amplitude (N_1) [V]	:	2.262E+02
Peak derivative (N_2) [V/s]	:	3.018E+08
Peak impulse (N_3) [V.s]	:	5.756E-03
Rectified total impulse (N_4) [V.s]	:	5.756E-03
Sq. root. action integral (N_5) [V.s$^{1/2}$]	:	8.512E-01
Time to peak (Δt_{max}) [s]	:	1.403E-05
10-90 rise-time (Δt_{10-90}) [s]	:	3.742E-06
Max. rate of rise (t_{rm})[s]	:	7.497E-07
FWHM (Δt_{50-50}) [s]	:	1.777E-05
Fall time (Δt_f) [s]	:	1.852E-05
Peak spectral amplitude ($R_{max(f)}$) [V/Hz]	:	5.719E-03
Average frequency (f_0^{avg} (TD)) [Hz]	:	NaN
Center frequency (f_0 (FD)) [Hz]	:	NaN
-3dB Bandwidth (BW_{-3dB}) [Hz]	:	7.014E+03
90% Bandwidth (BW_{90}) [Hz]	:	1.008E+04
Band-ratio (br)	:	1.008E+04
Average quality factor (Q (TD))	:	NaN
Quality factor (Q (FD))	:	NaN

A-2.3 BAE Non Linear Transmission Line in [A-3]

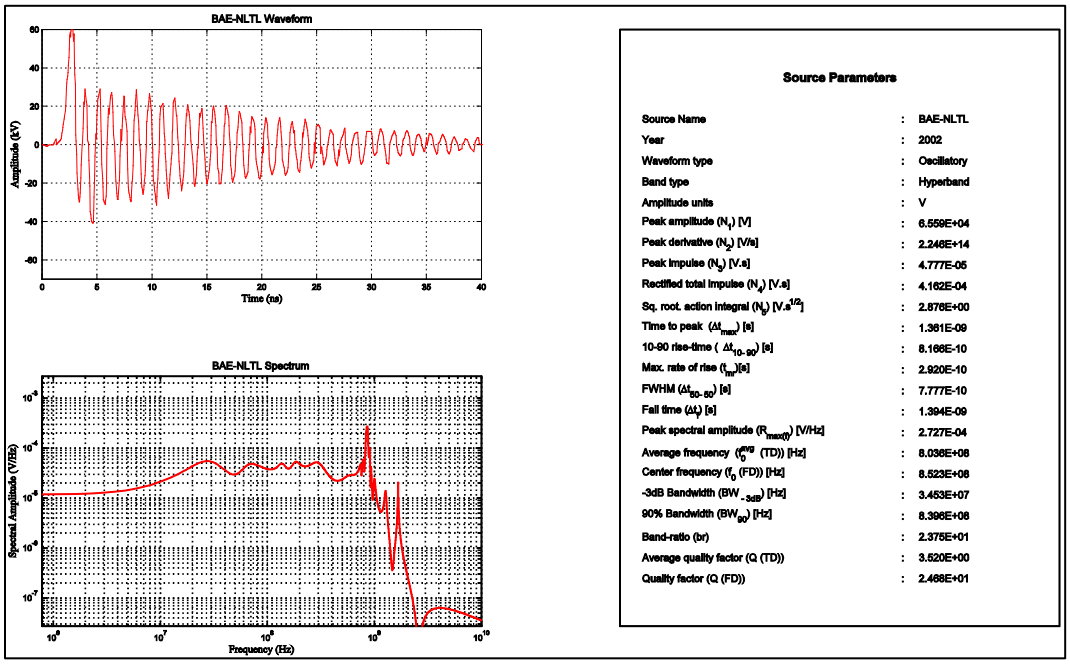

Source Parameters

Source Name	:	BAE-NLTL
Year	:	2002
Waveform type	:	Oscillatory
Band type	:	Hyperband
Amplitude units	:	V
Peak amplitude (N_1) [V]	:	6.559E+04
Peak derivative (N_2) [V/s]	:	2.246E+14
Peak Impulse (N_3) [V.s]	:	4.777E-05
Rectified total impulse (N_4) [V.s]	:	4.162E-04
Sq. root. action integral (N_5) [V.s$^{1/2}$]	:	2.676E+00
Time to peak (Δt_{max}) [s]	:	1.361E-09
10-90 rise-time (Δt_{10-90}) [s]	:	8.166E-10
Max. rate of rise (t_{mr})[s]	:	2.920E-10
FWHM (Δt_{50-50}) [s]	:	7.777E-10
Fall time (Δt_f) [s]	:	1.394E-09
Peak spectral amplitude ($R_{max(f)}$) [V/Hz]	:	2.727E-04
Average frequency (f_0^{avg} (TD)) [Hz]	:	8.036E+08
Center frequency (f_0 (FD)) [Hz]	:	8.523E+08
-3dB Bandwidth (BW_{-3dB}) [Hz]	:	3.453E+07
90% Bandwidth (BW_{90}) [Hz]	:	8.398E+08
Band-ratio (br)	:	2.375E+01
Average quality factor (Q (TD))	:	3.520E+00
Quality factor (Q (FD))	:	2.468E+01

A-2.4 H.V. pulser in [A-4]

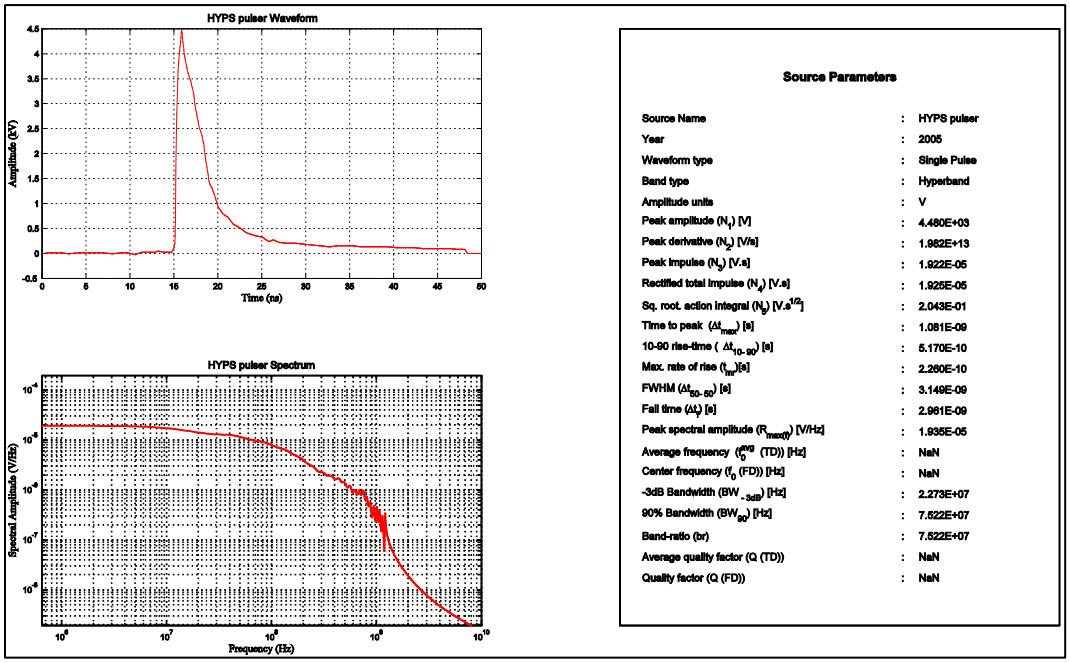

Source Parameters

Source Name	:	HYPS pulser
Year	:	2005
Waveform type	:	Single Pulse
Band type	:	Hyperband
Amplitude units	:	V
Peak amplitude (N_1) [V]	:	4.480E+03
Peak derivative (N_2) [V/s]	:	1.982E+13
Peak Impulse (N_3) [V.s]	:	1.922E-05
Rectified total impulse (N_4) [V.s]	:	1.925E-05
Sq. root. action integral (N_5) [V.s$^{1/2}$]	:	2.043E-01
Time to peak (Δt_{max}) [s]	:	1.081E-09
10-90 rise-time (Δt_{10-90}) [s]	:	5.170E-10
Max. rate of rise (t_{mr})[s]	:	2.260E-10
FWHM (Δt_{50-50}) [s]	:	3.149E-09
Fall time (Δt_f) [s]	:	2.961E-09
Peak spectral amplitude ($R_{max(f)}$) [V/Hz]	:	1.935E-05
Average frequency (f_0^{avg} (TD)) [Hz]	:	NaN
Center frequency (f_0 (FD)) [Hz]	:	NaN
-3dB Bandwidth (BW_{-3dB}) [Hz]	:	2.273E+07
90% Bandwidth (BW_{90}) [Hz]	:	7.522E+07
Band-ratio (br)	:	7.522E+07
Average quality factor (Q (TD))	:	NaN
Quality factor (Q (FD))	:	NaN

A-2.5 Mid-voltage pulser in [A-4]

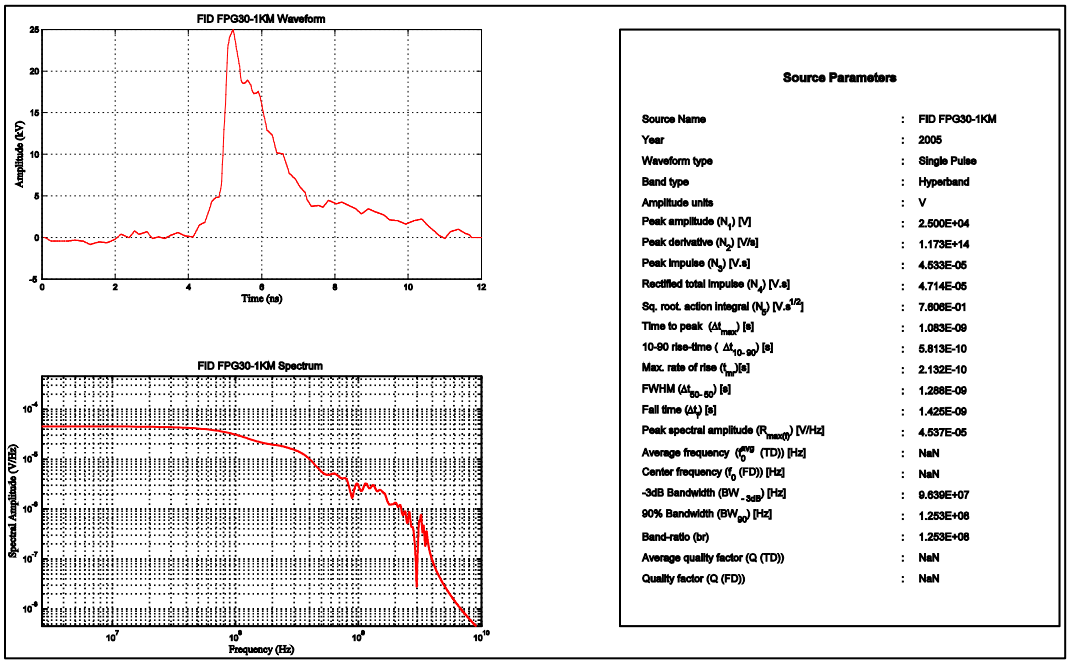

Source Parameters

Source Name	:	FID FPG30-1KM
Year	:	2005
Waveform type	:	Single Pulse
Band type	:	Hyperband
Amplitude units	:	V
Peak amplitude (N_1) [V]	:	2.500E+04
Peak derivative (N_2) [V/s]	:	1.173E+14
Peak impulse (N_3) [V.s]	:	4.533E-05
Rectified total impulse (N_4) [V.s]	:	4.714E-05
Sq. root. action integral (N_5) [V.s$^{1/2}$]	:	7.606E-01
Time to peak (Δt_{max}) [s]	:	1.083E-09
10-90 rise-time (Δt_{10-90}) [s]	:	5.813E-10
Max. rate of rise (t_{mr})[s]	:	2.132E-10
FWHM (Δt_{50-50}) [s]	:	1.288E-09
Fall time (Δt_f) [s]	:	1.425E-09
Peak spectral amplitude ($R_{max(f)}$) [V/Hz]	:	4.537E-05
Average frequency (f_0^{avg} (TD)) [Hz]	:	NaN
Center frequency (f_0 (FD)) [Hz]	:	NaN
-3dB Bandwidth (BW_{-3dB}) [Hz]	:	9.639E+07
90% Bandwidth (BW_{90}) [Hz]	:	1.253E+08
Band-ratio (br)	:	1.253E+08
Average quality factor (Q (TD))	:	NaN
Quality factor (Q (FD))	:	NaN

A-2.6 Voltage source in [A-5]

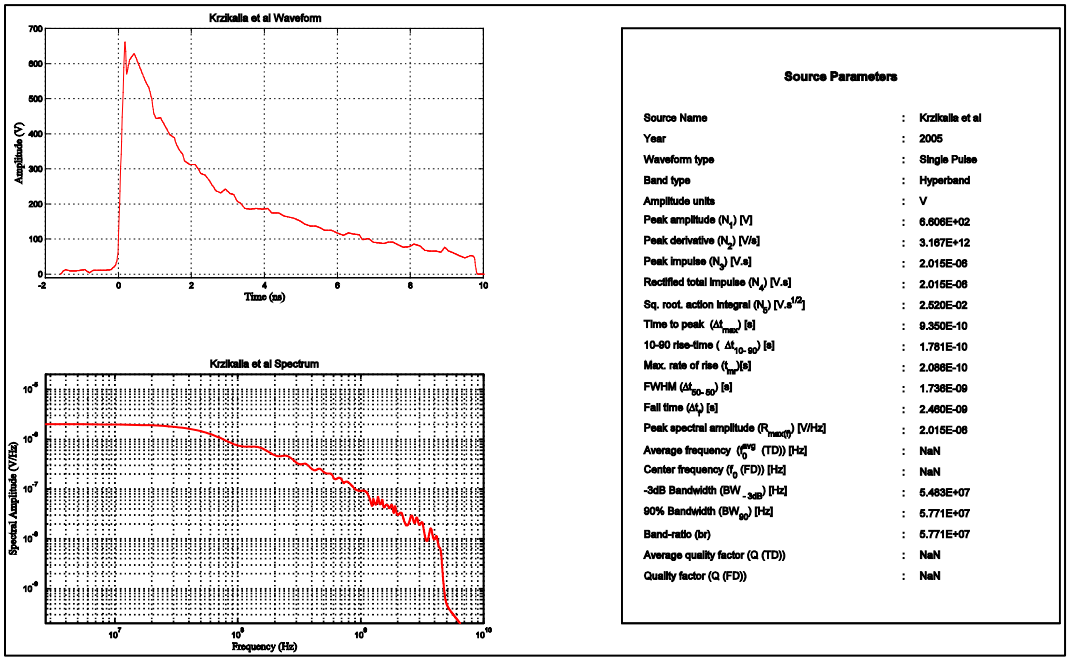

Source Parameters

Source Name	:	Krzikalla et al
Year	:	2005
Waveform type	:	Single Pulse
Band type	:	Hyperband
Amplitude units	:	V
Peak amplitude (N_1) [V]	:	6.606E+02
Peak derivative (N_2) [V/s]	:	3.167E+12
Peak impulse (N_3) [V.s]	:	2.015E-06
Rectified total impulse (N_4) [V.s]	:	2.015E-06
Sq. root. action integral (N_5) [V.s$^{1/2}$]	:	2.520E-02
Time to peak (Δt_{max}) [s]	:	9.350E-10
10-90 rise-time (Δt_{10-90}) [s]	:	1.761E-10
Max. rate of rise (t_{mr})[s]	:	2.086E-10
FWHM (Δt_{50-50}) [s]	:	1.736E-09
Fall time (Δt_f) [s]	:	2.460E-09
Peak spectral amplitude ($R_{max(f)}$) [V/Hz]	:	2.015E-06
Average frequency (f_0^{avg} (TD)) [Hz]	:	NaN
Center frequency (f_0 (FD)) [Hz]	:	NaN
-3dB Bandwidth (BW_{-3dB}) [Hz]	:	5.483E+07
90% Bandwidth (BW_{90}) [Hz]	:	5.771E+07
Band-ratio (br)	:	5.771E+07
Average quality factor (Q (TD))	:	NaN
Quality factor (Q (FD))	:	NaN

A-2.7 Power Spectra PGS-402 in [A-6]

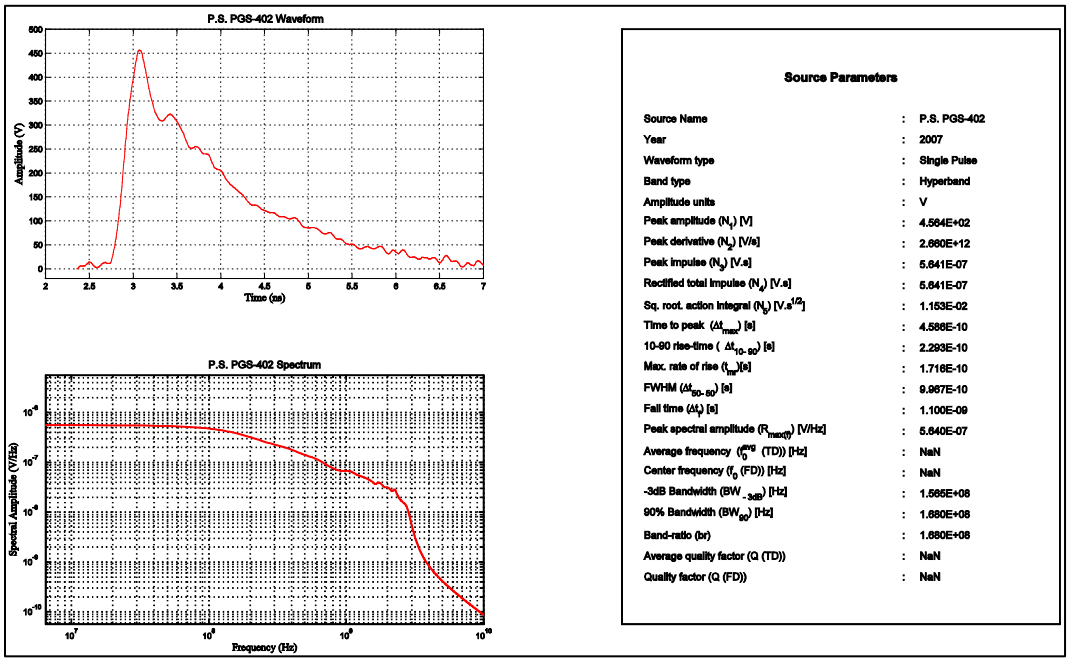

Source Parameters

Source Name	:	P.S. PGS-402
Year	:	2007
Waveform type	:	Single Pulse
Band type	:	Hyperband
Amplitude units	:	V
Peak amplitude (N_1) [V]	:	4.564E+02
Peak derivative (N_2) [V/s]	:	2.660E+12
Peak impulse (N_3) [V.s]	:	5.641E-07
Rectified total impulse (N_4) [V.s]	:	5.641E-07
Sq. root. action integral (N_0) [V.s$^{1/2}$]	:	1.153E-02
Time to peak (Δt_{max}) [s]	:	4.588E-10
10-90 rise-time (Δt_{10-90}) [s]	:	2.293E-10
Max. rate of rise (t_{mr})[s]	:	1.716E-10
FWHM (Δt_{50-50}) [s]	:	9.967E-10
Fall time (Δt_f) [s]	:	1.100E-09
Peak spectral amplitude ($R_{max(f)}$) [V/Hz]	:	5.640E-07
Average frequency (f_0^{avg} (TD)) [Hz]	:	NaN
Center frequency (f_0 (FD)) [Hz]	:	NaN
-3dB Bandwidth (BW_{-3dB}) [Hz]	:	1.565E+08
90% Bandwidth (BW_{90}) [Hz]	:	1.680E+08
Band-ratio (br)	:	1.680E+08
Average quality factor (Q (TD))	:	NaN
Quality factor (Q (FD))	:	NaN

A-2.8 RADAN 303B UWB Voltage Source in [A-7]

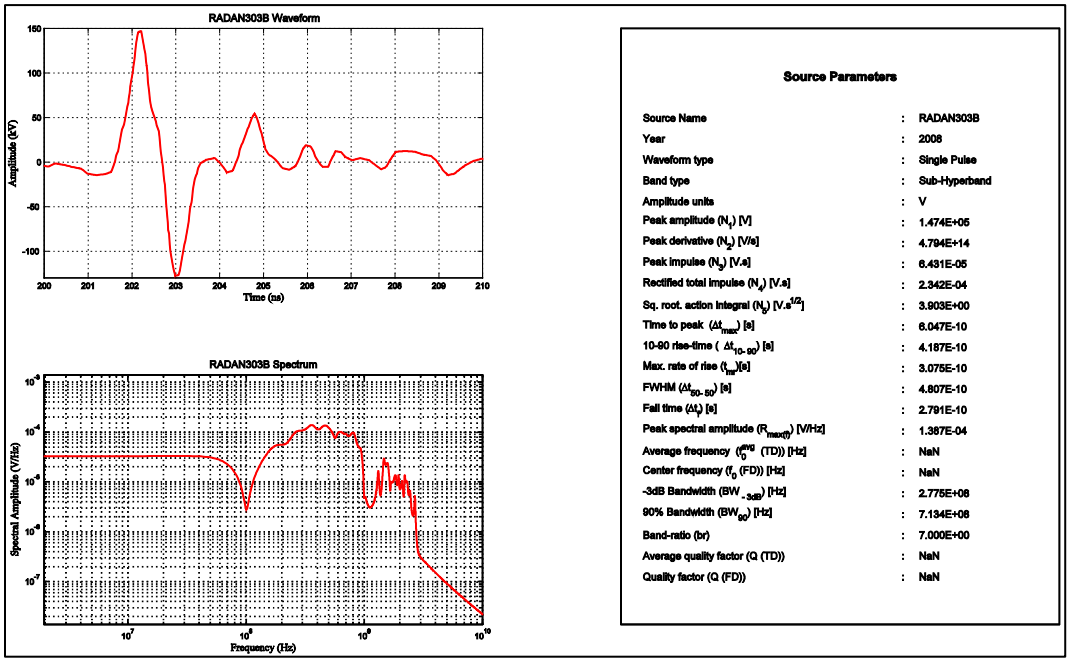

Source Parameters

Source Name	:	RADAN303B
Year	:	2008
Waveform type	:	Single Pulse
Band type	:	Sub-Hyperband
Amplitude units	:	V
Peak amplitude (N_1) [V]	:	1.474E+05
Peak derivative (N_2) [V/s]	:	4.794E+14
Peak impulse (N_3) [V.s]	:	6.431E-05
Rectified total impulse (N_4) [V.s]	:	2.342E-04
Sq. root. action integral (N_0) [V.s$^{1/2}$]	:	3.903E+00
Time to peak (Δt_{max}) [s]	:	6.047E-10
10-90 rise-time (Δt_{10-90}) [s]	:	4.187E-10
Max. rate of rise (t_{mr})[s]	:	3.075E-10
FWHM (Δt_{50-50}) [s]	:	4.807E-10
Fall time (Δt_f) [s]	:	2.791E-10
Peak spectral amplitude ($R_{max(f)}$) [V/Hz]	:	1.387E-04
Average frequency (f_0^{avg} (TD)) [Hz]	:	NaN
Center frequency (f_0 (FD)) [Hz]	:	NaN
-3dB Bandwidth (BW_{-3dB}) [Hz]	:	2.775E+08
90% Bandwidth (BW_{90}) [Hz]	:	7.134E+08
Band-ratio (br)	:	7.000E+00
Average quality factor (Q (TD))	:	NaN
Quality factor (Q (FD))	:	NaN

A-2.9 HYPS pulsed voltage source in [A-8]

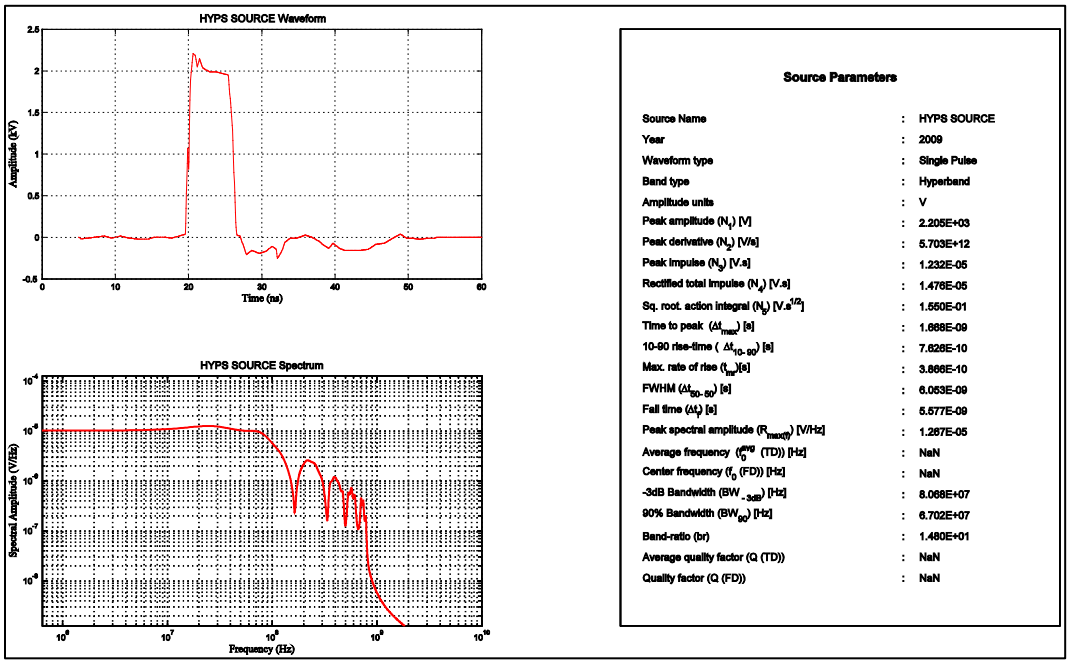

Source Parameters

Source Name	:	HYPS SOURCE
Year	:	2009
Waveform type	:	Single Pulse
Band type	:	Hyperband
Amplitude units	:	V
Peak amplitude (N_a) [V]	:	2.205E+03
Peak derivative (N_d) [V/s]	:	5.703E+12
Peak impulse (N_p) [V.s]	:	1.232E-05
Rectified total impulse (N_e) [V.s]	:	1.476E-05
Sq. root. action integral (N_b) [V.s$^{1/2}$]	:	1.550E-01
Time to peak (Δt_{max}) [s]	:	1.668E-09
10-90 rise-time (Δt_{10-90}) [s]	:	7.626E-10
Max. rate of rise (t_{rm})[s]	:	3.866E-10
FWHM (Δt_{50-50}) [s]	:	6.053E-09
Fall time (Δt_f) [s]	:	5.577E-09
Peak spectral amplitude ($R_{max(f)}$) [V/Hz]	:	1.287E-05
Average frequency (f_0^{avg} (TD)) [Hz]	:	NaN
Center frequency (f_0 (FD)) [Hz]	:	NaN
-3dB Bandwidth (BW_{-3dB}) [Hz]	:	8.068E+07
90% Bandwidth (BW_{90}) [Hz]	:	6.702E+07
Band-ratio (br)	:	1.480E+01
Average quality factor (Q (TD))	:	NaN
Quality factor (Q (FD))	:	NaN

A-2.10 Impulse Voltage Source in [A-9]

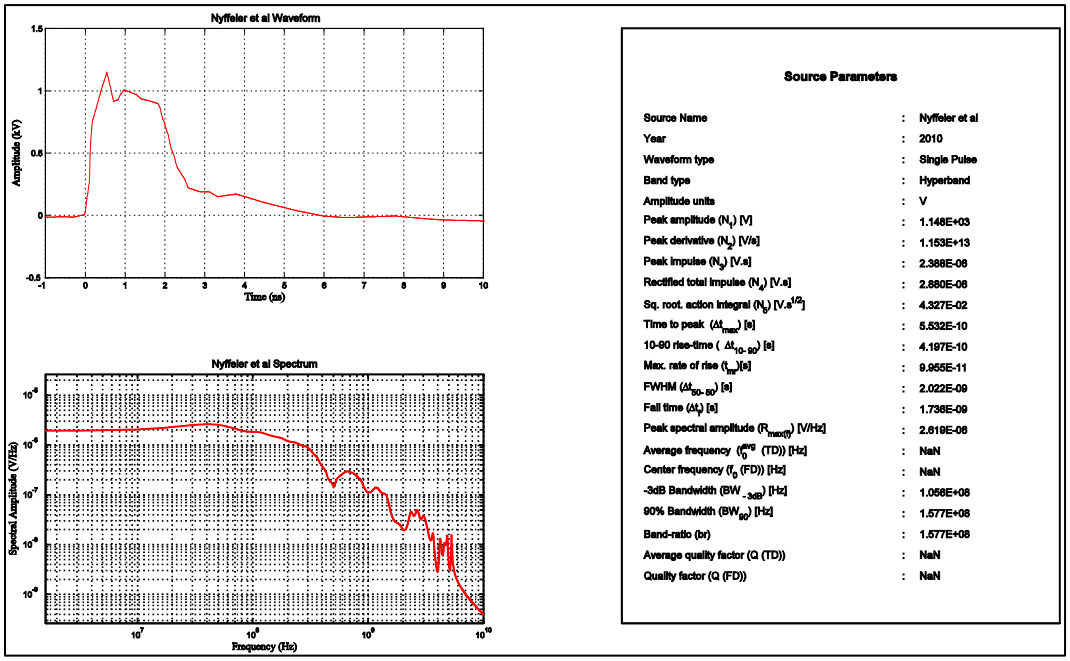

Source Parameters

Source Name	:	Nyffeler et al
Year	:	2010
Waveform type	:	Single Pulse
Band type	:	Hyperband
Amplitude units	:	V
Peak amplitude (N_a) [V]	:	1.148E+03
Peak derivative (N_d) [V/s]	:	1.153E+13
Peak impulse (N_p) [V.s]	:	2.388E-06
Rectified total impulse (N_e) [V.s]	:	2.880E-06
Sq. root. action integral (N_b) [V.s$^{1/2}$]	:	4.327E-02
Time to peak (Δt_{max}) [s]	:	5.532E-10
10-90 rise-time (Δt_{10-90}) [s]	:	4.197E-10
Max. rate of rise (t_{rm})[s]	:	9.955E-11
FWHM (Δt_{50-50}) [s]	:	2.022E-09
Fall time (Δt_f) [s]	:	1.736E-09
Peak spectral amplitude ($R_{max(f)}$) [V/Hz]	:	2.619E-06
Average frequency (f_0^{avg} (TD)) [Hz]	:	NaN
Center frequency (f_0 (FD)) [Hz]	:	NaN
-3dB Bandwidth (BW_{-3dB}) [Hz]	:	1.056E+08
90% Bandwidth (BW_{90}) [Hz]	:	1.577E+08
Band-ratio (br)	:	1.577E+08
Average quality factor (Q (TD))	:	NaN
Quality factor (Q (FD))	:	NaN

A-2.11 Stun Gun in [A-10]

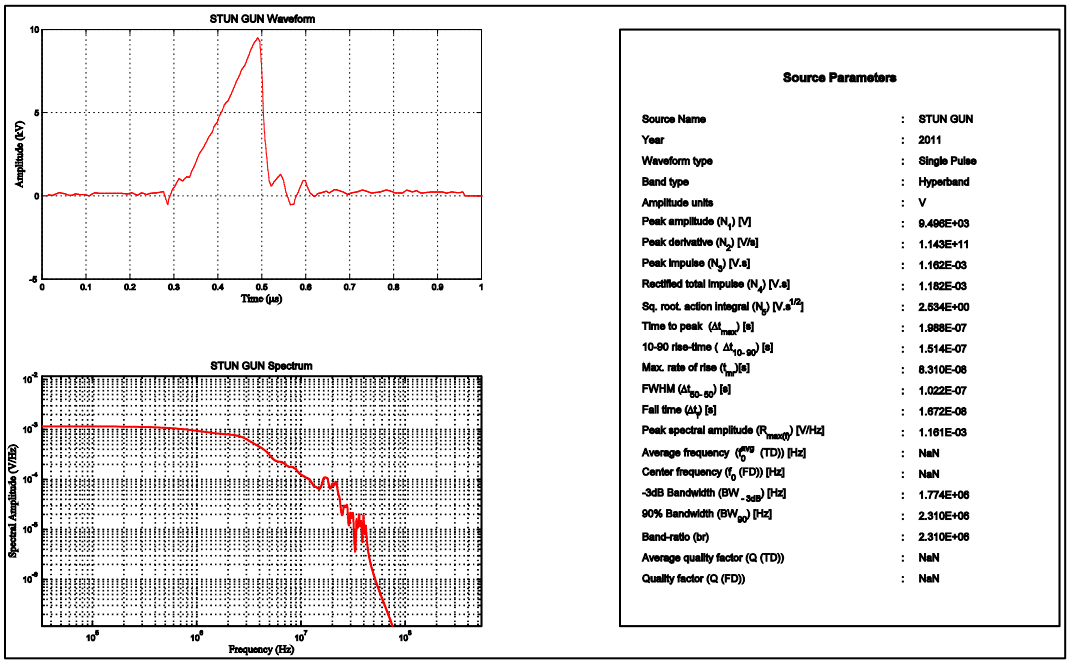

Source Parameters

Source Name	:	STUN GUN
Year	:	2011
Waveform type	:	Single Pulse
Band type	:	Hyperband
Amplitude units	:	V
Peak amplitude (N_1) [V]	:	9.498E+03
Peak derivative (N_2) [V/s]	:	1.143E+11
Peak impulse (N_3) [V.s]	:	1.162E-03
Rectified total impulse (N_4) [V.s]	:	1.182E-03
Sq. root. action integral (N_5) [V.s$^{1/2}$]	:	2.634E+00
Time to peak (Δt_{max}) [s]	:	1.988E-07
10-90 rise-time (Δt_{10-90}) [s]	:	1.514E-07
Max. rate of rise (t_{mr})[s]	:	8.310E-08
FWHM (Δt_{50-50}) [s]	:	1.022E-07
Fall time (Δt_f) [s]	:	1.672E-08
Peak spectral amplitude ($R_{max(f)}$) [V/Hz]	:	1.161E-03
Average frequency (f_0^{avg} (TD)) [Hz]	:	NaN
Center frequency (f_0 (FD)) [Hz]	:	NaN
-3dB Bandwidth (BW_{-3dB}) [Hz]	:	1.774E+06
90% Bandwidth (BW_{90}) [Hz]	:	2.310E+06
Band-ratio (br)	:	2.310E+06
Average quality factor (Q (TD))	:	NaN
Quality factor (Q (FD))	:	NaN

A-3 RADIATED SOURCES

A-3.1 H2 source in [A-3]

Measurement distance 10m

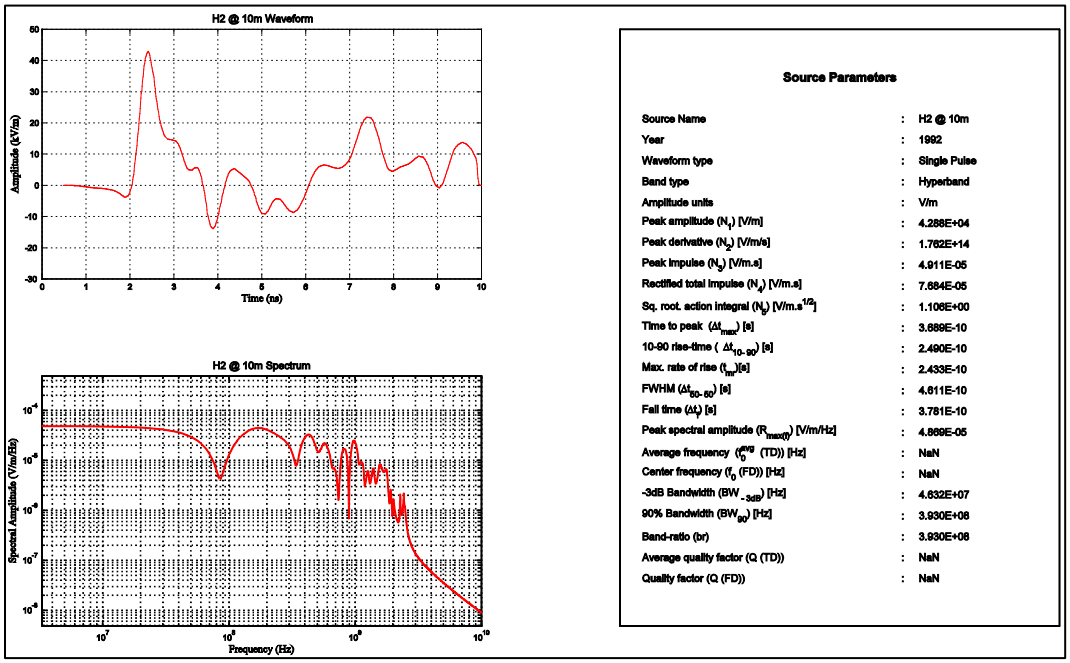

Source Parameters

Source Name	:	H2 @ 10m
Year	:	1992
Waveform type	:	Single Pulse
Band type	:	Hyperband
Amplitude units	:	V/m
Peak amplitude (N_1) [V/m]	:	4.288E+04
Peak derivative (N_2) [V/m/s]	:	1.762E+14
Peak Impulse (N_3) [V/m.s]	:	4.911E-05
Rectified total impulse (N_4) [V/m.s]	:	7.684E-05
Sq. root. action integral (N_5) [V/m.s$^{1/2}$]	:	1.108E+00
Time to peak (Δt_{max}) [s]	:	3.689E-10
10-90 rise-time (Δt_{10-90}) [s]	:	2.490E-10
Max. rate of rise (t_{rm})[s]	:	2.433E-10
FWHM (Δt_{50-50}) [s]	:	4.611E-10
Fall time (Δt_f) [s]	:	3.781E-10
Peak spectral amplitude ($R_{max(f)}$) [V/m/Hz]	:	4.869E-05
Average frequency (f_0^{avg} (TD)) [Hz]	:	NaN
Center frequency (f_0 (FD)) [Hz]	:	NaN
-3dB Bandwidth (BW_{-3dB}) [Hz]	:	4.632E+07
90% Bandwidth (BW_{90}) [Hz]	:	3.930E+08
Band-ratio (br)	:	3.930E+08
Average quality factor (Q (TD))	:	NaN
Quality factor (Q (FD))	:	NaN

A-3.2 IRA II in [A-3]

Measurement distance Not specified

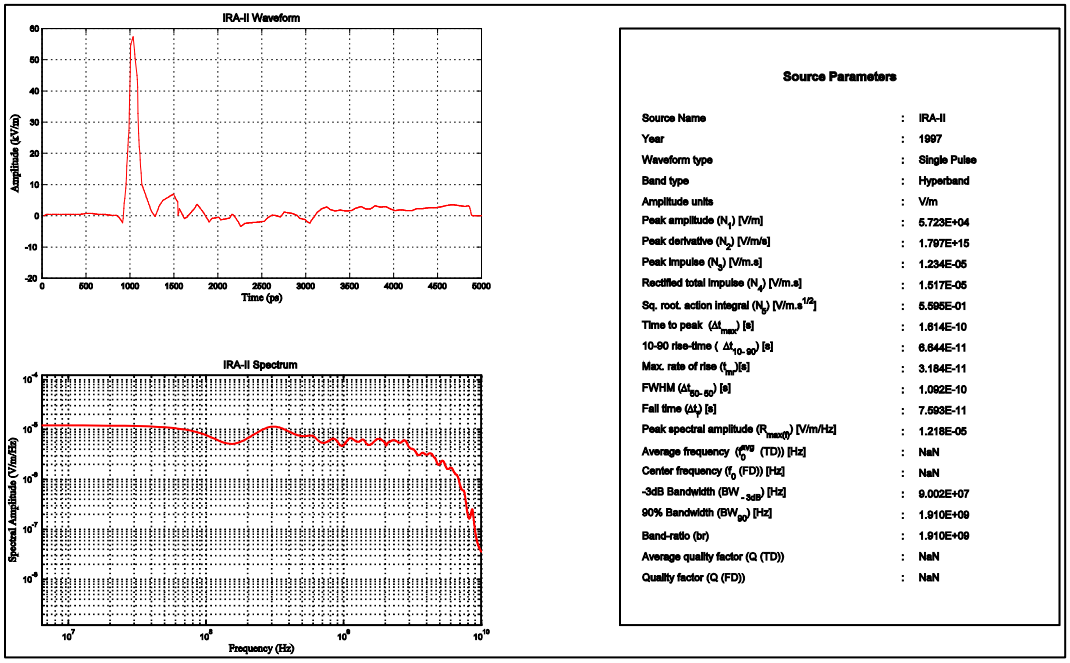

Source Parameters

Source Name	:	IRA-II
Year	:	1997
Waveform type	:	Single Pulse
Band type	:	Hyperband
Amplitude units	:	V/m
Peak amplitude (N_1) [V/m]	:	5.723E+04
Peak derivative (N_2) [V/m/s]	:	1.797E+15
Peak Impulse (N_3) [V/m.s]	:	1.234E-05
Rectified total impulse (N_4) [V/m.s]	:	1.517E-05
Sq. root. action integral (N_5) [V/m.s$^{1/2}$]	:	5.595E-01
Time to peak (Δt_{max}) [s]	:	1.614E-10
10-90 rise-time (Δt_{10-90}) [s]	:	6.644E-11
Max. rate of rise (t_{rm})[s]	:	3.184E-11
FWHM (Δt_{50-50}) [s]	:	1.092E-10
Fall time (Δt_f) [s]	:	7.593E-11
Peak spectral amplitude ($R_{max(f)}$) [V/m/Hz]	:	1.218E-05
Average frequency (f_0^{avg} (TD)) [Hz]	:	NaN
Center frequency (f_0 (FD)) [Hz]	:	NaN
-3dB Bandwidth (BW_{-3dB}) [Hz]	:	9.002E+07
90% Bandwidth (BW_{90}) [Hz]	:	1.910E+09
Band-ratio (br)	:	1.910E+09
Average quality factor (Q (TD))	:	NaN
Quality factor (Q (FD))	:	NaN

A-3.3 JOLT in [A-11]

Measurement distance 10m (analytical)

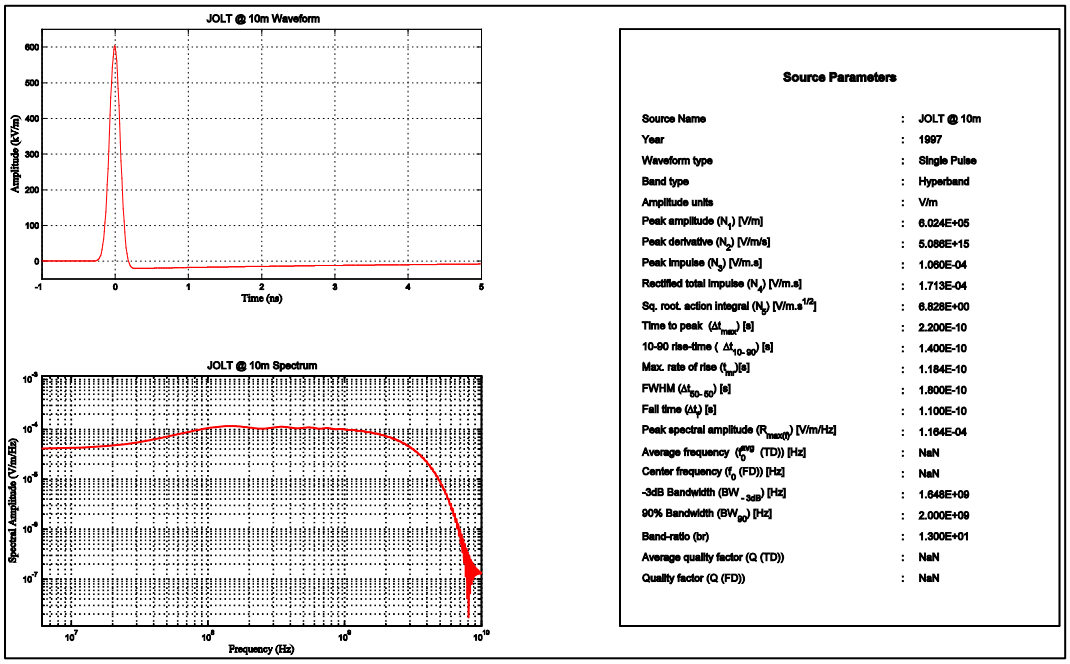

A-3.4 AFRL Solid State Generator in [A-3]

Measurement distance Not specified

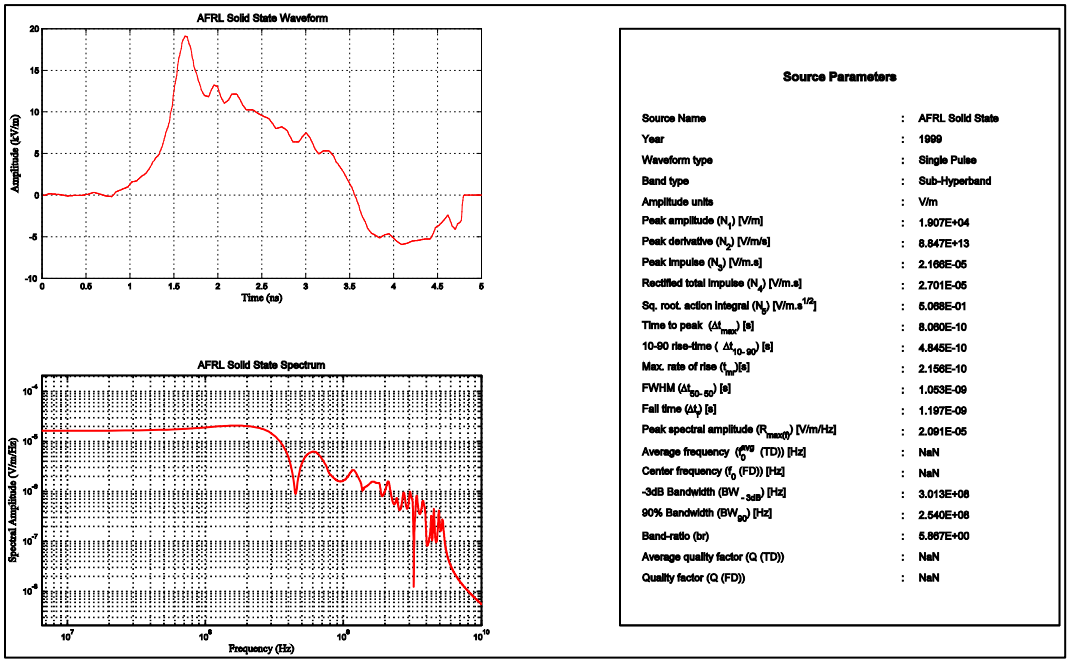

A-3.5 Marx Generator + Exponential TEM Horn Antenna in [A-12]

Measurement distance 100m

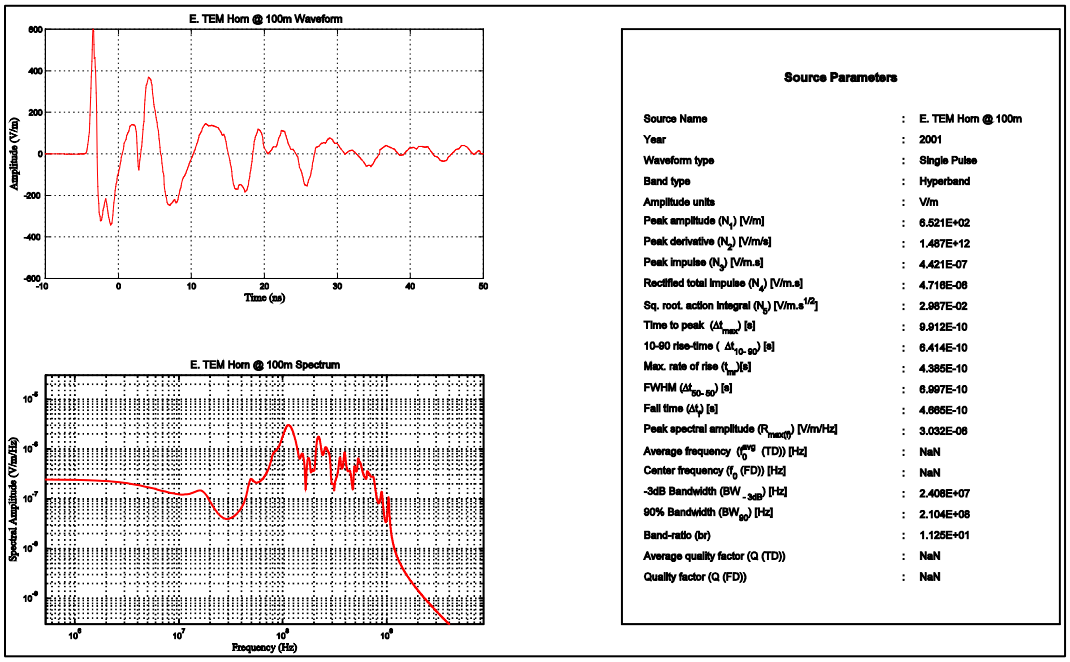

A-3.6 Marx Generator + Half TEM Horn Antenna in [A-12]

Measurement distance 100m

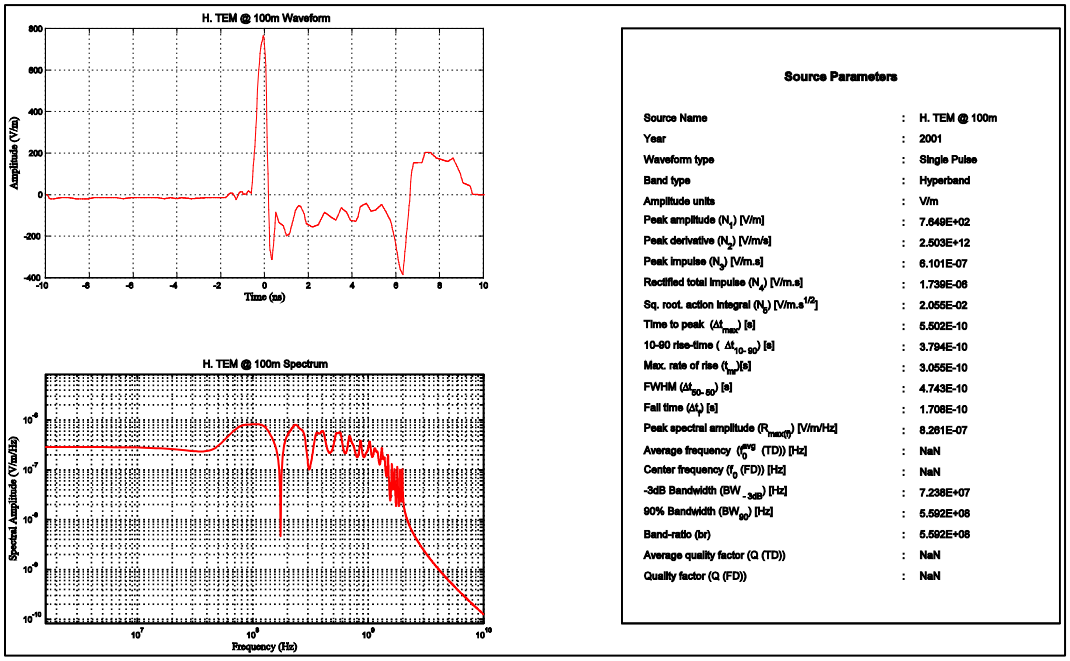

A-3.7 Marx Generator + Helical Antenna in [A-12]

Measurement distance 100m

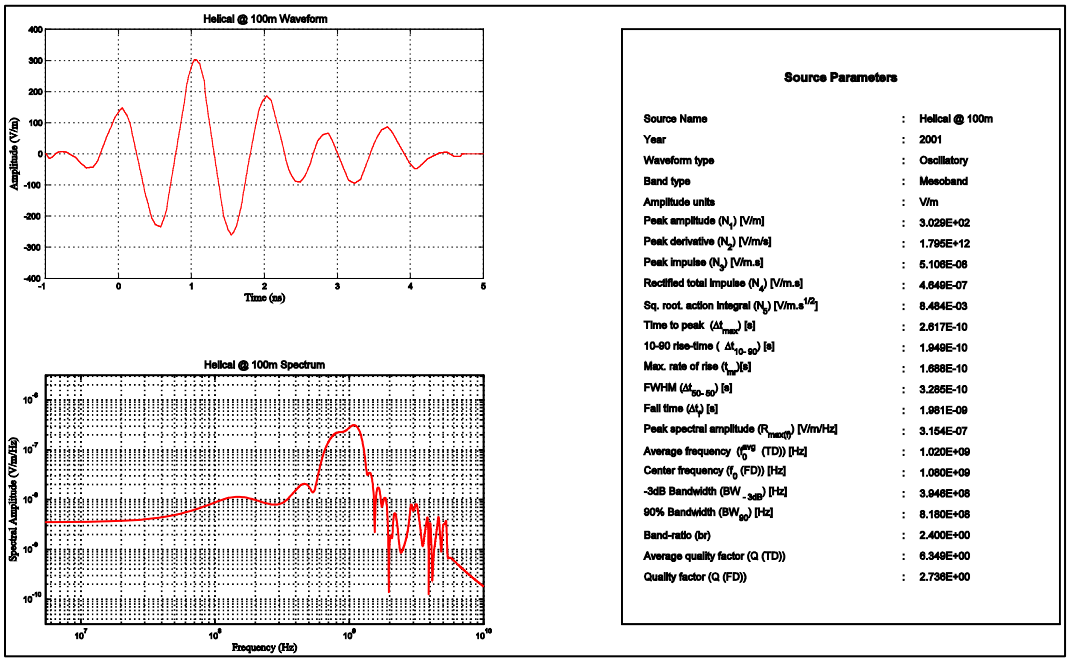

Source Parameters

Source Name	:	Helical @ 100m
Year	:	2001
Waveform type	:	Oscillatory
Band type	:	Mesoband
Amplitude units	:	V/m
Peak amplitude (N_1) [V/m]	:	3.029E+02
Peak derivative (N_2) [V/m/s]	:	1.795E+12
Peak impulse (N_3) [V/m.s]	:	5.106E-08
Rectified total impulse (N_4) [V/m.s]	:	4.649E-07
Sq. root. action integral (N_5) [V/m.s$^{1/2}$]	:	8.484E-03
Time to peak (Δt_{max}) [s]	:	2.617E-10
10-90 rise-time (Δt_{10-90}) [s]	:	1.949E-10
Max. rate of rise (t_{mr})[s]	:	1.688E-10
FWHM (Δt_{50-50}) [s]	:	3.285E-10
Fall time (Δt_f) [s]	:	1.981E-09
Peak spectral amplitude ($R_{max(f)}$) [V/m/Hz]	:	3.154E-07
Average frequency (f_0^{avg} (TD)) [Hz]	:	1.020E+09
Center frequency (f_0 (FD)) [Hz]	:	1.080E+09
-3dB Bandwidth (BW_{-3dB}) [Hz]	:	3.946E+08
90% Bandwidth (BW_{90}) [Hz]	:	8.180E+08
Band-ratio (br)	:	2.400E+00
Average quality factor (Q (TD))	:	6.349E+00
Quality factor (Q (FD))	:	2.736E+00

A-3.8 Marx Generator + Monopole Antenna in [A-12]

Measurement distance 100m

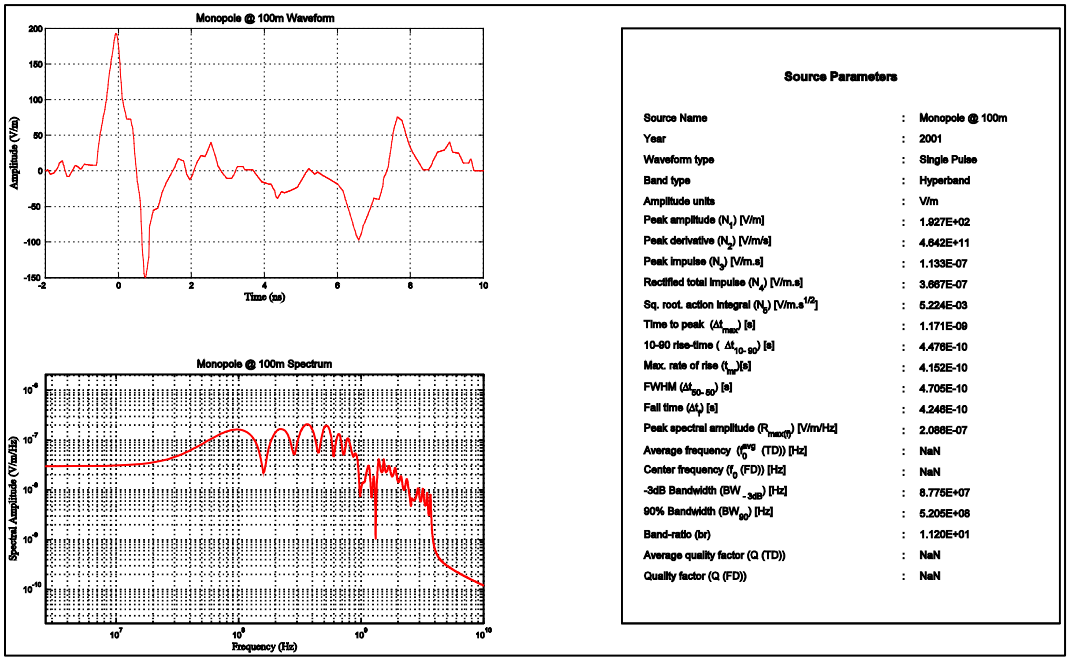

Source Parameters

Source Name	:	Monopole @ 100m
Year	:	2001
Waveform type	:	Single Pulse
Band type	:	Hyperband
Amplitude units	:	V/m
Peak amplitude (N_1) [V/m]	:	1.927E+02
Peak derivative (N_2) [V/m/s]	:	4.642E+11
Peak impulse (N_3) [V/m.s]	:	1.133E-07
Rectified total impulse (N_4) [V/m.s]	:	3.667E-07
Sq. root. action integral (N_5) [V/m.s$^{1/2}$]	:	5.224E-03
Time to peak (Δt_{max}) [s]	:	1.171E-09
10-90 rise-time (Δt_{10-90}) [s]	:	4.476E-10
Max. rate of rise (t_{mr})[s]	:	4.152E-10
FWHM (Δt_{50-50}) [s]	:	4.705E-10
Fall time (Δt_f) [s]	:	4.246E-10
Peak spectral amplitude ($R_{max(f)}$) [V/m/Hz]	:	2.088E-07
Average frequency (f_0^{avg} (TD)) [Hz]	:	NaN
Center frequency (f_0 (FD)) [Hz]	:	NaN
-3dB Bandwidth (BW_{-3dB}) [Hz]	:	8.775E+07
90% Bandwidth (BW_{90}) [Hz]	:	5.205E+08
Band-ratio (br)	:	1.120E+01
Average quality factor (Q (TD))	:	NaN
Quality factor (Q (FD))	:	NaN

A-3.9 DIEHL DS-110 Generator in [A-3]

Measurement distance 1m

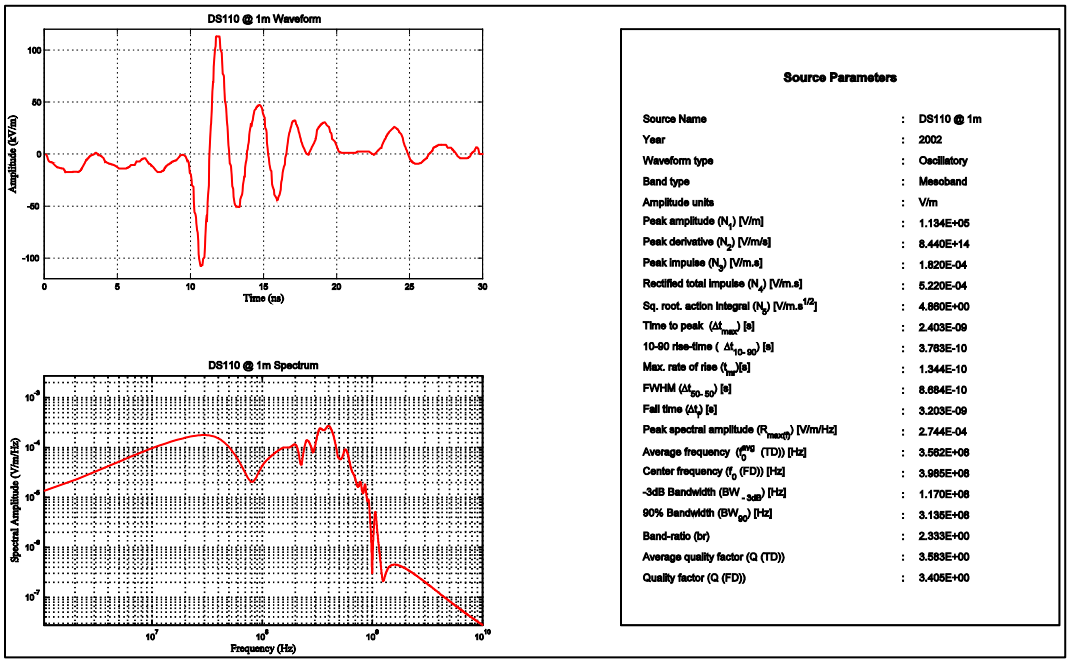

A-3.10 Compact resonant antenna source system in [A-13]

Measurement distance 15m

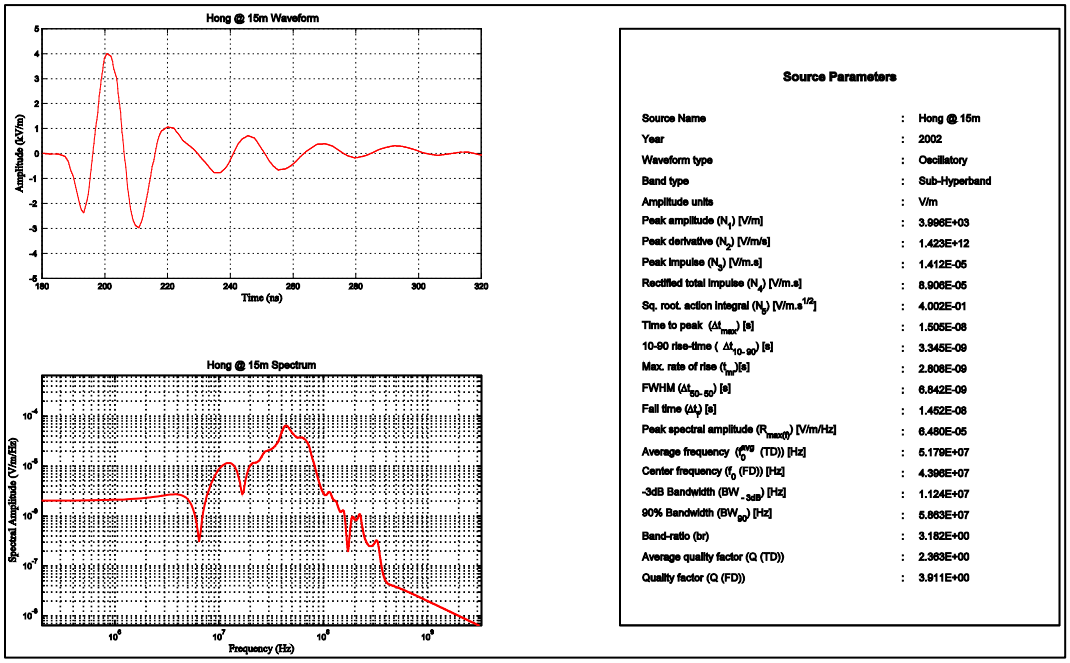

A-3.11 Para-IRA in [A-14]

Measurement distance 12.2m

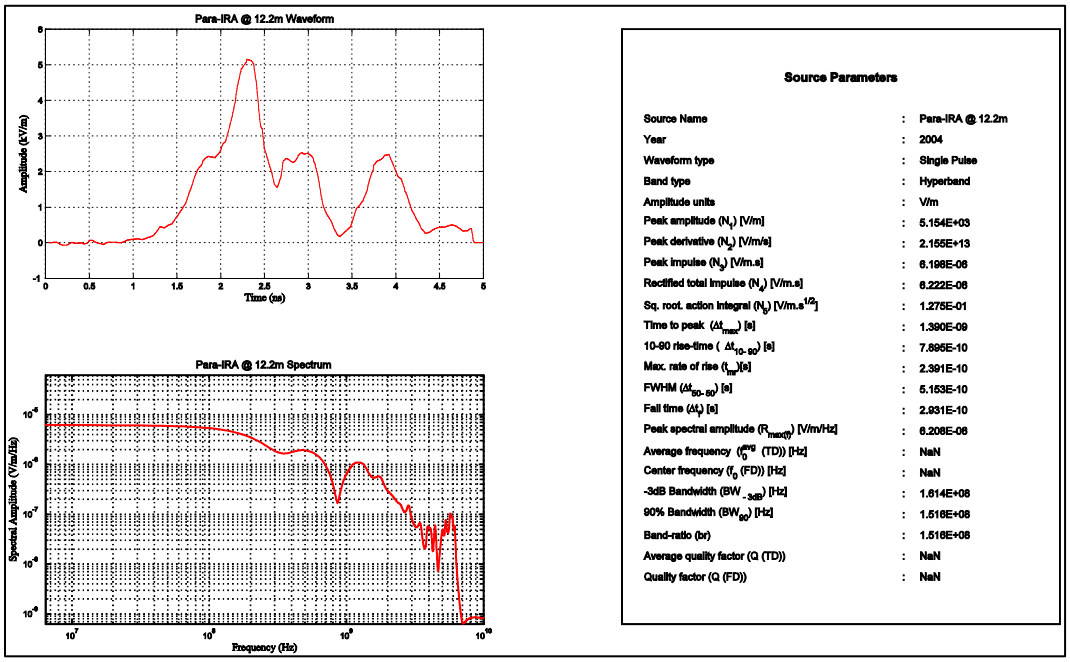

Source Parameters

Source Name	:	Para-IRA @ 12.2m
Year	:	2004
Waveform type	:	Single Pulse
Band type	:	Hyperband
Amplitude units	:	V/m
Peak amplitude (N_1) [V/m]	:	5.154E+03
Peak derivative (N_2) [V/m/s]	:	2.155E+13
Peak impulse (N_3) [V/m.s]	:	6.198E-06
Rectified total impulse (N_4) [V/m.s]	:	6.222E-06
Sq. root. action integral (N_5) [V/m.s$^{1/2}$]	:	1.275E-01
Time to peak (Δt_{max}) [s]	:	1.390E-09
10-90 rise-time (Δt_{10-90}) [s]	:	7.895E-10
Max. rate of rise (t_{mr})[s]	:	2.391E-10
FWHM (Δt_{50-50}) [s]	:	5.153E-10
Fall time (Δt_f) [s]	:	2.931E-10
Peak spectral amplitude ($R_{max(f)}$) [V/m/Hz]	:	6.208E-06
Average frequency (f_0^{avg} (TD)) [Hz]	:	NaN
Center frequency (f_0 (FD)) [Hz]	:	NaN
-3dB Bandwidth (BW_{-3dB}) [Hz]	:	1.614E+08
90% Bandwidth (BW_{90}) [Hz]	:	1.516E+08
Band-ratio (br)	:	1.516E+08
Average quality factor (Q (TD))	:	NaN
Quality factor (Q (FD))	:	NaN

A-3.12 IRA-6 in [A-4]

Measurement distance 20.4m

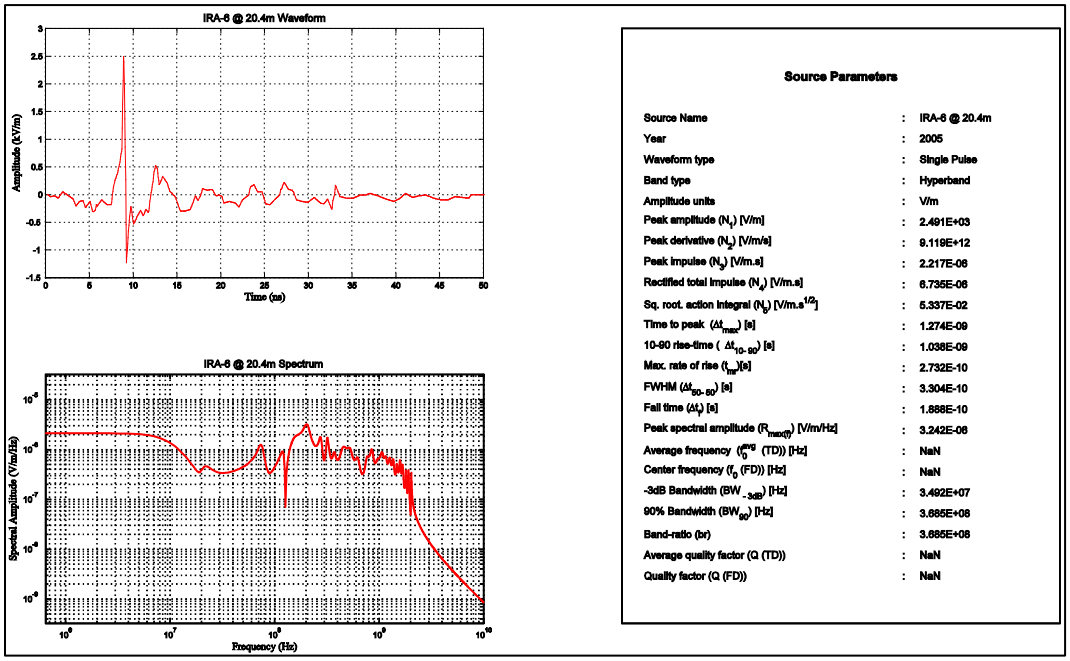

Source Parameters

Source Name	:	IRA-6 @ 20.4m
Year	:	2005
Waveform type	:	Single Pulse
Band type	:	Hyperband
Amplitude units	:	V/m
Peak amplitude (N_1) [V/m]	:	2.491E+03
Peak derivative (N_2) [V/m/s]	:	9.119E+12
Peak impulse (N_3) [V/m.s]	:	2.217E-06
Rectified total impulse (N_4) [V/m.s]	:	6.735E-06
Sq. root. action integral (N_5) [V/m.s$^{1/2}$]	:	5.337E-02
Time to peak (Δt_{max}) [s]	:	1.274E-09
10-90 rise-time (Δt_{10-90}) [s]	:	1.038E-09
Max. rate of rise (t_{mr})[s]	:	2.732E-10
FWHM (Δt_{50-50}) [s]	:	3.304E-10
Fall time (Δt_f) [s]	:	1.888E-10
Peak spectral amplitude ($R_{max(f)}$) [V/m/Hz]	:	3.242E-06
Average frequency (f_0^{avg} (TD)) [Hz]	:	NaN
Center frequency (f_0 (FD)) [Hz]	:	NaN
-3dB Bandwidth (BW_{-3dB}) [Hz]	:	3.492E+07
90% Bandwidth (BW_{90}) [Hz]	:	3.685E+08
Band-ratio (br)	:	3.685E+08
Average quality factor (Q (TD))	:	NaN
Quality factor (Q (FD))	:	NaN

A-3.13 High power compact microwave source in [A-15]

Measurement distance 9m

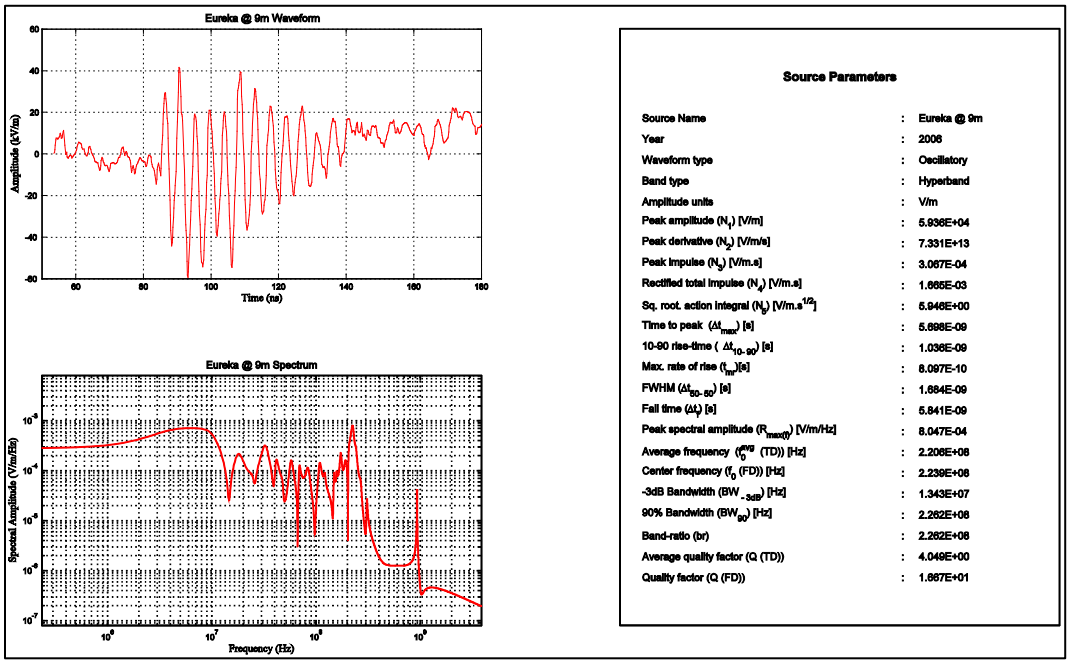

Source Parameters

Source Name	:	Eureka @ 9m
Year	:	2006
Waveform type	:	Oscillatory
Band type	:	Hyperband
Amplitude units	:	V/m
Peak amplitude (N_1) [V/m]	:	5.936E+04
Peak derivative (N_2) [V/m/s]	:	7.331E+13
Peak impulse (N_3) [V/m.s]	:	3.067E-04
Rectified total impulse (N_4) [V/m.s]	:	1.665E-03
Sq. root. action integral (N_5) [V/m.$s^{1/2}$]	:	5.946E+00
Time to peak (Δt_{max}) [s]	:	5.698E-09
10-90 rise-time (Δt_{10-90}) [s]	:	1.036E-09
Max. rate of rise (t_{mr})[s]	:	8.097E-10
FWHM (Δt_{50-50}) [s]	:	1.684E-09
Fall time (Δt_f) [s]	:	5.841E-09
Peak spectral amplitude ($R_{max(f)}$) [V/m/Hz]	:	8.047E-04
Average frequency (f_0^{avg} (TD)) [Hz]	:	2.206E+08
Center frequency (f_0 (FD)) [Hz]	:	2.239E+08
-3dB Bandwidth (BW_{-3dB}) [Hz]	:	1.343E+07
90% Bandwidth (BW_{90}) [Hz]	:	2.262E+08
Band-ratio (br)	:	2.262E+08
Average quality factor (Q (TD))	:	4.049E+00
Quality factor (Q (FD))	:	1.667E+01

A-3.14 UWB source, single Antenna in [A-16]

Measurement distance 10m

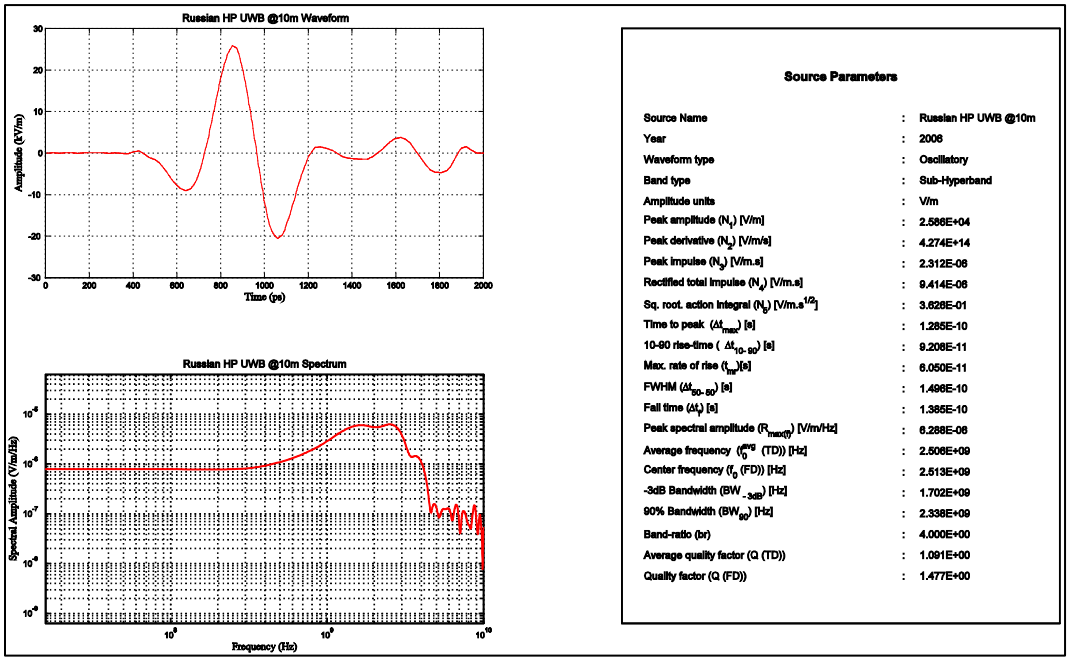

Source Parameters

Source Name	:	Russian HP UWB @10m
Year	:	2006
Waveform type	:	Oscillatory
Band type	:	Sub-Hyperband
Amplitude units	:	V/m
Peak amplitude (N_1) [V/m]	:	2.586E+04
Peak derivative (N_2) [V/m/s]	:	4.274E+14
Peak impulse (N_3) [V/m.s]	:	2.312E-06
Rectified total impulse (N_4) [V/m.s]	:	9.414E-06
Sq. root. action integral (N_5) [V/m.$s^{1/2}$]	:	3.628E-01
Time to peak (Δt_{max}) [s]	:	1.285E-10
10-90 rise-time (Δt_{10-90}) [s]	:	9.208E-11
Max. rate of rise (t_{mr})[s]	:	6.050E-11
FWHM (Δt_{50-50}) [s]	:	1.498E-10
Fall time (Δt_f) [s]	:	1.385E-10
Peak spectral amplitude ($R_{max(f)}$) [V/m/Hz]	:	6.288E-06
Average frequency (f_0^{avg} (TD)) [Hz]	:	2.506E+09
Center frequency (f_0 (FD)) [Hz]	:	2.513E+09
-3dB Bandwidth (BW_{-3dB}) [Hz]	:	1.702E+09
90% Bandwidth (BW_{90}) [Hz]	:	2.338E+09
Band-ratio (br)	:	4.000E+00
Average quality factor (Q (TD))	:	1.091E+00
Quality factor (Q (FD))	:	1.477E+00

A-3.15 George source + Valentine Antenna in [A-17]

Measurement distance 10m

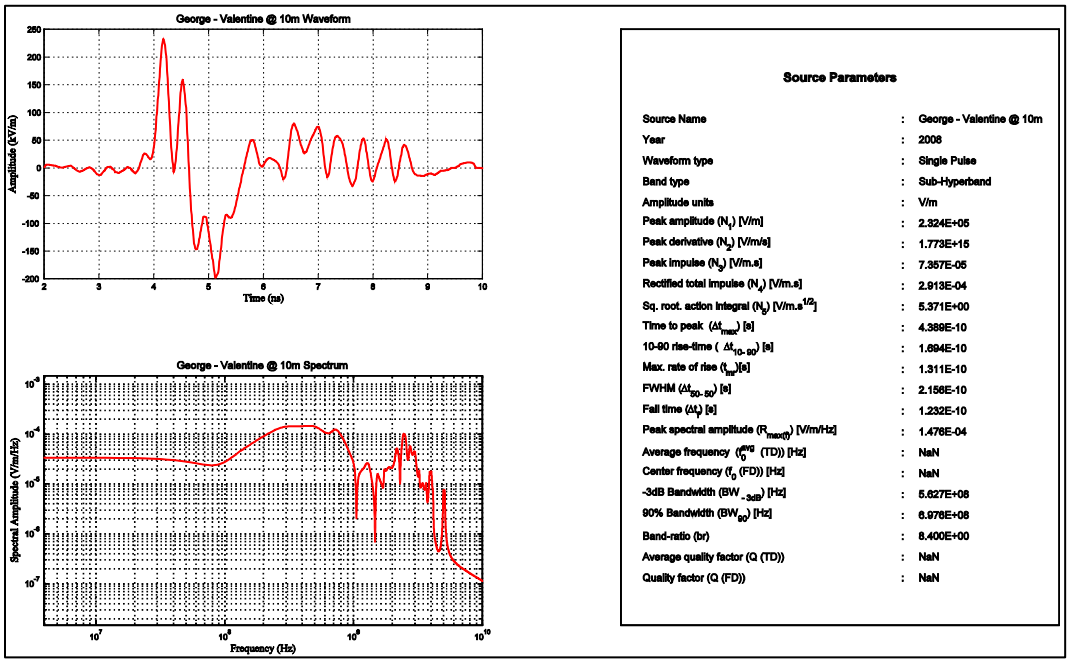

Source Parameters

Source Name	:	George - Valentine @ 10m
Year	:	2008
Waveform type	:	Single Pulse
Band type	:	Sub-Hyperband
Amplitude units	:	V/m
Peak amplitude (N_1) [V/m]	:	2.324E+05
Peak derivative (N_2) [V/m/s]	:	1.773E+15
Peak impulse (N_3) [V/m.s]	:	7.357E-05
Rectified total impulse (N_4) [V/m.s]	:	2.913E-04
Sq. root. action integral (N_5) [V/m.s$^{1/2}$]	:	5.371E+00
Time to peak (Δt_{max}) [s]	:	4.389E-10
10-90 rise-time (Δt_{10-90}) [s]	:	1.694E-10
Max. rate of rise (t_{rm})[s]	:	1.311E-10
FWHM (Δt_{50-50}) [s]	:	2.156E-10
Fall time (Δt_f) [s]	:	1.232E-10
Peak spectral amplitude ($R_{max(f)}$) [V/m/Hz]	:	1.476E-04
Average frequency (f_0^{avg} (TD)) [Hz]	:	NaN
Center frequency (f_0 (FD)) [Hz]	:	NaN
-3dB Bandwidth (BW_{-3dB}) [Hz]	:	5.627E+08
90% Bandwidth (BW_{90}) [Hz]	:	6.976E+08
Band-ratio (br)	:	8.400E+00
Average quality factor (Q (TD))	:	NaN
Quality factor (Q (FD))	:	NaN

A-3.16 Leonardo source + Valentine Antenna in [A-17]

Measurement distance 10m

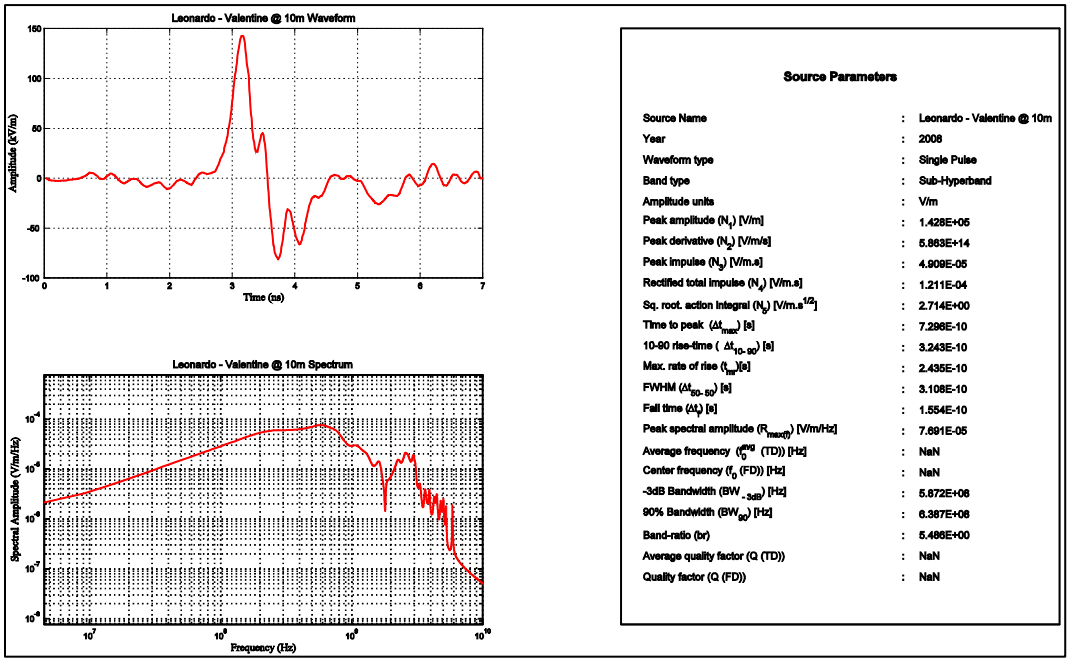

Source Parameters

Source Name	:	Leonardo - Valentine @ 10m
Year	:	2008
Waveform type	:	Single Pulse
Band type	:	Sub-Hyperband
Amplitude units	:	V/m
Peak amplitude (N_1) [V/m]	:	1.428E+05
Peak derivative (N_2) [V/m/s]	:	5.863E+14
Peak impulse (N_3) [V/m.s]	:	4.909E-05
Rectified total impulse (N_4) [V/m.s]	:	1.211E-04
Sq. root. action integral (N_5) [V/m.s$^{1/2}$]	:	2.714E+00
Time to peak (Δt_{max}) [s]	:	7.298E-10
10-90 rise-time (Δt_{10-90}) [s]	:	3.243E-10
Max. rate of rise (t_{rm})[s]	:	2.435E-10
FWHM (Δt_{50-50}) [s]	:	3.108E-10
Fall time (Δt_f) [s]	:	1.554E-10
Peak spectral amplitude ($R_{max(f)}$) [V/m/Hz]	:	7.691E-05
Average frequency (f_0^{avg} (TD)) [Hz]	:	NaN
Center frequency (f_0 (FD)) [Hz]	:	NaN
-3dB Bandwidth (BW_{-3dB}) [Hz]	:	5.872E+08
90% Bandwidth (BW_{90}) [Hz]	:	6.387E+08
Band-ratio (br)	:	5.486E+00
Average quality factor (Q (TD))	:	NaN
Quality factor (Q (FD))	:	NaN

A-3.17 GIMLI in [A-18]

Measurement distance 8m

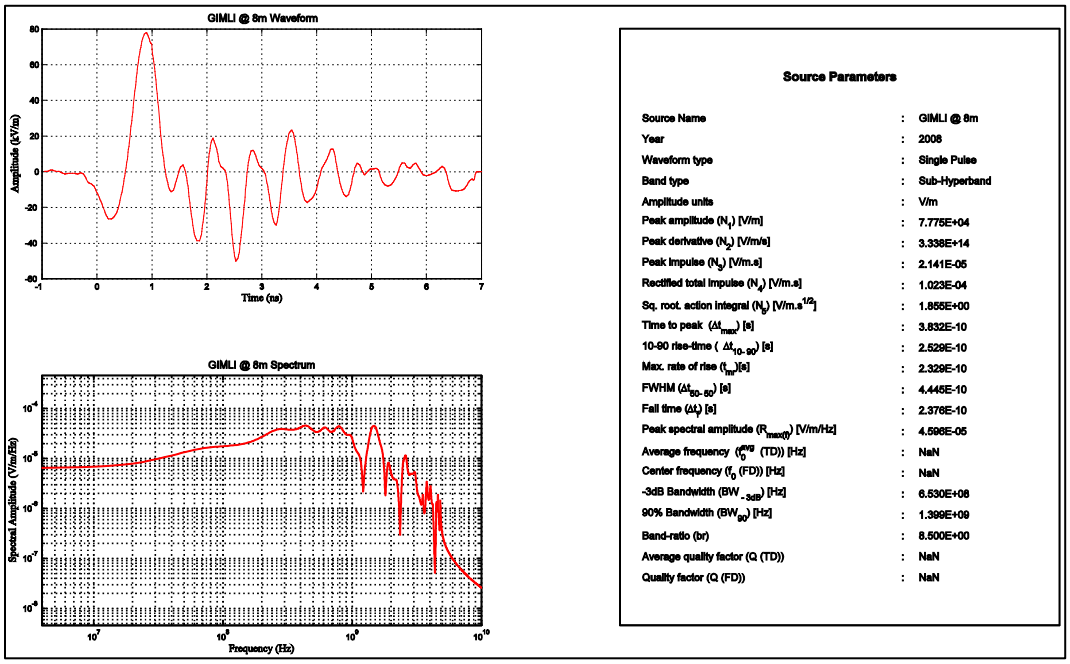

A-3.18 Ringing Dipole in [A-19]

Measurement distance 3m

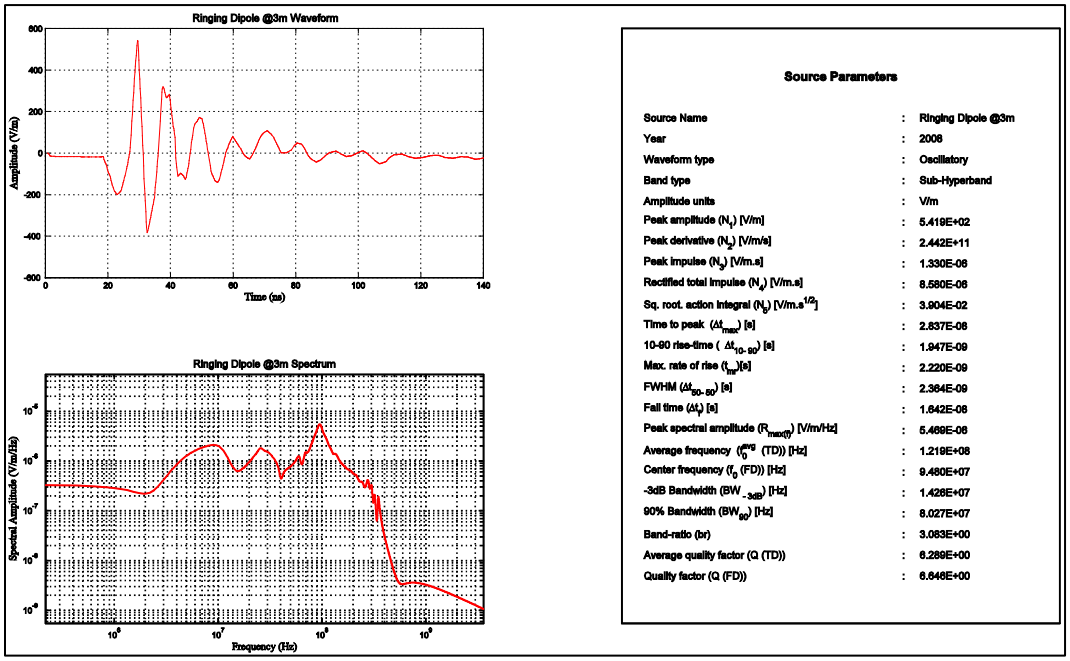

A-3.19 Ringing Log periodic antenna in [A-19]

Measurement distance 3m

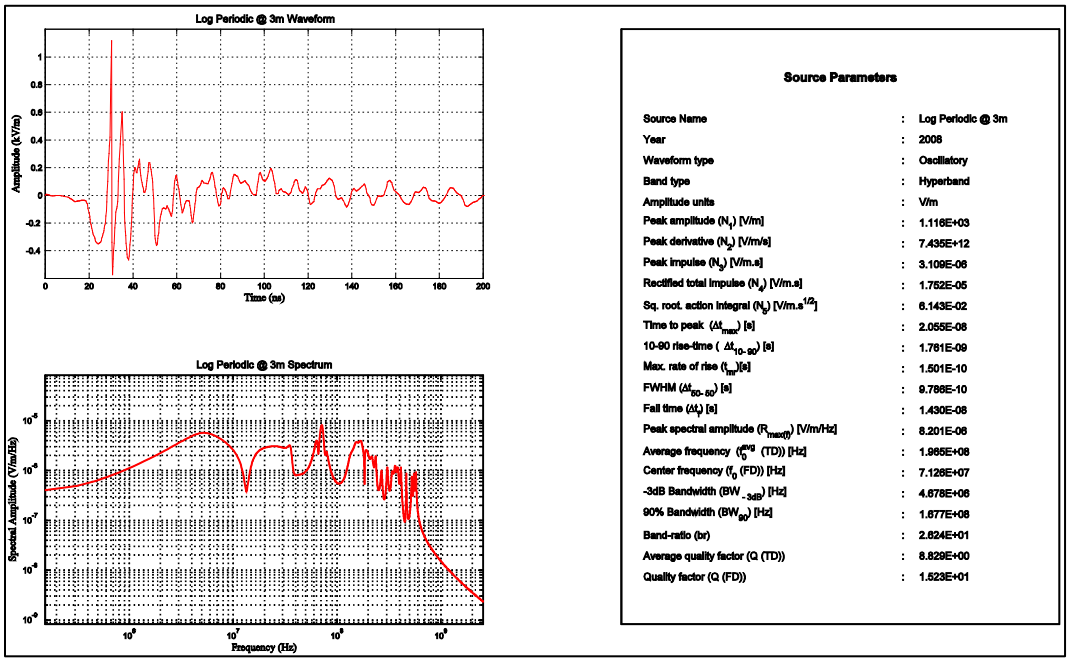

Source Parameters

Source Name	:	Log Periodic @ 3m
Year	:	2008
Waveform type	:	Oscillatory
Band type	:	Hyperband
Amplitude units	:	V/m
Peak amplitude (N_1) [V/m]	:	1.116E+03
Peak derivative (N_2) [V/m/s]	:	7.435E+12
Peak impulse (N_3) [V/m.s]	:	3.109E-06
Rectified total impulse (N_4) [V/m.s]	:	1.752E-05
Sq. root. action integral (N_5) [V/m.s$^{1/2}$]	:	6.143E-02
Time to peak (Δt_{max}) [s]	:	2.055E-08
10-90 rise-time (Δt_{10-90}) [s]	:	1.761E-09
Max. rate of rise (t_{mr})[s]	:	1.501E-10
FWHM (Δt_{50-50}) [s]	:	9.786E-10
Fall time (Δt_f) [s]	:	1.430E-08
Peak spectral amplitude ($R_{max(f)}$) [V/m/Hz]	:	8.201E-06
Average frequency (f_0^{avg} (TD)) [Hz]	:	1.965E+08
Center frequency (f_0 (FD)) [Hz]	:	7.126E+07
-3dB Bandwidth (BW_{-3dB}) [Hz]	:	4.678E+08
90% Bandwidth (BW_{90}) [Hz]	:	1.677E+08
Band-ratio (br)	:	2.624E+01
Average quality factor (Q (TD))	:	8.829E+00
Quality factor (Q (FD))	:	1.523E+01

A-3.20 HYPS Generator + IRA Antenna in [A-8]

Measurement distance 3m

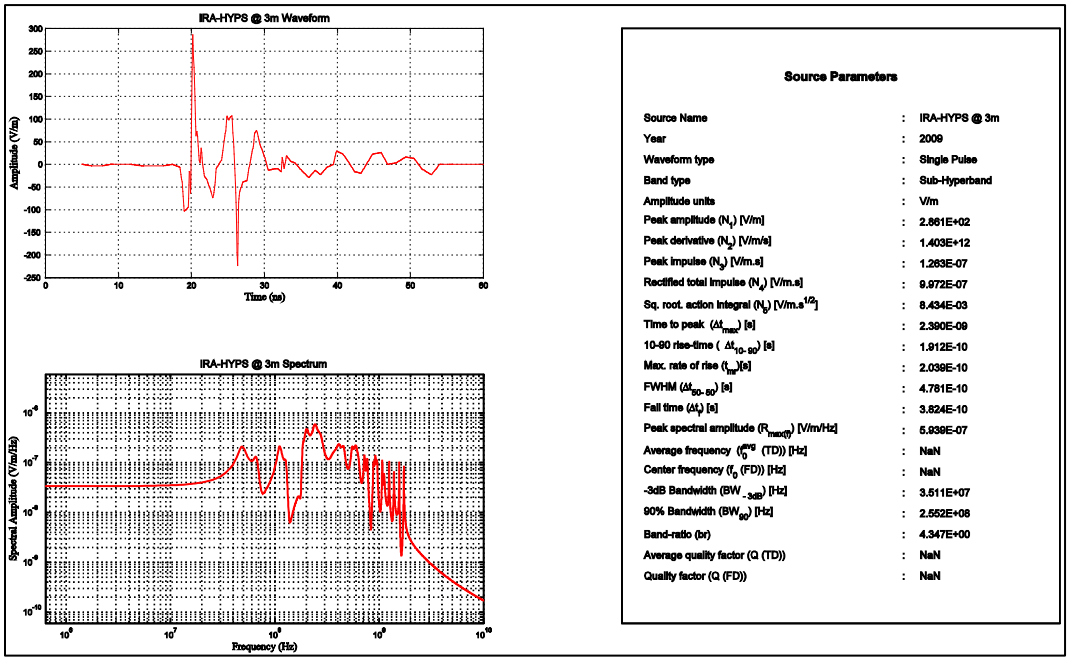

Source Parameters

Source Name	:	IRA-HYPS @ 3m
Year	:	2009
Waveform type	:	Single Pulse
Band type	:	Sub-Hyperband
Amplitude units	:	V/m
Peak amplitude (N_1) [V/m]	:	2.861E+02
Peak derivative (N_2) [V/m/s]	:	1.403E+12
Peak impulse (N_3) [V/m.s]	:	1.263E-07
Rectified total impulse (N_4) [V/m.s]	:	9.972E-07
Sq. root. action integral (N_5) [V/m.s$^{1/2}$]	:	8.434E-03
Time to peak (Δt_{max}) [s]	:	2.390E-09
10-90 rise-time (Δt_{10-90}) [s]	:	1.912E-10
Max. rate of rise (t_{mr})[s]	:	2.039E-10
FWHM (Δt_{50-50}) [s]	:	4.781E-10
Fall time (Δt_f) [s]	:	3.824E-10
Peak spectral amplitude ($R_{max(f)}$) [V/m/Hz]	:	5.939E-07
Average frequency (f_0^{avg} (TD)) [Hz]	:	NaN
Center frequency (f_0 (FD)) [Hz]	:	NaN
-3dB Bandwidth (BW_{-3dB}) [Hz]	:	3.511E+07
90% Bandwidth (BW_{90}) [Hz]	:	2.552E+08
Band-ratio (br)	:	4.347E+00
Average quality factor (Q (TD))	:	NaN
Quality factor (Q (FD))	:	NaN

A-3.21 MONTENA HIRA 140 in [A-20]

Measurement distance 30m

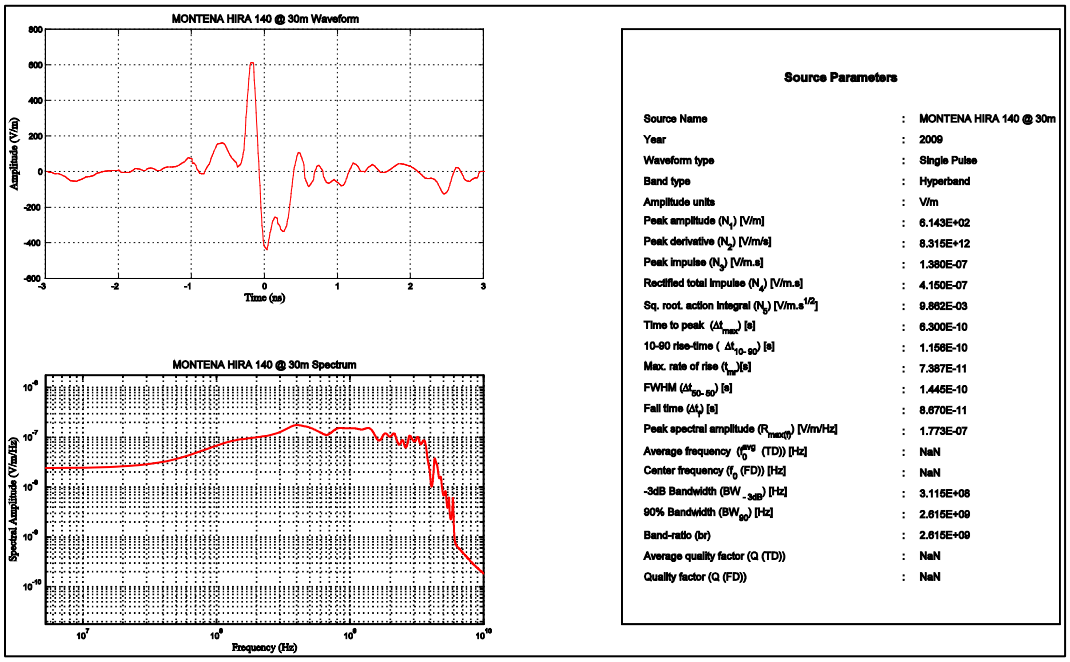

Source Parameters

Source Name	:	MONTENA HIRA 140 @ 30m
Year	:	2009
Waveform type	:	Single Pulse
Band type	:	Hyperband
Amplitude units	:	V/m
Peak amplitude (N_1) [V/m]	:	6.143E+02
Peak derivative (N_2) [V/m/s]	:	8.315E+12
Peak impulse (N_3) [V/m.s]	:	1.380E-07
Rectified total impulse (N_4) [V/m.s]	:	4.150E-07
Sq. root. action integral (N_5) [V/m.s$^{1/2}$]	:	9.862E-03
Time to peak (Δt_{max}) [s]	:	6.300E-10
10-90 rise-time (Δt_{10-90}) [s]	:	1.166E-10
Max. rate of rise (t_{mr})[s]	:	7.387E-11
FWHM (Δt_{50-50}) [s]	:	1.445E-10
Fall time (Δt_f) [s]	:	8.670E-11
Peak spectral amplitude ($R_{max(f)}$) [V/m/Hz]	:	1.773E-07
Average frequency (f_0^{avg} (TD)) [Hz]	:	NaN
Center frequency (f_0 (FD)) [Hz]	:	NaN
-3dB Bandwidth (BW_{-3dB}) [Hz]	:	3.115E+08
90% Bandwidth (BW_{90}) [Hz]	:	2.615E+09
Band-ratio (br)	:	2.615E+09
Average quality factor (Q (TD))	:	NaN
Quality factor (Q (FD))	:	NaN

A-3.22 SWO + Helical Antenna in [A-21]

Measurement distance 2m

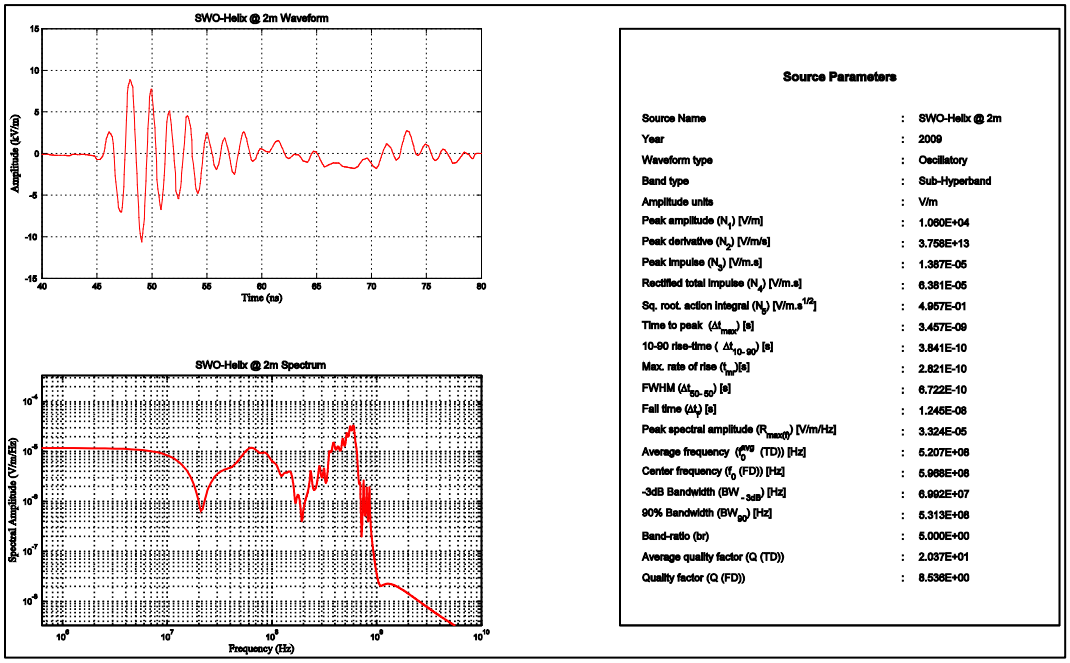

Source Parameters

Source Name	:	SWO-Helix @ 2m
Year	:	2009
Waveform type	:	Oscillatory
Band type	:	Sub-Hyperband
Amplitude units	:	V/m
Peak amplitude (N_1) [V/m]	:	1.060E+04
Peak derivative (N_2) [V/m/s]	:	3.758E+13
Peak impulse (N_3) [V/m.s]	:	1.387E-05
Rectified total impulse (N_4) [V/m.s]	:	6.381E-05
Sq. root. action integral (N_5) [V/m.s$^{1/2}$]	:	4.957E-01
Time to peak (Δt_{max}) [s]	:	3.457E-09
10-90 rise-time (Δt_{10-90}) [s]	:	3.841E-10
Max. rate of rise (t_{mr})[s]	:	2.821E-10
FWHM (Δt_{50-50}) [s]	:	6.722E-10
Fall time (Δt_f) [s]	:	1.245E-08
Peak spectral amplitude ($R_{max(f)}$) [V/m/Hz]	:	3.324E-05
Average frequency (f_0^{avg} (TD)) [Hz]	:	5.207E+08
Center frequency (f_0 (FD)) [Hz]	:	5.968E+08
-3dB Bandwidth (BW_{-3dB}) [Hz]	:	6.992E+07
90% Bandwidth (BW_{90}) [Hz]	:	5.313E+08
Band-ratio (br)	:	5.000E+00
Average quality factor (Q (TD))	:	2.037E+01
Quality factor (Q (FD))	:	8.538E+00

A-3.23 Biconical antenna in [A-22]

Measurement distance 1m

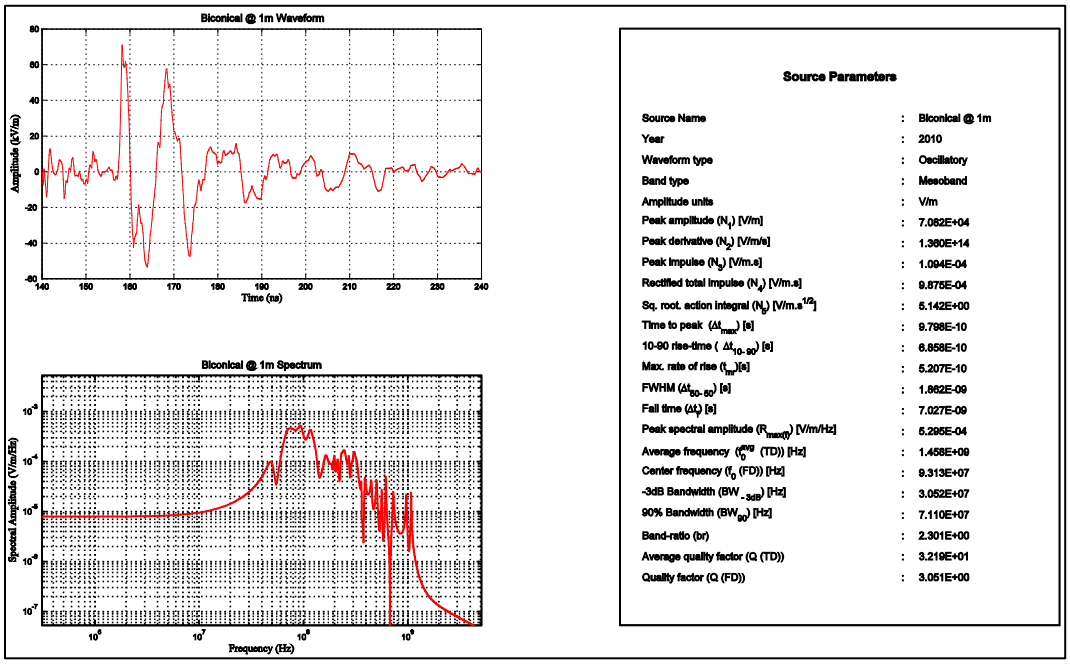

A-3.24 Spiral biconical antenna in [A-22]

Measurement distance 1m

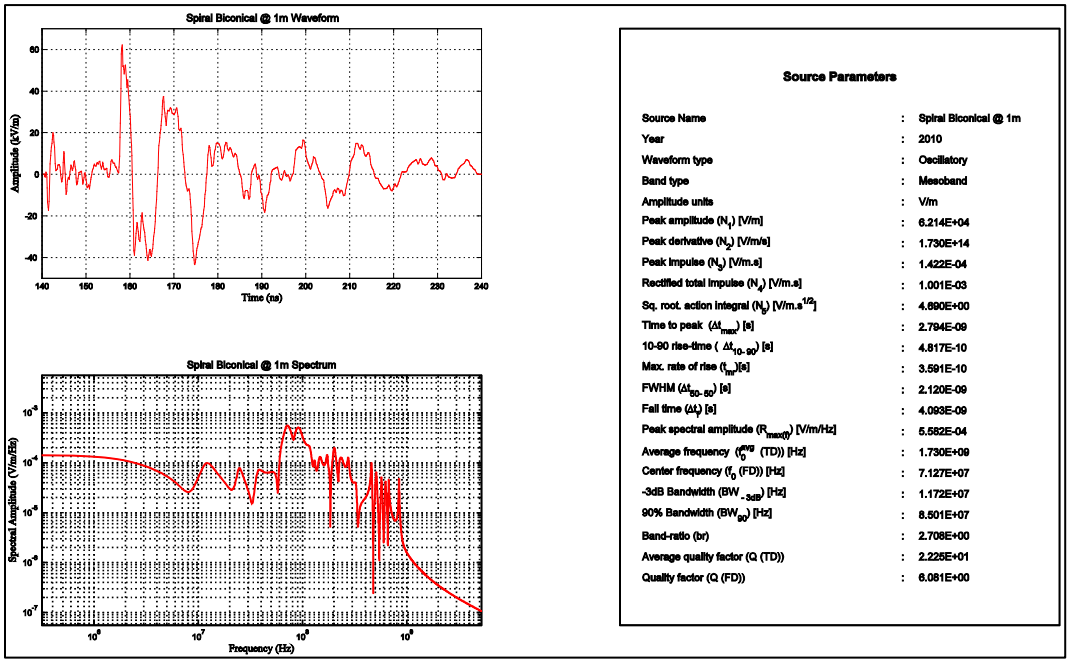

A-3.25 EPFL HIRA in [A-23]

Measurement distance 10m

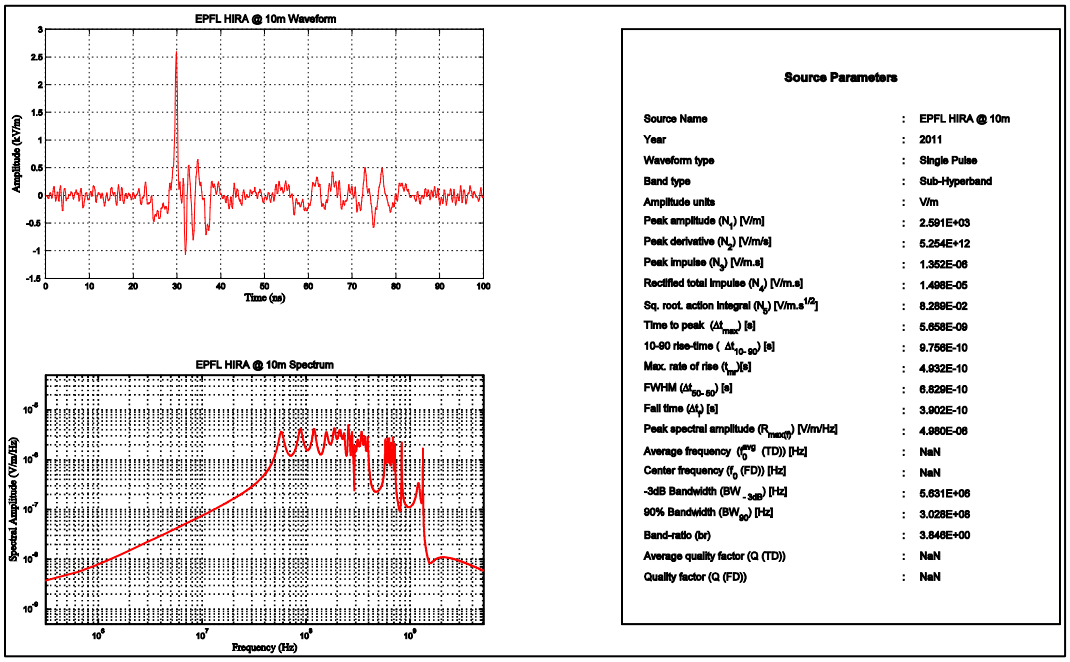

Source Parameters

Source Name	:	EPFL HIRA @ 10m
Year	:	2011
Waveform type	:	Single Pulse
Band type	:	Sub-Hyperband
Amplitude units	:	V/m
Peak amplitude (N_1) [V/m]	:	2.591E+03
Peak derivative (N_2) [V/m/s]	:	5.254E+12
Peak impulse (N_3) [V/m.s]	:	1.352E-06
Rectified total impulse (N_4) [V/m.s]	:	1.498E-05
Sq. root. action integral (N_5) [V/m.s$^{1/2}$]	:	8.289E-02
Time to peak (Δt_{max}) [s]	:	5.658E-09
10-90 rise-time (Δt_{10-90}) [s]	:	9.756E-10
Max. rate of rise (t_{mr})[s]	:	4.932E-10
FWHM (Δt_{50-50}) [s]	:	6.829E-10
Fall time (Δt_f) [s]	:	3.902E-10
Peak spectral amplitude ($R_{max(f)}$) [V/m/Hz]	:	4.980E-06
Average frequency (f_0^{avg} (TD)) [Hz]	:	NaN
Center frequency (f_0 (FD)) [Hz]	:	NaN
-3dB Bandwidth (BW_{-3dB}) [Hz]	:	5.631E+08
90% Bandwidth (BW_{90}) [Hz]	:	3.028E+08
Band-ratio (br)	:	3.846E+00
Average quality factor (Q (TD))	:	NaN
Quality factor (Q (FD))	:	NaN

A-3.26 GIMLI in [A-24]

Measurement distance 9m

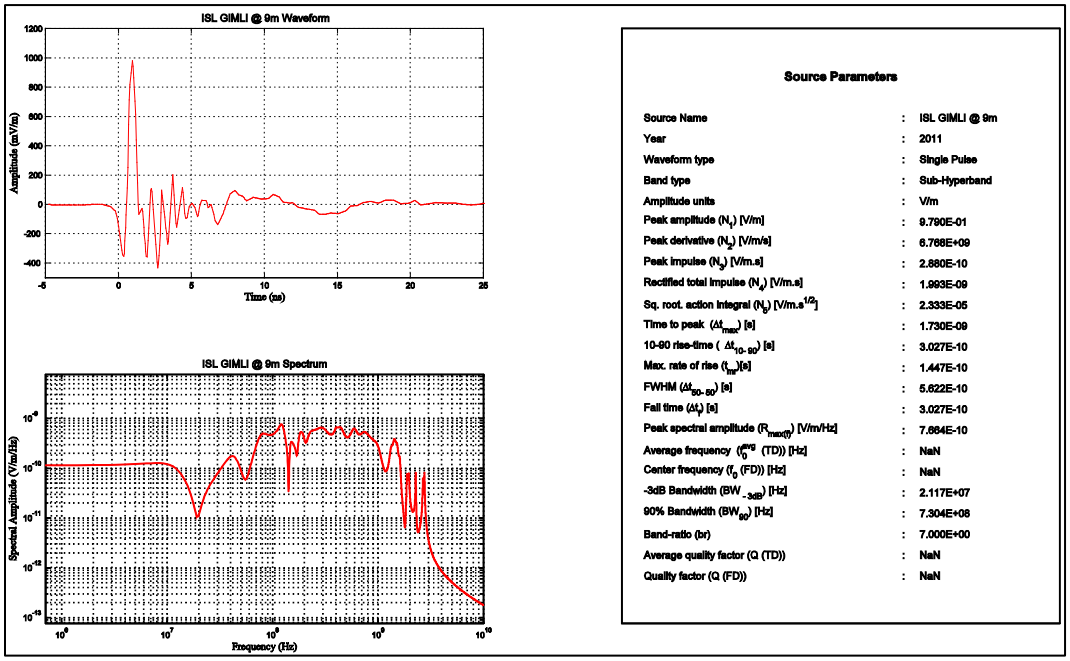

Source Parameters

Source Name	:	ISL GIMLI @ 9m
Year	:	2011
Waveform type	:	Single Pulse
Band type	:	Sub-Hyperband
Amplitude units	:	V/m
Peak amplitude (N_1) [V/m]	:	9.790E-01
Peak derivative (N_2) [V/m/s]	:	6.766E+09
Peak impulse (N_3) [V/m.s]	:	2.680E-10
Rectified total impulse (N_4) [V/m.s]	:	1.993E-09
Sq. root. action integral (N_5) [V/m.s$^{1/2}$]	:	2.333E-05
Time to peak (Δt_{max}) [s]	:	1.730E-09
10-90 rise-time (Δt_{10-90}) [s]	:	3.027E-10
Max. rate of rise (t_{mr})[s]	:	1.447E-10
FWHM (Δt_{50-50}) [s]	:	5.622E-10
Fall time (Δt_f) [s]	:	3.027E-10
Peak spectral amplitude ($R_{max(f)}$) [V/m/Hz]	:	7.664E-10
Average frequency (f_0^{avg} (TD)) [Hz]	:	NaN
Center frequency (f_0 (FD)) [Hz]	:	NaN
-3dB Bandwidth (BW_{-3dB}) [Hz]	:	2.117E+07
90% Bandwidth (BW_{90}) [Hz]	:	7.304E+08
Band-ratio (br)	:	7.000E+00
Average quality factor (Q (TD))	:	NaN
Quality factor (Q (FD))	:	NaN

A-3.27 EPFL SWO in [A-25]

Measurement distance 1m

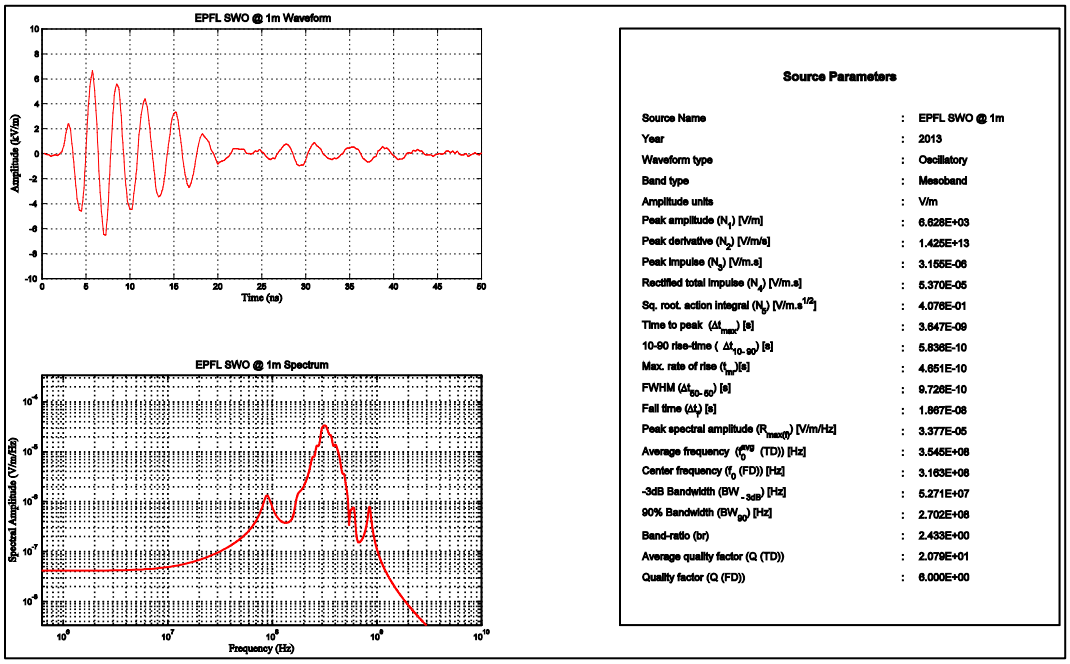

A-3.28 ISL HPM source in [A-26]

Measurement distance 10m

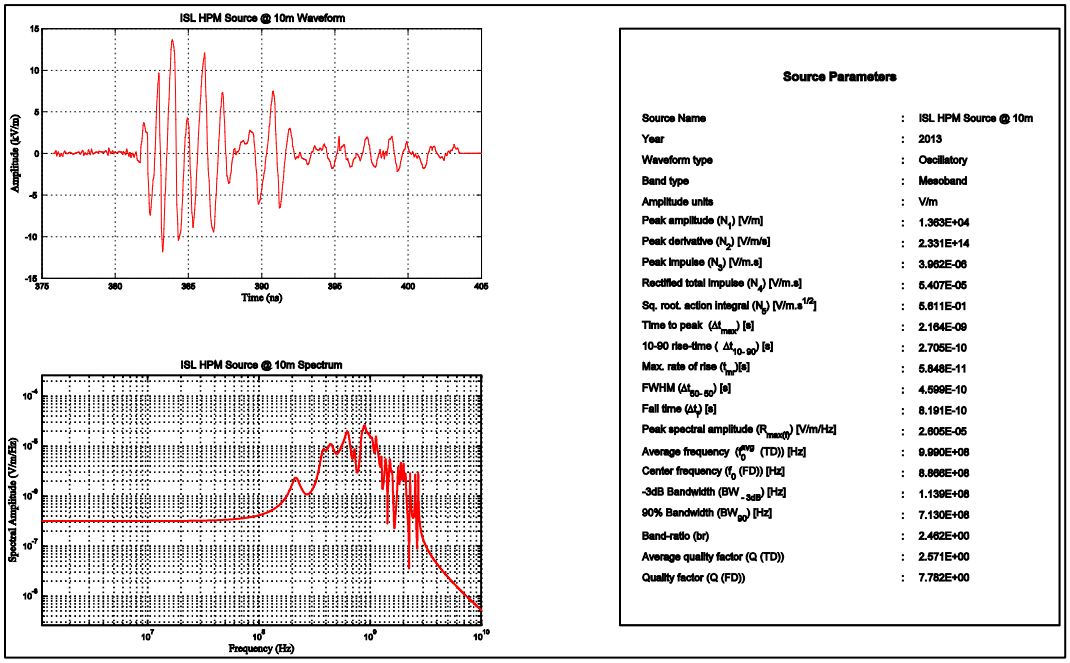

A-4 REFERENCES

[A- 1] J. S. H. Schoenberg, J. W. Burger, J. S. Tyo, M. D. Abdalla, M. C. Skipper, and W. R. Buchwald, "Ultra-wideband source using gallium arsenide photoconductive semiconductor switches," *Plasma Science, IEEE Transactions on,* vol. 25, pp. 327-334, 1997.

[A- 2] Y. V. Parfenov, L. N. Zdoukhov, W. A. Radasky, and M. Ianoz, "Conducted IEMI threats for commercial buildings," *Electromagnetic Compatibility, IEEE Transactions on,* vol. 46, pp. 404-411, 2004.

[A- 3] W. D. Prather, C. E. Baum, R. J. Torres, F. Sabath, and D. Nitsch, "Survey of worldwide high-power wideband capabilities," *Electromagnetic Compatibility, IEEE Transactions on,* vol. 46, pp. 335-344, 2004.

[A- 4] L. H. Bowen and E. G. Farr, "A High-Voltage Cable-Fed Impulse Radiating Antenna," *Sensor and Simulation Notes,* vol. 507, 2005.

[A- 5] R. Krzikalla and J. L. Haseborg, "HPEM protection on HF transmission lines," *Adv. Radio Sci.,* vol. 2, pp. 79-82, 2005.

[A- 6] D. Mansson, T. Nilsson, R. Thottappillil, and M. Backstrom, "Propagation of UWB Transients in Low-Voltage Installation Power Cables," *Electromagnetic Compatibility, IEEE Transactions on,* vol. 49, pp. 585-592, 2007.

[A- 7] D. Mansson, R. Thottappillil, T. Nilsson, O. Lunden, and M. Backstrom, "Susceptibility of Civilian GPS Receivers to Electromagnetic Radiation," *Electromagnetic Compatibility, IEEE Transactions on,* vol. 50, pp. 434-437, 2008.

[A- 8] ITU, "High-power electromagnetic immunity guide for telecommunication systems," in *K. 81* ed, 2009.

[A- 9] M. Nyffeler, A. W. Kaelin, D. Rolle, P. F. Bertholet, and A. Jaquier, "Behavior of combined Lightning HEMP Protection Devices to HPEM Overvoltage Input Signals," in *AMEREM 2010*, Ottawa, Canada, 2010.

[A- 10] J. H. Hagmann, S. Dickmann, and S. Potthast, "Application and propagation of transient pulses on power supply networks," in *EMC Europe 2011 York*, 2011, pp. 7-12.

[A- 11] C. E. Baum, W. L. Baker, W. D. Prather, J. M. Lehr, J. P. O'Loughlin, D. V. Giri*, et al.*, "JOLT: A Highly Directive, Very Intensive, Impulse-Like Radiator," *Sensor and Simulation 0480,* November 2003.

[A- 12] J. R. Mayes, W. J. Carey, W. C. Nunnally, and L. Altgilbers, "The Marx generator as an ultra wideband source," in *Pulsed Power Plasma Science, 2001. IEEE Conference Record - Abstracts*, 2001, p. 510.

[A- 13] K. D. Hong and S. W. Braidwood, "Resonant antenna-source system for generation of high-power wideband pulses," *Plasma Science, IEEE Transactions on,* vol. 30, pp. 1705-1711, 2002.

[A- 14] L. M. Atchley, E. G. Farr, D. E. Ellibee, and L. Altgilbers, "Further Developments in Ultra-Wideband Antennas Built Into Parachutes," *Sensor and Simulation Notes 495,* 2004.

[A- 15] Eureka, "High-Power Compact Microwave Source for Vehicle Immobilization," Eureka Aerospace, Pasadena, CA2006.

[A- 16] A. Efremov, V. Koshelev, B. Kovalchuk, V. Plisko, and K. Sukhushin, "High-power sources of ultra-wideband radiation with subnanosecond pulse lengths," *Instruments and Experimental Techniques,* vol. 54, pp. 70-76, 2011.

[A- 17]B. Cadilhon, "Etude et réalisation d'un ensemble autonome d'émission d'ondes électromagnétiques de fortes puissances," DOCTEUR, ECOLE DOCTORALE DES SCIENCES EXACTES ET DE LEURS APPLICATIONS, UNIVERSITE DE PAU ET DES PAYS DE L'ADOUR, 2008.
[A- 18]B. Martin, "Etude et conception d'un étage de mise en forme d'impulsions ultra-large-bande de forte puissance," DOCTEUR, Université de Limoges, 2008.
[A- 19]D. Belt, J. Mankowski, J. Walter, J. Dickens, and M. Kristiansen, "Analysis of Mesoband Single Element Pulsed Ring-Down Antennas for Implementation in Phased Array Systems," in *IEEE International Power Modulators and High Voltage Conference, Proceedings of the 2008*, 2008, pp. 152-155.
[A- 20]M. Sallin and B. Daout, "Technical Note - TN16 -Half Impulse Radiating Antenna Type HIRA140 Measurements and simulations," Montena Technologies, Rossens, Switzerland2009.
[A- 21]D. V. Giri, F. M. Tesche, M. D. Abdalla, M. C. Skipper, and M. Nyffeler, "Switched Oscillators and Their Integration Into Helical Antennas," *Plasma Science, IEEE Transactions on,* vol. 38, pp. 1411-1426, 2010.
[A- 22]M. Armanious, "DESIGN AND ANALYSIS OF A HIGH POWER MODERATE BAND RADIATOR USING A SWITCHED OSCILLATOR," DOCTOR OF PHILOSOPHY, COLLEGE OF OPTICAL SCIENCES, THE UNIVERSITY OF ARIZONA, 2010.
[A- 23]F. Vega, "DESIGN OF A HIGH POWER ULTRA WIDEBAND SYSTEM USING A FAST IMPULSE CURRENT GENERATOR," Doctor of Philosophy, Electrical and Electronics Engineering Department, National University of Colombia, 2011.
[A- 24]P. Delmote, J. P. Duperoux, F. Bieth, and S. Pinguet, "UWB at ISL: The GIMLI project and other applications," in *High Power Microwave Defense and Security Workshop*, Saint Louis, 2011.
[A- 25]F. Vega, "Analytical Methods for the Study and Design of Integrated Switched Oscillators and Antennas for Mesoband Radiation," DOCTEUR ÈS SCIENCES, FACULTÉ DES SCIENCES ET TECHNIQUES DE L'INGÉNIEUR, ÉCOLE POLYTECHNIQUE FÉDÉRALE DE LAUSANNE, 2013.
[A- 26]P. Delmote, F. Bieth, S. Pinguet, and J. Michel, "Embedded HPM source , design and outdoor experiments," in *ISL Symposium "Electrical Engineering"*, Saint-Louis, France, 2013.

SYSTEM DESIGN AND ASSESSMENT NOTES

NOTE 41

8 July 2014

APPENDIX B

COLLECTION OF POTENTIAL IEMI SOURCES REPORTED IN THE LITERATURE

Corresponding author: nicolas.mora@epfl.ch

TABLE OF CONTENTS

B-1 INTRODUCTION

This appendix presents a database containing relevant characteristics of potential conducted and radiated IEMI sources that have been reported in the literature (peer reviewed journal articles, , standards, books, conference articles, reports, conference presentations, manuals, and brochures). Most of the information about the sources has been obtained throughout the analyzed reports, and with the aid of the "wavecards" presented in Appendix A (if available). The information that could not be obtained from the readings, or parameters like the classification according to the technological level, cost level, or portability, have been obtained from the authors' best knowledge according to their expertise in the subject. The fields where no information is available or the characteristic does not apply to the studied source have been filled with "N/A".

Depending on the kind of source (conducted or radiated), the following characteristics are listed in the database:

1. Conducted Sources

   (i) *Year:* the year of the source construction (if available) or the publication year of the document that reports the source (for the first time).

   (ii) *Source Name:* the name that was used to identify the source in the database

   (iii) *Peak Voltage (kV):* the maximum voltage in kV that can be generated by the source

   (iv) *PRF (Hz):* the pulse repetition frequency of the source in Hz, as explained in Eq. 2.10.

   (v) Average/ center frequency: the average frequency of the source (only for mesoband or CW sources, or sub-hyperband sources with a very low band ratio).

   (vi) Band type: the band-type of the source according to its band-ratio, as it was explained in Tab 3.1 if the source waveform is available in the wavecards. Else, the band-type is inferred according to the information available from the publication.

   (vii) Technology Level: the classification of the source according to the technological sophistication criteria proposed by Giri and Tesche in [B-1] and reviewed in Section 3.4 of this note.

   (viii) Cost Level: the classification of the source according to its cost as proposed by Sabath and Garbe in [B-2] and reviewed in Section 3.4 of this note.

   (ix) Portability level: the classification of the source according to its portaibility level as proposed by ITU in [B-3] and reviewed in Section 3.5 of this note.

   (x) Reference: the reference from which the information about the source has been obtained.

(xi) *Wavecard:* the name of the wave-card associated to the source (if available in Appendix A).

2. Radiated Sources

(i) *Year:* the year of the source construction (if available) or the publication year of the document that reports the source (for the first time).

(ii) *Source Name:* the name that was used to identify the source in the database

(iii) *Peak Field (kV/m):* the reported peak electric field in kV/m generated by the source at a given distance

(iv) *Test distance (m):* the distance in m at which the peak electric field has been measured

(v) *Far Voltage (kV):* the far-field generated by the source as explained in Section 3.3 of this note.

(vi) *Vpeak (pulser) (kV):* the peak voltage in kV generated by the source's main pulser

(vii) *rEp/Vp*: the far-voltage/ pulser-peak-voltage ratio as explained in Section 3.3 of this note.

(viii) *rise-time* $_{10\text{-}90}$ *(ps):* the 10-90 rise time of the source in ps obtained from the wave-card (if available), else it is inferred from the information available in the publication.

(ix) *PRF (Hz):* the pulse repetition frequency of the source in Hz, as explained in Eq. 2.10.

(x) *Min frequency (MHz):* the minimum frequency of the source in MHz (only for mesoband or CW sources, or sub-hyperband sources with a very low band ratio).

(xi) *Average/ center frequency (MHz):* the average/center frequency of the source in MHz (only for mesoband or CW sources, or sub-hyperband sources with a very low band ratio).

(xii) *Max frequency(MHz)*: the maximum frequency of the source in MHz (only for mesoband or CW sources, or sub-hyperband sources with a very low band ratio).

(xiii) *Band type:* the band-type of the source according to its band-ratio, as it was explained in Tab 3.1 if the source waveform is available in the wave-cards. Else, the band-type is inferred according to the information available from the publication.

(xiv) Technology Level: the classification of the source according to the technological sophistication criteria proposed by Giri and Tesche in [B-1] and reviewed in Section 3.4 of this note.

(xv) Cost Level: the classification of the source according to its cost as proposed by Sabath and Garbe in [B-2] and reviewed in Section 3.4 of this note.

(xvi) Portability level: the classification of the source according to its portaibility level as proposed by ITU in [B-3] and reviewed in Section 3.5 of this note.

(xvii) Primary source DC voltage: the DC charging voltage of the Marx generator of primary source of the pulser.

(xviii) Pulser: brief description of the source pulser

(xix) Output antenna: brief description of the source antenna

(xx) Reference: the reference from which the information about the source has been obtained.

(xxi) Wavecard: the name of the wavecard associated to the source (if available in Appendix A).

B-2 CONDUCTED SOURCES

Year	Source name	Peak Voltage (kV)	PRF (Hz)	Average/center frequency	Band type	Technology Level (Giri-2004)	Cost Level (Sabath Garbe-2009)	Portability Level (ITU - 2009)	Reference	Wavecard
1997	FET Based Pulse Modulator	70	2000	N/A	Hyperband	2	2	2	[B-4]	1997 GaAs Source
2000	Pulse test source	1.5	5	N/A	Hyperband	2	2	2	[B-5]	2000 Parfenov et al
2002	BAE non linear transmission line	65	1000	10 MHz-2000MHz	Hyperband	3	2	2	[B-6]	2002 BAE-NLTL
2003	FID FPG Series	0.05	10000	N/A	Hyperband	3	2	2	[B-6]	N/A
2005	FID FPG30-1KM	25	N/A	N/A	Hyperband	3	2	2	[B-7]	2005 FID FPG30-1KM
2005	HYPS pulser	4.5	N/A	N/A	Hyperband	3	2	2	[B-7]	2005 HYPS pulser
2005	Kentech PBG3	12.5	800	N/A	Hyperband	3	2	2	[B-8]	2005 Krzikalla et al
2007	Power spectra PGS-402	0.45	N/A	N/A	Hyperband	2	2	2	[B-9]	2007 P.S. PGS-402
2008	Radan 303B UWB Voltage source	150	25	N/A	Sub-hyperband	3	3	3	[B-10]	2008 RADAN303B
2009	HYPS pulsed voltage source	2.2	N/A	N/A	Hyperband	2	2	2	[B-3]	2009 HYPS Source
2009	Compact lightning surge generator	10	N/A	N/A	Hyperband	2	2	2	[B-3]	N/A
2009	Lightning surge generator	25	N/A	N/A	Hyperband	2	2	3	[B-3]	N/A
2009	Lightning surge generator	50	N/A	N/A	Hyperband	2	2	4	[B-3]	N/A
2009	CW generator	0.24	N/A	1 Hz - 10MHz	Hypoband	2	2	2	[B-3]	N/A
2009	Commercial power supply	0.24	N/A	50 Hz	Hypoband	1	1	2	[B-3]	N/A
2010	Impulse voltage source	4	1000	N/A	Hyperband	2	2	2	[B-11]	2010 Nyffeler et al
2011	Typical stun gun	10	N/A	N/A	Hyperband	1	1	1	[B-12]	2011 STUN GUN
2012	Montena EMP80K-5-500	80	0.01	N/A	Hyperband	3	2	2	[B-13]	N/A
2012	Montena EMP300K-5-500	80	0.01	N/A	Hyperband	3	3	2	[B-13]	N/A
2012	Montena IPP3K-4MS	3	0.02	N/A	Hyperband	3	2	2	[B-13]	N/A
2012	Montena CLP40K	25	N/A	30MHz-300MHz	Mesoband	3	2	2	[B-13]	N/A

B-3 RADIATED SOURCES

Year	Source name	Peak Field (kV/m)	Test distance (m)	Far Voltage (kV)	Vpeak (pulser) (kV)	rEp/Vp	rise-time 10-90 (ps)	PRF (Hz)	Min Freq. (MHz)	Avg /center Freq. (MHz)	Max Freq. (MHz)	Band type	Technology Level (Giri Tesche-2004)	Cost Level (Sabath Garbe-2009)	Portability Level (ITU - 2009)	Primary Source DC Voltage (kV)	Pulser	Output Antenna	Ref	Wavecard
1992	H-2	43	10	430	300	1.43	238	N/A	N/A	N/A	N/A	Hyperband	3	3	4	300	PFL 300kV/250ps/2ns	TEM Horn	[B-6]	1992 H2 @ 10m
1994	Prototype IRA	23	2	1281	120	10.68	99	200	N/A	N/A	N/A	Hyperband	3	3	4	30	Switched capacitor pulser ±60kV/100ps/20ns	IRA	[B-14]	N/A
1997	IRA II	41.6	16.6	690	144	4.79	70	400	N/A	N/A	N/A	Hyperband	3	3	4	N/A	Switched capacitor pulser ±75kV/85ps/20ns	IRA	[B-15]	1997 IRA-II
1997	JOLT	62	85	5300	1000	5.30	80	600	N/A	N/A	N/A	Hyperband	3	4	4	50	Switched capacitor pulser 1MV/180ps/5ns	HIRA	[B-16]	1997 JOLT @ 10m
1997	PCSS UWB source	6.5	0.65	N/A	13	N/A	330	2000	N/A	500	N/A	N/A	3	2	3	13	PCSS switched Blumlein 13kV/420ps/900ps	TEM Horn	[B-4]	N/A
1997	PCSS UWB source	6.5	0.65	N/A	13	N/A	330	2000	N/A	165	N/A	N/A	3	2	3	13	PCSS switched Blumlein 13kV/420ps/1.8ns	TEM Horn	[B-4]	N/A
1998	Swiss IRA	1.4	5	10	2.8	3.57	N/A	800	N/A	N/A	N/A	Hyperband	3	3	4	N/A	Switched capacitor pulser 2.8 kV/100ps/4ns	IRA	[B-15]	N/A
1999	AFRL Solid State Array	20	1	20	17	1.18	484	N/A	N/A	N/A	N/A	Sub-hyperband	3	3	3	17	17kV PCSS Blumlein	4 TEM Horns	[B-6]	1999 AFRL Solid State
2001	Marx + E. TEM Horn	0.652	100	65.2	150	0.43	641	N/A	N/A	N/A	N/A	Hyperband	2	2	3	10	Marx Generator 150kV/400ps	Exponential TEM Horn	[B-17]	2001 E. TEM Horn @ 100m
2001	Marx + H. TEM Horn	0.743	100	74.3	150	0.50	379	N/A	N/A	N/A	N/A	Hyperband	2	2	3	10	Marx Generator 150kV/400ps	Half TEM Horn	[B-17]	2001 H. TEM @ 100m
2001	Marx + Helical	0.3	100	30	150	0.20	N/A	N/A	N/A	1000	N/A	Mesoband	2	2	3	10	Marx Generator 150kV/400ps	Helical	[B-17]	2001 Helical @ 100m
2001	Marx + Monopole	0.2	100	20	150	0.13	447	N/A	N/A	N/A	N/A	Hyperband	2	2	3	10	Marx Generator 150kV/400ps	Monopole	[B-17]	2001 Monopole @ 100m

Year	Source name	Peak Field (kV/m)	Test distance (m)	Far Voltage (kV)	Vpeak (pulser) (kV)	rEp/Vp	rise-time 10-90 (ps)	PRF (Hz)	Min Freq. (MHz)	Avg /center Freq. (MHz)	Max Freq. (MHz)	Band type	Technology Level (Giri Tesche-2004)	Cost Level (Sabath Garbe-2009)	Portability Level (ITU - 2009)	Primary Source DC Voltage (kV)	Pulser	Output Antenna	Ref	Wavecard
2001	WIS HIRA	22	11	242	100	2.42	N/A	N/A	N/A	N/A	N/A	Hyperband	3	3	4	100	Switched PFL pulser 100 kV/300ps /650ps	HIRA	[B-18]	N/A
2001	TNO IRA	7	1	34	9	3.78	N/A	800	N/A	N/A	N/A	Hyperband	3	3	4	N/A	Switched capacitor pulser 9 kV/100ps /4ns	IRA	[B-15]	N/A
2002	DS-110	125	1	125	400	0.31	N/A	N/A	N/A	350	N/A	Mesoband	3	3	2	50	400kV Marx Generator	Coil	[B-6]	2002 DS110 @ 1m
2002	Compact Biconical resonant system	4	15	60	200	0.30	N/A	N/A	N/A	43	N/A	Sub-hyperband	2	2	3	24	Capacitive bank+ Tesla Trafo. Pulser 200kV	Bicone	[B-19]	2002 Hong @ 15m
2002	DS-350	300	1	300	1000	0.30	N/A	50	N/A	100	N/A	Mesoband	3	3	3	N/A	1MV Marx Generator	Multirod Dipole Antenna	[B-6]	N/A
2003	Univ. Of Magdeburg IRA	7	1	34	9	3.78	N/A	800	N/A	N/A	N/A	Hyperband	3	3	4	N/A	Switched capacitor pulser 9 kV/100ps /4ns	IRA	[B-15]	N/A
2003	RAS-FGD800	18	3	N/A	0.8	N/A	75	5000	N/A	N/A	N/A	N/A	3	2	N/A	N/A	800V Pulser	Combination of magnetic and electric dipoles	[B-6]	N/A
2003	THOR	68	10	680	1000	0.68	200	N/A	N/A	N/A	N/A	Sub-hyperband	3	4	3	*	1MV pulser	TEM Horn	[B-6]	N/A
2003	MATRIX	6	15	90	150	0.60	N/A	N/A	180	N/A	600	Mesoband	3	3	4	150	Switched oscillator	HIRA	[B-6]	N/A
2004	Para - IRA	5	12.2	61	80	0.76	789	N/A	N/A	N/A	N/A	Hyperband	3	3	3	30	80 kV/ 220 ps Marx	Parachute IRA	[B-20]	2004 Para-IRA @ 12.2m
2004	Microwave oven + waveguide	0.079	6	0.474	4	0.12	N/A	N/A	N/A	2045	N/A	Hypoband	1	1	2	4	Microwave oven	Open-ended waveguide	[B-15]	N/A
2004	Microwave oven + horn	0.337	6	2.022	4	0.51	N/A	N/A	N/A	2045	N/A	Hypoband	1	1	3	4	Microwave oven	Pyramidal horn	[B-15]	N/A
2004	Microwave oven + reflector	0.78	6	4.68	4	1.17	N/A	N/A	N/A	2045	N/A	Hypoband	1	1	3	4	Microwave oven	Parabolic reflector	[B-15]	N/A
2005	IRA-6	2.8	20.4	57.12	30	1.90	1038	N/A	N/A	N/A	N/A	Hyperband	3	3	3	N/A	30kV/150ps FID Pulser	IRA	[B-7]	2005 IRA-6 @ 20.4 m
2005	Texas Tech Vircator	290	1.5	N/A	250	N/A	N/A	10.00	3000	4800	6000	Hypoband	3	4	4	21	Marx Generator 250kV	Open-ended waveguide	[B-21]	N/A
2005	FOI Vircator	18.8	1	N/A	250	N/A	N/A	N/A	1000	N/A	5000	Hypoband	3	4	4	30	Vircator	Open-ended waveguide	[B-22]	N/A

Year	Source name	Peak Field (kV/m)	Test distance (m)	Far Voltage (kV)	Vpeak (pulser) (kV)	rEp/Vp	rise-time 10-90 (ps)	PRF (Hz)	Min Freq. (MHz)	Avg /center Freq. (MHz)	Max Freq. (MHz)	Band type	Technology Level (Giri Tesche-2004)	Cost Level (Sabath Garbe-2009)	Portability Level (ITU - 2009)	Primary Source DC Voltage (kV)	Pulser	Output Antenna	Ref	Wavecard
2005	IRA-6	0.6	20.4	12.24	4.5	2.72	N/A	N/A	N/A	N/A	N/A	Hyperband	3	3	3	N/A	4.5kV/547ps Pulser	IRA	[B-7]	N/A
2006	EUREKA -High Power Compact Microwave Source	68	10	680	600	1.13	N/A	100.00	N/A	350	N/A	Mesoband	3	3	3	40	600kV Marx Generator+ Blumlein	TEM Horn	[B-23]	2006 Eureka @ 9m
2006	Russian HP UWB source	26	10	260	200	1.30	92	100	N/A	N/A	N/A	Sub-hyperband	3	4	3	N/A	Bipolar Pulse former - 160kV/200kV/500ps duration	Horn	[B-24]	2008 Russian HP UWB
2006	Russian HP UWB source (array)	69	10	690	200	3.45	N/A	100	N/A	N/A	N/A	Hyperband	3	4	3	N/A	Bipolar Pulse former - 160kV/200kV/500ps duration	16-Horns array	[B-24]	N/A
2008	George +Valentine Antenna	23.2	10	232	200	1.16	170.00	350.00	N/A	N/A	N/A	Sub-hyperband	3	3	3	60	200 kV/300ps Marx	Valentine	[B-25]	2008 George-Valentine @ 10m
2008	GIMLI repetitive	77.7	8	621.6	207	3	252	200	N/A	N/A	N/A	Sub-hyperband	3	4	3	30	250kV Marx/400ps	TEM Horn	[B-26]	2008 GIMLI @ 8m
2008	Leonardo +PFL+Valentine Antenna	14.2	10	142	98	1.45	280	120	N/A	N/A	N/A	Sub-hyperband	3	3	3	60	200 kV/2ns Marx	Valentine	[B-25]	2008 Leonardo-Valentine @ 10m
2008	Ringing log-periodic antenna	1.1	3	N/A	75	N/A	N/A	N/A	N/A	71	N/A	Hyperband	2	2	3	75	Self discharged antenna	Log-periodic	[B-27]	2008 Log Periodic @ 3m
2008	Ringing dipole	0.542	3	N/A	75	N/A	N/A	N/A	N/A	95	N/A	Sub-hyperband	2	2	3	75	Self discharged antenna	Dipole	[B-27]	2008 Ringing Dipole @ 3m
2009	IRA (Farr Research) + HYPS Generator	0.27	3	N/A	2	N/A	190	N/A	N/A	N/A	N/A	Sub-hyperband	3	3	3	*	HYPS Pulser 2kV/230ps/6ns	IRA	[B-3]	2009 IRA-HYPS @ 3m
2009	Montena HIRA 140	0.65	30	19.5	10	1.95	116	N/A	N/A	N/A	N/A	Sub-hyperband	3	3	4	N/A	10kV/140ps Pulser	HIRA	[B-28]	2009 MONTENA HIRA 140 @ 30 m
2009	SWO + Helical antenna	10	2	N/A	30	N/A	N/A	10	N/A	596	N/A	Sub-hyperband	3	3	3	0.012	30 kV Switched oscillator	Helical	[B-29, 30]	2009 SWO-Helix @ 2m
2010	Biconical Antenna excited by ultrafast switch	70	1	N/A	380	N/A	N/A	N/A	N/A	93	N/A	Mesoband	3	2	3	N/A	380 kV Marx	Bicone	[B-31]	2010 Biconical @ 1m

Year	Source name	Peak Field (kV/m)	Test distance (m)	Far Voltage (kV)	Vpeak (pulser) (kV)	rEp/Vp	rise-time 10-90 (ps)	PRF (Hz)	Min Freq. (MHz)	Avg /center Freq. (MHz)	Max Freq. (MHz)	Band type	Technology Level (Giri Tesche-2004)	Cost Level (Sabath Garbe-2009)	Portability Level (ITU - 2009)	Primary Source DC Voltage (kV)	Pulser	Output Antenna	Ref	Wavecard
2010	Spiral Biconical Antenna excited by ultrafast switch	62	1	N/A	380	N/A	N/A	N/A	N/A	71	N/A	Mesoband	3	2	3	N/A	380 kV Marx	Spiral Bicone	[B-31]	2010 Spiral Biconical @ 1m
2010	2GHz MATRIX Oscillator	N/A	N/A	N/A	65	N/A	N/A	N/A	N/A	2000	N/A	Mesoband	3	3	2	65	65 kV Switched oscillator	Bicone	[B-32]	N/A
2010	HPM WBTS	N/A	N/A	N/A	2000	N/A	N/A	100	200	N/A	6000	Mesoband	3	4	4	50kV	2MV/300 ps Marx	Helical	[B-33]	N/A
2011	EPFL HIRA	2.7	10	27	23	1.17	665	100	N/A	N/A	N/A	Sub-hyperband	3	3	4	50	Switched PFL pulser 23kV/600ps/2.1ns	HIRA	[B-34]	2011 EPFL HIRA @ 10m
2011	ISL GIMLI	140	10	1400	400	3.5	302	N/A	N/A	N/A	N/A	Sub-hyperband	3	4	3	30	400 kV Marx	TEM Horn	[B-35]	2011 ISL GIMLI @9m
2011	Standard F - Diehl HPEMcase	90	1	N/A	300	N/A	N/A	10	N/A	350	N/A	Mesoband	3	3	2	50	300kV Marx	Coil	[B-36]	N/A
2011	Plus F - Diehl HPEMcase	135	1	N/A	600	N/A	N/A	10	N/A	350	N/A	Mesoband	3	3	2	50	600kV Marx	Coil	[B-36]	N/A
2011	Standard F - Diehl HPEMcase + Reflector	150	1	N/A	300	N/A	N/A	10	N/A	350	N/A	Mesoband	3	3	2	50	300kV Marx	Coil	[B-36]	N/A
2011	Plus F - Diehl HPEMcase	225	1	N/A	600	N/A	N/A	10	N/A	350	N/A	Mesoband	3	3	2	50	600kV Marx	Coil	[B-36]	N/A
2011	Standard T -Diehl HPEMcase	20-80	1	N/A	300	N/A	N/A	10 Hz	120	N/A	280	Mesoband	3	3	2	50	300kV Marx	Tunable Coil	[B-36]	N/A
2011	1GHz MATRIX Oscillator	N/A	N/A	N/A	50	N/A	N/A	N/A	N/A	1000	N/A	Mesoband	3	3	2	50	50 kV Switched oscillator	Bicone	[B-37]	N/A
2012	Montena HIRA 180S	7.3	20	147	30	4.90	116	N/A	N/A	N/A	N/A	Hyperband	3	3	4	N/A	30kV/130ps Pulser	HIRA	[B-38]	N/A
2013	EPFL Switching Oscillator	6.6	1	N/A	30	N/A	N/A	N/A	N/A	317	N/A	Mesoband	3	2	2	N/A	30 kV Switched oscillator	Monopole	[B-39]	2013 EPFL SWO @ 1m
2013	ISL-Embedded HPM Source	35	10	350	350	1.00	N/A	110.00	380	N/A	1200	Mesoband	3	4	3	40	440 kV Marx	Helical	[B-40]	2013 ISL HPM Source @ 10m

B-4 REFERENCES

[B- 1] D. V. Giri and F. M. Tesche, "Classification of intentional electromagnetic environments (IEME)," *Electromagnetic Compatibility, IEEE Transactions on,* vol. 46, pp. 322-328, 2004.

[B- 2] F. Sabath and H. Garbe, "Risk potential of radiated HPEM environments," in *Electromagnetic Compatibility, 2009. EMC 2009. IEEE International Symposium on*, 2009, pp. 226-231.

[B- 3] ITU, "High-power electromagnetic immunity guide for telecommunication systems," in *K. 81* ed, 2009.

[B- 4] J. S. H. Schoenberg, J. W. Burger, J. S. Tyo, M. D. Abdalla, M. C. Skipper, and W. R. Buchwald, "Ultra-wideband source using gallium arsenide photoconductive semiconductor switches," *Plasma Science, IEEE Transactions on,* vol. 25, pp. 327-334, 1997.

[B- 5] Y. V. Parfenov, L. N. Zdoukhov, W. A. Radasky, and M. Ianoz, "Conducted IEMI threats for commercial buildings," *Electromagnetic Compatibility, IEEE Transactions on,* vol. 46, pp. 404-411, 2004.

[B- 6] W. D. Prather, C. E. Baum, R. J. Torres, F. Sabath, and D. Nitsch, "Survey of worldwide high-power wideband capabilities," *Electromagnetic Compatibility, IEEE Transactions on,* vol. 46, pp. 335-344, 2004.

[B- 7] L. H. Bowen and E. G. Farr, "A High-Voltage Cable-Fed Impulse Radiating Antenna," *Sensor and Simulation Notes,* vol. 507, 2005.

[B- 8] R. Krzikalla and J. L. Haseborg, "HPEM protection on HF transmission lines," *Adv. Radio Sci.,* vol. 2, pp. 79-82, 2005.

[B- 9] D. Mansson, T. Nilsson, R. Thottappillil, and M. Backstrom, "Propagation of UWB Transients in Low-Voltage Installation Power Cables," *Electromagnetic Compatibility, IEEE Transactions on,* vol. 49, pp. 585-592, 2007.

[B- 10] D. Mansson, R. Thottappillil, T. Nilsson, O. Lunden, and M. Backstrom, "Susceptibility of Civilian GPS Receivers to Electromagnetic Radiation," *Electromagnetic Compatibility, IEEE Transactions on,* vol. 50, pp. 434-437, 2008.

[B- 11] M. Nyffeler, A. W. Kaelin, D. Rolle, P. F. Bertholet, and A. Jaquier, "Behavior of combined Lightning HEMP Protection Devices to HPEM Overvoltage Input Signals," in *AMEREM 2010*, Ottawa, Canada, 2010.

[B- 12] J. H. Hagmann, S. Dickmann, and S. Potthast, "Application and propagation of transient pulses on power supply networks," in *EMC Europe 2011 York*, 2011, pp. 7-12.

[B- 13] MONTENA, "Pulsed Current Injection Test System according to MIL-STD-188-125/1&2," MONTENA, Ed., ed. Rossens, Switzerland, 2012.

[B- 14] D. V. Giri, H. Lackner, I. D. Smith, D. W. Morton, C. E. Baum, J. R. Marek*, et al.*, "Design, fabrication, and testing of a paraboloidal reflector antenna and pulser system for impulse-like waveforms," *Plasma Science, IEEE Transactions on,* vol. 25, pp. 318-326, 1997.

[B- 15] D. V. Giri, *High-power electromagnetic radiators : nonlethal weapons and other applications*. Cambridge, MA: Harvard University Press, 2004.

[B- 16] C. E. Baum, W. L. Baker, W. D. Prather, J. M. Lehr, J. P. O'Loughlin, D. V. Giri*, et al.*, "JOLT: A Highly Directive, Very Intensive, Impulse-Like Radiator," *Sensor and Simulation 0480,* November 2003.

[B- 17] J. R. Mayes, W. J. Carey, W. C. Nunnally, and L. Altgilbers, "The Marx generator as an ultra wideband source," in *Pulsed Power Plasma Science, 2001. IEEE Conference Record - Abstracts*, 2001, p. 510.

[B- 18] F. Sabath, M. Jung, and T. H. G. G. Weise, "Design and setup of a short pulse simulator for susceptibility investigations," *Sensor and Simulation Notes,* vol. 460, 2001.
[B- 19] K. D. Hong and S. W. Braidwood, "Resonant antenna-source system for generation of high-power wideband pulses," *Plasma Science, IEEE Transactions on,* vol. 30, pp. 1705-1711, 2002.
[B- 20] L. M. Atchley, E. G. Farr, D. E. Ellibee, and L. Altgilbers, "Further Developments in Ultra-Wideband Antennas Built Into Parachutes," *Sensor and Simulation Notes 495,* 2004.
[B- 21] Y. J. Chen, "COMPACT, REPETITIVE MARX GENERATOR AND HPM GENERATION WITH THE VIRCATOR," Master of Science, Electrical Engineering, Texas Tech University, 2005.
[B- 22] B. M. Novac, M. Istenic, L. Jing, I. R. Smith, J. Brown, M. Hubbard*, et al.*, "A 10-GW Pulsed Power Supply for HPM Sources," *Plasma Science, IEEE Transactions on,* vol. 34, pp. 1814-1821, 2006.
[B- 23] Eureka, "High-Power Compact Microwave Source for Vehicle Immobilization," Eureka Aerospace, Pasadena, CA2006.
[B- 24] A. M. Efremov, V. I. Koshelev, B. M. Kovalchuk, V. V. Plisko, and K. N. Sukchushin, "High-Power Sources of Ultrawideband Radiation with Subnanosecond Pulse Length," presented at the 14th International Symposium on High Current Electronics, Tomsk, Russia, 2006.
[B- 25] B. Cadilhon, "Etude et réalisation d'un ensemble autonome d'émission d'ondes électromagnétiques de fortes puissances," DOCTEUR, ECOLE DOCTORALE DES SCIENCES EXACTES ET DE LEURS APPLICATIONS, UNIVERSITE DE PAU ET DES PAYS DE L'ADOUR, 2008.
[B- 26] B. Martin, "Etude et conception d'un étage de mise en forme d'impulsions ultra-large-bande de forte puissance," DOCTEUR, Université de Limoges, 2008.
[B- 27] D. Belt, J. Mankowski, J. Walter, J. Dickens, and M. Kristiansen, "Analysis of Mesoband Single Element Pulsed Ring-Down Antennas for Implementation in Phased Array Systems," in *IEEE International Power Modulators and High Voltage Conference, Proceedings of the 2008*, 2008, pp. 152-155.
[B- 28] M. Sallin and B. Daout, "Technical Note - TN16 -Half Impulse Radiating Antenna Type HIRA140 Measurements and simulations," Montena Technologies, Rossens, Switzerland2009.
[B- 29] D. V. Giri, F. M. Tesche, M. D. Abdalla, M. C. Skipper, and M. Nyffeler, "Switched Oscillators and Their Integration into Helical Antennas," *Circuit and Electromagnetic System Design Notes,* vol. 58, 2009.
[B- 30] D. V. Giri, F. M. Tesche, M. D. Abdalla, M. C. Skipper, and M. Nyffeler, "Switched Oscillators and Their Integration Into Helical Antennas," *Plasma Science, IEEE Transactions on,* vol. 38, pp. 1411-1426, 2010.
[B- 31] M. Armanious, "DESIGN AND ANALYSIS OF A HIGH POWER MODERATE BAND RADIATOR USING A SWITCHED OSCILLATOR," DOCTOR OF PHILOSOPHY, COLLEGE OF OPTICAL SCIENCES, THE UNIVERSITY OF ARIZONA, 2010.
[B- 32] M. Armanious, J. S. Tyo, M. C. Skipper, M. D. Abdalla, W. D. Prather, and J. E. Lawrance, "Interaction Between Geometric Parameters and Output Waveforms in High-Power Quarter-Wave Oscillators," *Plasma Science, IEEE Transactions on,* vol. 38, pp. 1124-1131, 2010.

[B- 33] D. Morton, J. Banister, T. DaSilva, J. Levine, T. Naff, I. Smith*, et al.*, "HPM WBTS, a transportable high-power wide-band microwave source," in *Power Modulator and High Voltage Conference (IPMHVC), 2010 IEEE International*, 2010, pp. 186-189.

[B- 34] F. Vega, "DESIGN OF A HIGH POWER ULTRA WIDEBAND SYSTEM USING A FAST IMPULSE CURRENT GENERATOR," Doctor of Philosophy, Electrical and Electronics Engineering Department, National University of Colombia, 2011.

[B- 35] P. Delmote, J. P. Duperoux, F. Bieth, and S. Pinguet, "UWB HPM at ISL: The GIMLI project and other applications," in *High Power Microwave Defense & Security Workshop*, Saint-Louis, France, 2011.

[B- 36] DIEHL, "HPEM Case Brochure," DIEHL, Ed., ed, 2011.

[B- 37] M. Armanious, J. S. Tyo, M. C. Skipper, M. D. Abdalla, W. D. Prather, and G. Gruen, "Electrostatic field management and electrodynamic modeling of switched quarter-wave oscillators," *Dielectrics and Electrical Insulation, IEEE Transactions on,* vol. 18, pp. 1054-1065, 2011.

[B- 38] MONTENA, "Impulse Radiating Antennas - Brochure," MONTENA, Ed., ed. Rossens, Switzerland, 2012.

[B- 39] F. Vega, "Analytical Methods for the Study and Design of Integrated Switched Oscillators and Antennas for Mesoband Radiation," DOCTEUR ÈS SCIENCES, FACULTÉ DES SCIENCES ET TECHNIQUES DE L'INGÉNIEUR, ÉCOLE POLYTECHNIQUE FÉDÉRALE DE LAUSANNE, 2013.

[B- 40] P. Delmote, F. Bieth, S. Pinguet, and J. Michel, "Embedded HPM source , design and outdoor experiments," in *ISL Symposium "Electrical Engineering"*, Saint-Louis, France, 2013.